RESEARCH & REVIEWS IN SCIENCE AND MATHEMATICS

MAY 2021

VOLUME 1

EDITORS

PROF. DR. HASAN AKGÜL
PROF. DR. HASAN HÜSEYİN DOĞAN
ASSOC. PROF. DR. MEHMET YÜKSEL
DR. ONUR KARAMAN

AUTHORS

MÜSLÜM AYKUT AKGÜN
E. NİHAL ERCAN
BELGİN ERDEM
ESİN KIRAY
ERGİN KARİPTAŞ
ŞENER TULUMOĞLU
ASLI AKILLI
EMİNE PINAR PAKSUZ
ABDURRAHMAN DÜNDAR
BARBAROS AKKURT
ALTUĞ MERT SEVİM
MURAT AYHAN

gece kitaplığı

İmtiyaz Sahibi / Publisher • Yaşar Hız
Genel Yayın Yönetmeni / Editor in Chief • Eda Altunel
Kapak & İç Tasarım / Cover & Interior Design • Gece Kitaplığı
Editörler/ Edıtors • PROF. DR. HASAN AKGÜL
PROF. DR. HASAN HÜSEYİN DOĞAN
ASSOC. PROF. DR. MEHMET YÜKSEL
DR. ONUR KARAMAN
Birinci Basım / First Edition • © May 2021
ISBN • 978-625-7793-86-5

Gece Kitaplığı / Gece Publishing
Türkiye Adres / Turkey Address: Kızılay Mah. Fevzi Çakmak 1. Sokak Ümit Apt. No: 22/A Çankaya / Ankara / TR
Telefon / Phone: +90 312 384 80 40
web: www.gecekitapligi.com
e-mail: gecekitapligi@gmail.com

Baskı & Cilt / Printing & Volume
Sertifika / Certificate No: 47083

Research & Reviews in Science and Mathematics

May 2021

Volume 1

EDITORS

PROF. DR. HASAN AKGÜL

PROF. DR. HASAN HÜSEYİN DOĞAN

ASSOC. PROF. DR. MEHMET YÜKSEL

DR. ONUR KARAMAN

gece kitaplığı

CONTENTS

CHAPTER 1

TIMELIKE INCLINED CURVES AND
B_2-SLANT HELICES IN R_2^4

Müslüm Aykut AKGÜN 1

CHAPTER 2

THE BIG BANG

E.Nihal ERCAN 15

CHAPTER 3

CHARACTERIZATION OF PROBIOTIC ABILITIES OF LACTIC ACID BACTERIA FROM TRADITIONAL PICKLE JUICE AND SHALGAM

Belgin ERDEM, Esin KIRAY, Ergin KARİPTAŞ,
Şener TULUMOĞLU, Aslı AKILLI 33

CHAPTER 4

GENERAL CHARACTERISTICS OF BATS

Emine Pınar PAKSUZ 51

CHAPTER 5

AN INVESTIGATION ON PHYSICOCHEMICAL PARAMETERS AND POTENTIAL USE OF WASTE FRUIT PEELS AS CARBON SOURCES FOR α -AMYLASE PRODUCTION FROM BACILLUS LICHENIFORMIS

Abdurrahman DÜNDAR 67

CHAPTER 6

SOME EXAMPLES FOR SCHIFF BASE METAL COMPLEXES TO REFLECT THEIR CATALYTIC ACTIVITIES

Barbaros AKKURT, Altuğ Mert SEVİM 81

CHAPTER 7

THEORETICAL INVESTIGATION OF PLATINUM ANALOGUES USED IN CHEMOTHERAPY TREATMEN

Murat AYHAN 105

Chapter 1

TIMELIKE INCLINED CURVES AND B_2-SLANT HELICES IN R_2^4

Müslüm Aykut AKGÜN [1]

1 Department of Mathematics, Technical Sciences High School, Adiyaman University, TURKEY
E-mail:muslumakgun@adiyaman.edu.tr

1 Preliminaries

The Semi-Euclidean space R_2^4 is the standart vector space equipped with an indefinite flat metric $\langle , \rangle$ given by

$$\langle , \rangle = dx_1^2 + dx_2^2 - dx_3^2 - dx_4^2$$

where (x_1, x_2, x_3, x_4) is a rectangular coordinate system of R_2^4. A vector v in R_2^4 is called a spacelike, timelike or null(lightlike) if respectively hold $\langle v, v\rangle > 0$, $\langle v, v\rangle < 0$ or $\langle v, v\rangle = 0$ and $v \neq 0 = (0,0,0,0)$. The norm of a vector v is given by $\| v \| = \sqrt{|\langle v, v\rangle|}$. Two vectors v and w are said to be orthogonal if $\langle v, w\rangle = 0$.[9]

An arbitrary curve $\alpha: I \to R_2^4$ can locally be spacelike, timelike or null if respectively all of its velocity vectors $\alpha'(s)$ are spacelike, timelike or null.

Let $\{T(s), N(s), B_1(s), B_2(s)\}$ be the moving Frenet frame along the curve $\alpha(s)$ in R_2^4. Then T, N, B_1, B_2 are the tangent, the principal normal, the first binormal and the second binormal fields respectively and let $\nabla_T T$ is spacelike.

Let α be a timelike curve in R_2^4, parametrized by arclength function of s. The following case occur for the timelike curve α. Let the vector N is spacelike, B_1 and B_2 be null. In this case there exists only one Frenet frame $\{T, N, B_1, B_2\}$ for which $\alpha(s)$ is a timelike curve with Frenet equations

$$\begin{aligned} \nabla_T T &= k_1 N \\ \nabla_T N &= -k_1 T - k_2 B_1 \\ \nabla_T B_1 &= -k_2 N - k_3 B_2 \\ \nabla_T B_2 &= k_3 B_1 \end{aligned} \qquad (1)$$

where T, N, B_1 and B_2 are mutually orthogonal vectors satisfying the equations

$$\langle N,N\rangle = \langle B_1,B_2\rangle = 1,\quad \langle B_1,B_1\rangle = \langle B_2,B_2\rangle = 0,\quad \langle T,T\rangle = -1 \qquad (2)$$

Recall that the functions $k_1 = k_1(s)$, $k_2 = k_2(s)$ and $k_3 = k_3(s)$ are called the first, the second and the third curvature of the spacelike curve $\alpha(s)$, respectively and we will assume throughout this work that all the three curvatures satisfy $k_i(s) \neq 0,\ 1 \leq i \leq 3$.

2 Main Results

Let $\alpha(s)$ be a non-geodesic timelike curve in R_2^4 and let $\{T,N,B_1,B_2\}$ denotes the Frenet frame of the curve $\alpha(s)$. A timelike curve in R_2^4 is said to be an inclined curve if its tangent vector forms a constant angle with a constant vector U. From the definition of the inclined curve we can write

$$T.U = \eta cosh\theta \qquad (3)$$

where U is a timelike constant vector and $\eta = \mp 1$. Differentiating both sides of this equations we have

$$k_1 NU = 0 \qquad (4)$$

Thus we arrive $N \perp U$. Considering this we can compose U as

$$U = u_1 T + u_2 B_1 + u_3 B_2 \qquad (5)$$

where $u_i,\ 1 \leq i \leq 3$ are arbitrary functions. Differentiating (5) and considering Frenet equations, we have

$$0 = u'_1 T + (u_1 k_1(s) - u_2 k_2(s))N + (u_3 k_3(s) + u'_2)B_1 + (u'_3 - u_2 k_3(s))B_2 \qquad (6)$$

From (6) we find the equations

$$\begin{cases} u'_1 = 0 \\ u_1 k_1(s) - u_2 k_2(s) = 0 \\ u_3 k_3(s) + u'_2 = 0 \\ u'_3 - u_2 k_3(s) = 0 \end{cases} \qquad (7)$$

By using the equations above we have

$$u_1 = c = cons, \tag{8}$$

$$u_2 = c\frac{k_1(s)}{k_2(s)} = \frac{1}{k_3(s)}\frac{du_3}{ds} \tag{9}$$

and

$$u_3 = -\frac{c}{k_3(s)}\frac{d}{ds}\frac{k_1(s)}{k_2(s)} \tag{10}$$

From (7) and (10) we have

$$\frac{du_2}{ds} = -k_3(s)u_3 \tag{11}$$

Differentiating u_2 we have

$$\frac{d}{ds}\left(-\frac{1}{k_3(s)}\frac{du_3}{ds}\right) = -\frac{d}{ds}(c^2u_2) \tag{12}$$

From (7)we find

$$\frac{d}{ds}\left(\frac{1}{k_3(s)}\frac{du_3}{ds}\right) = -k_3(s)u_3 \tag{13}$$

By a direct computation we have the differential equation

$$\frac{d}{ds}\left(\frac{1}{k_3(s)}\frac{du_3}{ds}\right) + k_3(s)u_3 = 0 \tag{14}$$

By using exchange variable $t = \int_0^s k_3(s)ds$ in (14) we find

$$\frac{d^2u_3}{dt^2} + u_3 = 0 \tag{15}$$

The general solution of (15) is

$$u_3 = c_1 cost + c_2 sint \tag{16}$$

where $c_1, c_2 \in R$. Replacing variable $t = \int_0^s k_1(s)ds$ in (16) we have

$$u_3 = -\frac{c}{k_3(s)}\frac{d}{ds}\left(\frac{k_1(s)}{k_2(s)}\right) = c_1 cos\left(\int_0^s k_3(s)ds\right) + c_2 sin\left(\int_0^s k_3(s)ds\right) \tag{17}$$

Considering equation (7) we have

$$u_2 = c\frac{k_1(s)}{k_2(s)} = c_1 sin(\int_0^s k_3(s)ds) - c_2 cos(\int_0^s k_3(s)ds) \quad (18)$$

From the equations above we find

$$c_1 = -\frac{c}{k_3(s)}\frac{d}{ds}(\frac{k_1(s)}{k_2(s)})cos(\int_0^s k_3(s)ds) + c\frac{k_1(s)}{k_2(s)}sin(\int_0^s k_3(s)ds) \quad (19)$$

and

$$c_2 = -c\frac{k_1(s)}{k_2(s)}cos(\int_0^s k_3(s)ds) - \frac{c}{k_3(s)}\frac{d}{ds}(\frac{k_1(s)}{k_2(s)})sin(\int_0^s k_3(s)ds) \quad (20)$$

By taking $A_1 = c_1 + c_2$ and $A_2 = c_1 - c_2$, if we calculate $c_1^2 + c_2^2$ we find

$$c^2(\frac{k_1(s)}{k_2(s)})^2 + \frac{c^2}{k_3^2(s)}[\frac{d}{ds}(\frac{k_1(s)}{k_2(s)})]^2 = cons. \quad (21)$$

or

$$(\frac{k_1(s)}{k_2(s)})^2 + \frac{1}{k_3^2(s)}[\frac{d}{ds}(\frac{k_1(s)}{k_2(s)})]^2 = cons. \quad (22)$$

Conversely, let us consider vector given by

$$U = \{T + \frac{k_1(s)}{k_2(s)}B_1 - \frac{1}{k_3(s)}\frac{d}{ds}(\frac{k_1(s)}{k_2(s)})B_2\}\eta cosh\theta \quad (23)$$

Differentiating vector U and considering differential equation of (23) we obtain

$$\frac{dU}{ds} = 0$$

Thus U is a constant vector and so the curve $\alpha(s)$ is an inclined curve in R_2^4. So we have the following theorem.

Theorem 2.1 *Let $\alpha = \alpha(s)$ be a timelike curve in R_2^4. α is an inclined curve if and only if*

$$(\frac{k_1(s)}{k_2(s)})^2 + \frac{1}{k_3^2(s)}\{\frac{d}{ds}(\frac{k_1(s)}{k_2(s)})\}^2 = cons. \quad (24)$$

Corollary 2.2 *Let $\alpha = \alpha(s)$ be a timelike curve in R_2^4. α is an inclined curve if and only if*

$$k_3(s)\frac{k_1(s)}{k_2(s)} + \frac{d}{ds}\left[\frac{1}{k_3(s)}\frac{d}{ds}\left(\frac{k_1(s)}{k_2(s)}\right)\right] = 0. \quad (25)$$

Now let us solve the equation (25) respect to $\frac{k_1}{k_2}$. If we use exchange variable $t = \int_0^s k_3(s)ds$ in (25) we have

$$\frac{d^2}{dt^2}\left(\frac{k_1}{k_2}\right) + \left(\frac{k_1}{k_2}\right) = 0. \quad (26)$$

So we arrive

$$\frac{k_1}{k_2} = W_1 cos\int_0^s k_3(s)ds + W_2 sin\int_0^s k_3(s)ds. \quad (27)$$

where W_1 and W_2 are real numbers.

Now we will give a different characterization for inclined curves. Let α be an inclined curve in R_2^4. By differentiaing (24) with respect to s we get

$$\left(\frac{k_1}{k_2}\right)\left(\frac{k_1}{k_2}\right)' + \frac{1}{k_3}\left(\frac{k_1}{k_2}\right)'\left[\left(\frac{1}{k_3}\right)\left(\frac{k_1}{k_2}\right)'\right]' = 0 \quad (28)$$

and hence

$$\frac{1}{k_3}\left(\frac{k_1}{k_2}\right)' = -\frac{\left(\frac{k_1}{k_2}\right)\left(\frac{k_1}{k_2}\right)'}{\left[\left(\frac{1}{k_3}\right)\left(\frac{k_1}{k_2}\right)'\right]'} \quad (29)$$

If we define a function $f(s)$ as

$$f(s) = -\frac{\left(\frac{k_1}{k_2}\right)\left(\frac{k_1}{k_2}\right)'}{\left[\left(\frac{1}{k_3}\right)\left(\frac{k_1}{k_2}\right)'\right]'} \quad (30)$$

then

$$f(s) = -\frac{1}{k_3(s)}\left(\frac{k_1}{k_2}\right)' = W_1 sin\int_0^s k_3(s)ds - W_2 cos\int_0^s k_3(s)ds. \quad (31)$$

By using (27) and (30) we have

$$f'(s) = -\frac{k_1 k_3}{k_2}. \quad (32)$$

Conversely, consider the function

$$f(s) = -\frac{1}{k_3}(\frac{k_1}{k_2})' = W_1 sin \int_0^s k_3(s)ds - W_2 cos \int_0^s k_3(s)ds$$

and assume that $f'(s) = -\frac{k_1 k_3}{k_2}$. We compute

$$\frac{d}{ds}[(\frac{k_1(s)}{k_2(s)})^2 + \frac{1}{k_3^2(s)}\{(\frac{k_1(s)}{k_2(s)})'\}^2] = \frac{d}{ds}[\frac{1}{k_3^2}(f'(s))^2 + f^2(s)] := \varphi(s) \quad (33)$$

As $f(s)f'(s) = -(\frac{k_1}{k_2})(\frac{k_1}{k_2})'$ and $f''(s) = -k'_3(\frac{k_1}{k_2}) - k_3(\frac{k_1}{k_2})'$ we obtain

$$f'(s)f''(s) = k_3 k'_3(\frac{k_1}{k_2})^2 + k_3^2(\frac{k_1}{k_2})(\frac{k_1}{k_2})'. \quad (34)$$

As consequence of above computations

$$\varphi(s) = 2(ff' + \frac{f'f''}{k_3^2} - \frac{(f')^2 k'_3}{k_3^3}) = 0 \quad (35)$$

that is the function $(\frac{k_1(s)}{k_2(s)})^2 + \frac{1}{k_3^2(s)}\{(\frac{k_1(s)}{k_2(s)})'\}^2$ is constant. Therefore we have the following theorem.

Theorem 2.3 *Let α be a unit speed timelike curve in R_2^4. Then α is an inclined curve if and only if the function $f(s) = -\frac{1}{k_3(s)}(\frac{k_1}{k_2})' = W_1 sin \int_0^s k_3(s)ds - W_2 cos \int_0^s k_3(s)ds$ satisfies $f'(s) = -\frac{k_1 k_3}{k_2}$ where k_1, k_2 and k_3 are the curvatures of α.*

Now let $\alpha(s)$ be a timelike curve in R_2^4 and let $\{T, N, B_1, B_2\}$ denotes the Frenet frame of the curve $\alpha(s)$. We call $\alpha(s)$ as timelike B_2-slant helix if its second binormal vector makes a constant angle with a fixed direction in a vector U. From the definition of the B_2-slant helix we can write

$B_2.U = cosh\vartheta$

where U is a spacelike constant vector. Differentiating both sides of this equations we have

$k_3 B_1 . U = 0$

Since $k_3 \neq 0$ we arrive $B_1 \perp U$. Considering this we can compose U as

$$U = u_1 T + u_2 N + u_3 B_2 \tag{36}$$

where u_i, $1 \leq i \leq 3$ are arbitrary functions. Differentiating (36) and considering Frenet equations, we have

$$0 = (u'_1 - u_2 k_1)T + (u_1 k_1(s) + u'_2)N + (u_2 k_2(s) - u_3 k_3(s))B_1 + u'_3 B_2 \tag{37}$$

From (37) we find the equations

$$\begin{cases} u'_1 - u_2 k_1 = 0 \\ u_1 k_1(s) + u'_2 = 0 \\ -u_2 k_2(s) + u_3 k_3(s) = 0 \\ u'_3 = 0 \end{cases} \tag{38}$$

By using the equations above we have $u_3 = c = cons$,

$$u_2 = c\frac{k_3(s)}{k_2(s)} = \frac{1}{k_1(s)}\frac{du_1}{ds}. \tag{39}$$

and

$$u_1 = -\frac{c}{k_1(s)}\frac{d}{ds}\frac{k_3(s)}{k_2(s)}. \tag{40}$$

From (38) and (40) we have

$$\frac{du_1}{ds} = k_1(s)u_2. \tag{41}$$

Differentiating u_1 we have

$$\frac{d}{ds}\left(-\frac{1}{k_1(s)}\frac{du_2}{ds}\right) = k_1(s)u_2. \tag{42}$$

By a direct computation we have the differential equation

$$\frac{d}{ds}\left(\frac{1}{k_1(s)}\frac{du_2}{ds}\right) + k_1(s)u_2 = 0. \tag{43}$$

By using exchange variable $t = \int_0^s k_1(s)ds$ in (43) we find

$$\frac{d^2u_2}{dt^2} + u_2 = 0. \tag{44}$$

The general solution of (44) is

$$u_2 = m_1 cost + m_2 sint \tag{45}$$

where $m_1, m_2 \in R$. Replacing variable $t = \int_0^s k_1(s)ds$ in (45) we have

$$u_2 = c\frac{k_3(s)}{k_2(s)} = m_1 cos(\int_0^s k_1(s)ds) + m_2 sin(\int_0^s k_1(s)ds). \tag{46}$$

Considering equation (38) we have

$$u_1 = -\frac{c}{k_1(s)}\frac{d}{ds}(\frac{k_3(s)}{k_2(s)}) = -m_1 sin(\int_0^s k_1(s)ds) + m_2 cos(\int_0^s k_1(s)ds). \tag{47}$$

From the equations above we find

$$m_1 = -\frac{c}{k_1(s)}\frac{d}{ds}(\frac{k_3(s)}{k_2(s)})cos(\int_0^s k_1(s)ds) + c\frac{k_3(s)}{k_2(s)}sin(\int_0^s k_1(s)ds) \tag{48}$$

and

$$m_2 = c\frac{k_3(s)}{k_2(s)}cos(\int_0^s k_1(s)ds) - \frac{c}{k_1(s)}\frac{d}{ds}(\frac{k_3(s)}{k_2(s)})sin(\int_0^s k_1(s)ds). \tag{49}$$

By taking $B_1 = m_1 + m_2$ and $B_2 = m_1 - m_2$, if we calculate $B_1^2 + B_2^2$ we find

$$c^2(\frac{k_3(s)}{k_2(s)})^2 + \frac{c^2}{k_1^2(s)}[\frac{d}{ds}(\frac{k_3(s)}{k_2(s)})]^2 = constant \tag{50}$$

or

$$(\frac{k_3(s)}{k_2(s)})^2 + \frac{1}{k_1^2(s)}[\frac{d}{ds}(\frac{k_3(s)}{k_2(s)})]^2 = constant. \tag{51}$$

Conversely, let us consider vector given by

$$U = \{-\frac{1}{k_1(s)}\frac{d}{ds}(\frac{k_3(s)}{k_2(s)})T + \frac{k_3(s)}{k_2(s)}N + B_2\}cosh\vartheta. \quad (52)$$

Differentiating vector U and considering differential equation of (50) we obtain $\frac{dU}{ds} = 0$.

Thus U is a constant vector and so the curve $\alpha(s)$ is a timelike B_2 slant helix in R_2^4. As a result we can give the following theorem.

Theorem 2.4 *Let $\alpha = \alpha(s)$ be a timelike curve in R_2^4. α is a timelike B_2 slant helix if and only if*

$$(\frac{k_3(s)}{k_2(s)})^2 + \frac{1}{k_1^2(s)}\{\frac{d}{ds}(\frac{k_3(s)}{k_2(s)})\}^2 = constant. \quad (53)$$

Corollary 2.5 *Let $\alpha = \alpha(s)$ be a timelike curve in R_2^4. α is a B_2-slant helix if and only if*

$$k_1(s)\frac{k_3(s)}{k_2(s)} - \frac{d}{ds}[\frac{1}{k_1(s)}\frac{d}{ds}(\frac{k_3(s)}{k_2(s)})] = 0. \quad (54)$$

Now let us solve the equation (54) respect to $\frac{k_3}{k_2}$. If we use exchange variable $t = \int_0^s k_1(s)ds$ in (54) we have

$$\frac{d^2}{dt^2}(\frac{k_3}{k_2}) + (\frac{k_3}{k_2}) = 0. \quad (55)$$

So we arrive

$$\frac{k_3}{k_2} = L_1 cos\int_0^s k_1(s)ds + L_2 sin\int_0^s k_1(s)ds. \quad (56)$$

where L_1 and L_2 are real numbers.

Now we will give a different characterization for B_2-slant helices. Let α be a timelike B_2-slant helix in R_2^4. By differentiaing (53) with respect to s we get

$$(\frac{k_3}{k_2})(\frac{k_3}{k_2})' + \frac{1}{k_1}(\frac{k_3}{k_2})'[(\frac{1}{k_1})(\frac{k_3}{k_2})']' = 0 \quad (57)$$

and hence

$$\frac{1}{k_1}\left(\frac{k_3}{k_2}\right)' = -\frac{\left(\frac{k_3}{k_2}\right)\left(\frac{k_3}{k_2}\right)'}{\left[\left(\frac{1}{k_1}\right)\left(\frac{k_3}{k_2}\right)'\right]'} \tag{58}$$

If we define a function $f(s)$ as

$$f(s) = -\frac{\left(\frac{k_3}{k_2}\right)\left(\frac{k_3}{k_2}\right)'}{\left[\left(\frac{1}{k_1}\right)\left(\frac{k_3}{k_2}\right)'\right]'} \tag{59}$$

then

$$f(s) = -\frac{1}{k_1(s)}\left(\frac{k_3}{k_2}\right)' = L_1 sin\int_0^s k_1(s)ds - L_2 cos\int_0^s k_1(s)ds. \tag{60}$$

By using (57) and (60) we have

$$f'(s) = -\frac{k_1 k_3}{k_2}. \tag{61}$$

Conversely, consider the function

$$f(s) = -\frac{1}{k_1}\left(\frac{k_3}{k_2}\right)' = L_1 sin\int_0^s k_1(s)ds - L_2 cos\int_0^s k_1(s)ds$$

and assume that $f'(s) = -\frac{k_1 k_3}{k_2}$. We compute

$$\frac{d}{ds}\left[\left(\frac{k_3(s)}{k_2(s)}\right)^2 + \frac{1}{k_1^2(s)}\left\{\left(\frac{k_3(s)}{k_2(s)}\right)'\right\}^2\right] = \frac{d}{ds}\left[\frac{1}{k_1^2}(f'(s))^2 + f^2(s)\right] := \varphi(s) \tag{62}$$

As $f(s)f'(s) = -\left(\frac{k_3}{k_2}\right)\left(\frac{k_3}{k_2}\right)'$ and $f''(s) = -k'_1\left(\frac{k_3}{k_2}\right) - k_1\left(\frac{k_3}{k_2}\right)'$ we obtain

$$f'(s)f''(s) = k_1 k'_1\left(\frac{k_3}{k_2}\right)^2 + k_1^2\left(\frac{k_3}{k_2}\right)\left(\frac{k_3}{k_2}\right)'. \tag{63}$$

As consequence of above computations

$$\varphi(s) = 2\left(ff' + \frac{f'f''}{k_1^2} - \frac{(f')^2 k'_1}{k_1^3}\right) = 0 \tag{64}$$

that is the function $\left(\frac{k_3(s)}{k_2(s)}\right)^2 + \frac{1}{k_1^2(s)}\left\{\left(\frac{k_3(s)}{k_2(s)}\right)'\right\}^2$ is constant. Therefore we have the following theorem.

Theorem 2.6 *Let α be a unit speed timelike curve in R_2^4. Then α is a B_2 -slant helix if and only if the function $f(s) = -\frac{1}{k_1(s)}\left(\frac{k_3}{k_2}\right)' = L_1 sin\int_0^s k_1(s)ds - L_2 cos\int_0^s k_1(s)ds$ satisfies $f'(s) = -\frac{k_1 k_3}{k_2}$, where k_1, k_2 and k_3 are the curvatures of α.*

References

[1] A. Fernandez, A. Gimenez, and P. Lucas, Null helices in Lorentzian space forms, Int. J. Mod. Phys. A. 16 (2001), 4845-4863.

[2] A. Magden, On the Curves of Constant Slope, YTU Fen Bilimleri Dergisi, 4,(1993), 103-109.

[3] A. T. Ali, R. Lopez, Timelike B_2-slant Helices in Minkowski space E_1^4, arXiv, 0810, 1460v1[math.DG], 8 Oct 2008.

[4] A. T. Ali, R. Lopez, Slant Helices in Euclidean 4-space E^4, arXiv, 0901, 3324v1[math.DG], 21 Jan 2009.

[5] C. Camci, K. Ilarslan, L. Kula, H.H. HacisalihoÄŸlu, Harmonic Curvatures and Generalized Helices in E^n, Chaos,Solitions and Fractals 40 (2009), 2590-2596.

[6] H. Kocayigit, M. Onder, Timelike Curves of Constant Slope in Minkowski Space E_1^4, BU/JST, 1, (2007), 311-318.

[7] H. Kocayigit, M. Onder, M. Kazaz, Spacelike Helices in Minkowski 4-Space E_1^4, Anna Del Universita Di Ferrera, (2010), Vol.56, IS 2, pp 335-343.

[8] H. Kocayigit, M. Onder, M. Kazaz, Spacelike B_2-slant Helices in Minkowski 4-Space E_1^4, Int. Journal of Physical Sciences, 5(5)(2010), 470-475.

[9] İlarslan, K., Nesovic, E., Spacelike and timelike normal curves, Publications de l'Institut Mathematique, 85(99), 111-118, 2009.

[10] L. Kula, Y. Yayli, On Slant Helix and its Spherical Indicatrix, Appl. Math. Comp., 169, (2005), 600-607.

[11] S. Izumiya, N. Takeuchi, New Special Curves and Developable Surfaces, Turk. J. Math., 28(2004), 531-537.

[12] S. Keles, S. Y. Perktas and E. Kilic, Biharmonic Curves in LP-Sasakian Manifolds, Bulletin of the Malasyian Mathematical Society, (2) 33(2), 2010, 325-344

[13] S. Yilmaz, M. Turgut, On the Characterizations of Inclined Curves in Minkowski Spacetime E_1^4, Int. Math. Forum, 3, (2008), no.16, 783-792.

Chapter 2

THE BIG BANG

E.Nihal ERCAN [1]

1 Boğaziçi Üniversity , Physics Department

The Big Bang is the cosmological model that expresses the evolution of the universe, arguing that the universe originated from an extremely dense and hot spot about 13.8 billion years ago. The basic idea of the model is that the universe is expanding from a hot and dense initial state at a certain time in the past.

First proposed by Alexander Friedmann and Georges Lemaître in the 1920s, this theory, which assumes that the universe had a beginning, has gained wide acceptance among scientists, especially physicists, as it is supported by many evidence. This model is based on the general theory of relativity and the first Big Bang model was prepared by Alexander Friedmann. The model was later defended by George Gamow and other physicists.

After Edwin Hubble discovered redshift in distant galaxies in 1929, this observation was thought to be evidence that very distant galaxies and galaxy clusters have apparent velocity relative to position. Those moving the fastest in sight are the furthest. They should have been together in the past, as the distance between galaxy clusters has increased.

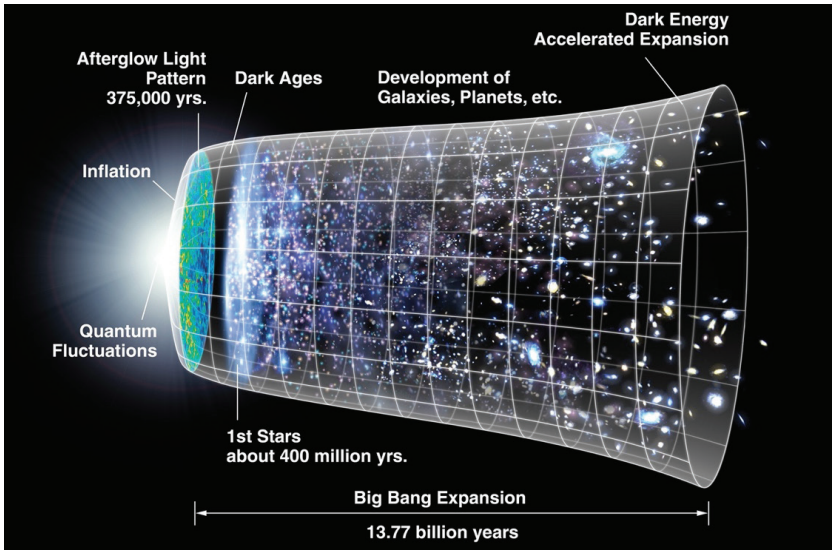

Figure 1. *Credict see reference[1*]*

According to the Big Bang model, the universe was in an extremely dense and hot state in its original state before expanding. The abundance of light elements in the cosmos we observe today is consistent with the results of the first nucleosynthesis accepted by the Big Bang model, and coincides with predictions that light elements were formed during nuclear processes in the first minutes of rapid expansion and cooling. According to these estimates, the ratio of hydrogen and helium in the universe matches the ratio of hydrogen and helium that, according to theoretical calculations,

should have remained from the Big Bang. If the universe had not had a beginning, the hydrogen in the universe would have burned completely and turned into helium. In these first minutes, the cooling universe must have allowed the formation of certain amounts of hydrogen, helium and lithium, allowing some nuclei to form.

The term Big Bang was first used by British physicist Fred Hoyle in 1949. Hoyle is a scientist who contributed to how light elements can form some heavy elements.

Figure 2. *Credict: see reference[2*]*

The Big Bang model is basically based on Albert Einstein's theory of general relativity and the cosmological principle. The general theory of relativity explains the gravitational interactions of all bodies without error. The discovery of general relativity by Albert Einstein in 1915 is considered the beginning of modern cosmology, which made it possible to describe the gradual evolution of the universe and the physical system of the universe.

Einstein was also the first scientist to use general relativity in this way when describing space in its entirety, proposing a solution stemming from general relativity. This model gave birth to a new concept at Einstein's initiative at that time: the cosmological principle. According to the cosmological principle, man does not have a privileged position in the universe, the universe is homogeneous and isotropic. In other words, the universe is homogeneous in space, regardless of the place and direction from which it is viewed; More precisely, the general appearance of the universe does not depend on the observer's position and the direction he is looking. This was considered a very ambitious hypothesis at the time. Because while discussing whether there were objects outside the Milky Way at that time, no convincing observation could provide an opportunity to confirm the existence of objects outside of the Milky Way. The cosmological principle, in explaining the macro properties of the universe, implies that the universe has no boundaries, so the Big Bang does not occur at a specific point in the vacuum, but simultaneously throughout the entire

space. The universe is homogeneous and isotropic. These two assumptions made it possible to calculate the history of the universe after Planck's time. Scientists are still trying to pinpoint important events that occurred before Planck's time.

Einstein concluded in his calculations that he made with his general relativity theory in 1915 that the universe could not be stationary. But back then the general acceptance was that the universe was static; so Einstein added the cosmological constant factor to his equations to fix his result and changed his first solution in his equations, but later developments showed he was wrong. For example, in the 1920s, Edwin Hubble discovered that nebulae are out of our galaxy and are moving away from our galaxy, and their speed of motion is proportional to their distance from our galaxy.

Before Hubble's discovery, many physicists like Willem de Sitter, Georges Lemaître, and Alexandre Friedmann had come up with other solutions to describe a universe expansion. His models were immediately accepted when the expansion of the universe was discovered. Thus, a universe that has been expanding for billions of years has been defined.

OBSERVATIONAL EVIDENCE AND COSMOLOGICAL BACKGROUND

Two conclusive observational evidence confirms the Big Bang model. The discovery of the cosmic microwave background radiation, which can be called the remnant of the hot age of the history of the universe, and the measurement of the release of light elements, that is, the measurement of the release of different isotopes of hydrogen, helium and lithium formed during the first hot phase.

These two observations took place in the early second half of the 20th century. Thus, the Big Bang became established in cosmology as the model that defines the observable universe. In addition to the almost perfect coincidence of this model with cosmological observations, other evidence began to emerge to confirm the model.

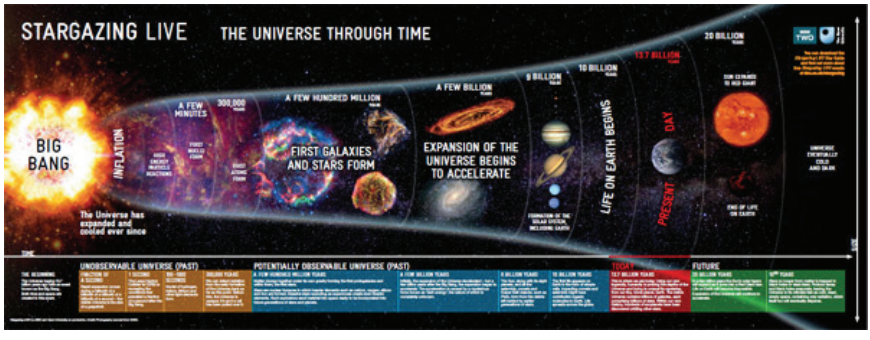

Figure 3. *Credict : see reference [3*]*

Cosmic Microwave Background Radiation:

The expansion shows that the universe was denser in the past. Georges Lemaître spoke for the first time in 1934 about the possibility of the universe getting warmer; however, the real discovery of this began only since the 1940s. George Gamov suggested that, similar to the redshift in radiation of distant astrophysical bodies, the universe should be filled with a radiation that loses energy with its expansion. Gamow actually understood that the strong densities in the primitive universe must have allowed a thermal equilibrium to be established between the atoms and then the existence of the radiation emitted by these atoms. Gamow improved Lemaitre's calculations in the 1940s and put forward a thesis based on the Big Bang. There had to be a certain amount of radiation left over from the Big Bang. Also, this luminosity must be uniform throughout the universe. This radiation is supposed to have an intensity equal to the density of the universe, and therefore this radiation must still be present even if its intensity is extremely reduced. Gamow, along with Ralph Alpher and Robert Herman, was the first to understand that the current heat of this radiation can be calculated from the age of the universe, the density of matter, and the release of helium. Gamow's discovery was led by Penzias and Wilson in their observations in the 1960s to measure obscure radio waves from the outer parts of the Milky Way. Penzias and Wilson also received the 1978 Nobel Prize in Physics for detecting radiation from all over the sky. The cosmic background, discovered in 1965, is one of the clearest evidence of the Big Bang. Since the discovery of the powerful nuclear force and the realization that it is the energy source of the stars, the question of explaining the release of various chemical elements in the universe has arisen. Around the 1950s, this oscillation, stellar nucleosynthesis and initial nucleosynthesis were created by evaluating the different processes suggested by two different views. Big Bang supporters were aware of the opinion that all elements, from helium to uranium, were produced during the initial hot phase of the universe. The current understanding is based on both hypotheses. Accordingly, helium and lithium were indeed produced during the initial nucleosynthesis. According to the Big Bang model, their oscillations are tightly linked to a single parameter that has been maintained since the first nucleosynthesis. At the same time, an increase in helium splitting is observed inside nearby galaxies, which is evidence of stellar nucleosynthesis.

The Evolutionary picture of Galaxies:

Figure 4: *Credict see reference***[***4*]*** *The "Hubble Ultra Deep Field" picture of space.*

The Big Bang model assumes that the homogeneous universe was more homogeneous in the past than it is today. His proof was provided by observing the radiating cosmic background.

Cosmic background radiation shows an extraordinary isotropy. In this case, the astrophysical structures did not exist in the early period of the Big Bang, they must have formed gradually later. The process of origin of their formation has been known since the work of James Jeans in 1902; this process is known as Jeans Indecision. According to the Big Bang model, the galaxies we observe today formed later, and in the past these early galaxies were not very similar to the neighboring galaxies we observe in our immediate environment. Although the speed of light is an enormous speed, it is a certain speed, so we only need to look at distant celestial bodies to understand what the universe was like in the past. Observations of distant galaxies that show redshift properties according to Hubble's Law, indeed, show that the first galaxies were sufficiently different from the second. At that time there was more intergalactic interaction; Few giant galaxies appeared after the intergalactic merger events.

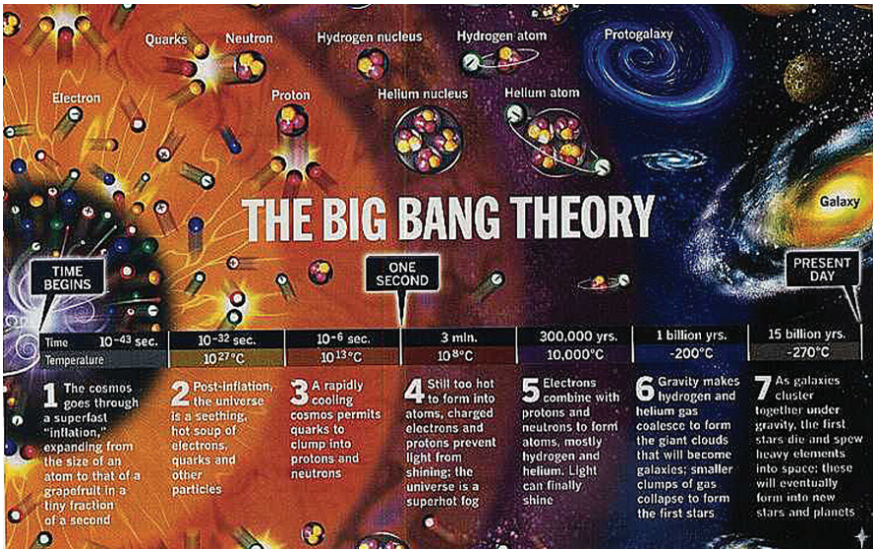

Figure 5: *Credict see reference [5*]*

Our universe is extremely less dense and cold in the present than it was in the past. Although there are some hot astrophysical objects, the radiation to which the universe is now exposed is very weak. The low density of stars in the universe plays a big role in this phenomenon, that is, the distance between a star at any point in the universe and the closest star to it is extremely large. Astronomical observation shows that stars and galaxies formed very early in the Big Bang. 300,000 years after the Big Bang era, the universe was a thousand times hotter and a billion times denser than it is now, while stars and galaxies did not yet exist. This is the period when the density of the universe allows light to spread. Previously, the main obstacle to the propagation of light was free electrons. During its cooling, these free electrons in the universe come together in atomic nuclei to form atoms. That is why this period is called the unification period. At the same time, since it is the period when light begins to spread, this period is also referred to as the separation period of matter and radiation. The radiation that we call the cosmic background radiation is the radiation that has continued from this period to the present day. A clearer map of the universe was drawn 380,000 years after the Big Bang, according to data from NASA's WMAP satellite in 2006. According to these results, it was determined that 12% of the universe consists of atoms, 15% of photons, 10% of neutrons and 63% of dark matter. These results also supported the relics of the period of unification.

300,000 years after the first period of the Big Bang, the universe consisted of electrons and atomic nuclei plasma. Atomic nuclei cannot exist when the temperature is high enough; In this case, a mixture of protons,

neutrons and electrons can be mentioned. The atomic nuclei formed in this phase, which started about one second after the start of the Big Bang and lasted about three minutes, are only hydrogen, helium and lithium nuclei. Therefore, this period is called first nucleosynthesis. Beyond a certain high temperature, interactions between electrons and photons can spontaneously create electron-positron pairs. Although these couples can disappear spontaneously, they are constantly recreated as the temperature exceeds a certain threshold. As the temperature decreases below this threshold, almost all of these pairs disappear as photons, leaving the excess electrons they formed. Heat was sufficient for the various interactions of electrons, photons and neutrinos, and these three types were in thermal equilibrium. When the universe cools, although electrons and photons continue to interact, neutrinos interact. This period is also the period when neutrinos leave. The existence of neutrinos is also indirectly confirmed by the equations of the first nucleosynthesis. During the next evolution of the universe, matter and antimatter perished in equal quantities, leaving behind the lightest excess of matter formed. Since this ordinary substance consists of particles called baryon, the stage in which the excess of the substance in question occurs is called baryogenesis. Little is known about this stage or process. For example, the temperature rating that occurs during this event varies according to the Big Bang models. A growing number of indications suggest that weak and strong electromagnetic forces are simply different aspects of a single interaction . This situation is now generally included in the scope of the Grand Unification Theory. It is thought that this interaction or force occurs at very high temperatures. So probably the universe must have gone through a phase in which the GUT found an area of application. Although its nature is still unknown, this stage must have been at the origin of baryogenesis and possibly dark matter. The universe grew considerably in a very short period of time. This phenomenon is called cosmic inflation. The Big Bang theory brought new issues to cosmology. It was assumed that the cause of the first sudden, rapid expansion initiated a process that led to the universe becoming homogeneous and isotropic. The inventor of the cosmic inflation concept was Alan Guth, who was the first to propose a scenario to describe such a process. Englert and Starobinsky are also known as other figures who worked on some of the problematic parts of this issue during the same period. He later showed that cosmic inflation, which contains traces of great astrophysical structures, will not only provide an opportunity to explain the homogeneity of the universe, but also reveal why the universe contains some contradictory phenomena. The history of the inflation must have taken place in an extremely hot and early period adjacent to the Great United Age and the Planck Age. The fact that the inflation scenario was in harmony with the observations made it a leading role in all matters related to the subject. The inflation phase is

an extremely rapid expansion of the universe over a period of time. This universe, whose density decreased due to expansion, was filled with a very homogeneous form of energy. This energy then very quickly turned into particles that could be set to interact and heat. These two phases that end inflation are called the pre-warming phase in terms of the explosive creation of the particles and the warming phase in terms of the thermalization of the particles. At temperatures such as the Planck heat, a field is entered where the current theories of physics no longer apply. This is an area where there will be a correction in the general theory of relativity, where the concepts of quantum mechanics are valid. Although it has not been put forward yet, a quantum theory of gravity, which may arise from string theory, which is still under development, will provide room for various speculations about the universe in the so-called Planck Age. Many authors such as Stephen Hawking have proposed various ways of research that will allow them to try to describe the universe in these periods. This area of research is today called quantum cosmology. The "cosmological standard model" is a logical consequence of the Big Bang view proposed in the first half of the 20th century. Its name is inspired by the standard model of particle physics. The cosmology standard model offers a definition of the universe that fits with the integrity of universe observations. It particularly emphasizes two points. The observable universe was born out of a dense and hot phase. A process during this phase enabled the region we could observe to be homogeneous, but also to show some exceptions. The current universe is full of many types of matter: photons, neutrinos, the particles that represent all kinds of electromagnetic radiation, the baryonic matter that make up the atoms, dark matter, and dark energy. Most of the astronomical observations now make use of these indispensable foundation stones when describing the universe as we know it. Cosmological research mainly aimed to describe these types of matter, their properties, and the accelerated expansion of the primeval universe. The three cornerstones of the cosmology standard model make it necessary to resort to physical phenomena not observed in the laboratory: Cosmic inflation, dark matter and dark energy.

Dark Matter:

Figure 6. *Credict see reference [6*]*

Various observations made in the 1970s and 1980s proved that there is not enough visible matter to explain the apparent effect of gravitational forces within and between galaxies. This determination naturally led to the conclusion that 90% of the matter in the universe consists of a type of matter that does not emit light or interact with normal baryonic matter. Dark matter, in short, is a type of matter that does not emit radiation or does not reflect electromagnetic rays directly enough to be detected. Evidence for the existence of dark matter is particularly in its gravitational effect on other matter.

Dark Energy: Observations showed that, according to supernova measurements, the expansion of the universe has accelerated since the universe reached half its current age. In explaining this acceleration, general relativity argued that some of the energy in the universe originated from an element with a large negative pressure. This element or energy is called dark energy today. The existence of dark energy is also understood in other ways. Negative pressure shows a kind of vacuum energy feature. But it can be said that the true nature of dark energy is a remnant of one of the Big Bang's great secrets. Although the energy density in matter decreases with the expansion of the universe, the density of dark energy remains constant. As a result, although matter has constituted a significant part of all the energy of the universe in the past and still constitutes a significant part, it is thought that in the distant future its contribution to the universe will decrease and dark energy will become more dominant.

When the Big Bang models were examined, it was seen that this type of model brought some problems with it. Before the changes were made, the plain Big Bang model did not seem very convincing; because it required the assumption of many physical quantities in extremely large and extremely

small quantities compared to conventional quantities. In other words, it seemed to require many parameters to be added to unexpected values in order to survive. In this case, the Big Bang, despite its success in explaining many observations, was a concept that posed many problems, but could not solve these problems itself, and therefore the solution it brought did not seem attractive. However, the scenarios added to the Big Bang models, especially the cosmic inflation scenario, managed to change the negative comments made in the early days of the theory. At first, there was no exact explanation for the homogeneous and isotropic nature of the universe. The reason why the universe evolved to the state we observe in our age was tried to be solved with the explanations of the operation based on the first conditions. In short, the discussion of how two extremely distant regions of the universe have the same characteristics, even though they were close to each other, did not have time to exchange any information in the past, is now called the horizon issue. Certain information about the state of the universe in the early period may have spread extremely rapidly throughout the universe. However, the obstacle to this solution is the special theory of relativity; The special theory of relativity proposes that nothing can move faster than light. However, although the expansion of the universe has been very rapid, the limits of special relativity may have been somewhat crossed. In fact, in such a case, the distance between the two regions of the universe may increase exponentially while the size of the observable universe remains constant. In other words, a region that was very small and homogeneous at the beginning has the opportunity to reach an extremely large size compared to the observable universe region. When this phase of constant rate of expansion is complete, the homogeneous region of the universe in which we are located may be considerably larger than what we have reached in our observations. Friedmann's equations show that such scenarios are possible, provided the existence of an atypical type of matter in the universe is acknowledged. Another issue encountered when examining the evolution of the universe is the question of the possible radius of curvature. General relativity reveals that if the distribution of matter in the universe is homogeneous, then the geometry of the universe depends on only one parameter, the spatial curvature. If the radius of curvature was greater than the size of the observable universe five billion years ago, it would have to be smaller than the size of the observable universe today, and its results should become visible. Since the curvature-related effects or consequences are still not visible, it can be said that the radius of curvature is significantly greater than the size of the observable universe during the nucleosynthesis period. This situation is called the flatness issue today. The radius of curvature is growing less rapidly than the size of the observable universe. However, if the law governing expansion is different from the law governing the expansion of a universe filled with ordinary matter, this

is no longer true. Assuming the presence of a type of material with non typical properties, the radius of curvature will grow faster than the size of the observable universe. If such an expansion phase happened in the past and lasted for a sufficiently long time, this can be explained by the fact that the radius of curvature is not measurable. Particle physics predicts that new particles gradually emerge during the cooling of the universe from its expansion. Some of these must have occurred during the process change, which is thought to have occurred in the primordial universe.

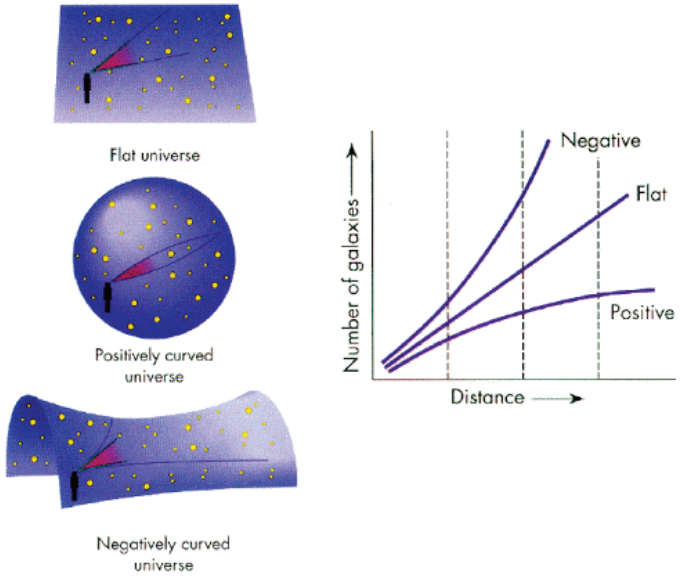

Figure 7. *Credict see reference [7*]*

These particles, some called monopoles or magnetic monopoles, had the property of being stable and had to be numerous and extremely heavy. If such particles had arisen, their contribution to the density of the universe should have been high. While particle physics predicts, the issue of such heavy particles, which have not been determined to actually exist because they have not been discovered, is called the monopoles issue. The magnetic monopoles issue can be solved with an accelerated expansion phase. This tends to reduce the density of all ordinary matter in the universe. In this case, however, a new issue arises: The accelerated expansion phase leaves behind a homogeneous, but materialless universe, as a spatial plane without bumps or troughs. The cosmic inflation proposed by Alan Guth in 1980s was a solution that solved all of these problems. An alternative solution to the cosmic inflation solution of monopoles, flatness, and horizon issues is presented by the Weyl curvature hypothesis.

Figure 8: *Credict see reference [8*]*

The observations show that the universe is homogeneous at large scales, but at the same time it contains deviations from homogeneity at small scales, ie it has the property of non-homogeneity. Today, it is known and explained how a small inhomogeneity in the distribution of matter under certain conditions grows and develops until it creates an important astrophysical body more dense than its environment. This is called the Jeans Indecision mechanism. Here, the first Big Bang models were insufficient to explain such turbulence or instability. Therefore, when the first Big Bang models were introduced, the issue of the formation of structures arose. The emergence of small escapes or deviations from homogeneity in the universe is due to the evolution undergoing to become the usual classical densities during the accelerated expansion phase.

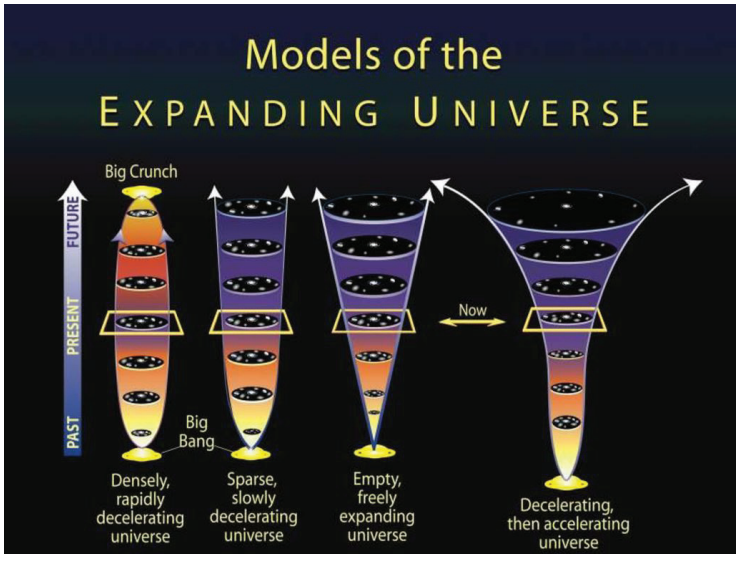

Figure 9. *Credict see reference [9*]*

Before the existence of dark energy was realized, cosmologists had devised two scenarios for the future of the universe. If the mass density of the universe was greater than the critical density, the universe would enter the process of collapse after reaching its maximum size. It would become denser and hotter and would complete this process in a state similar to its original state called the Great Crash. As an alternative to this scenario, if the density in the universe was equal to or below the critical density, the expansion would slow down but never stop. Star formation in interstellar gases would stop in all galaxies, and stars would turn into white dwarfs, neutron stars, and black holes. The collisions between them would result in gradual accumulations of mass, that is, the formation of larger masses and gradually becoming larger black holes. The average temperature of the universe would approach absolute zero. Also, if the proton remained unstable, baryonic matter would disappear, leaving behind only radiation and black holes. Eventually black holes would also disappear by emitting Hawking radiation. Thus, the entropy of the universe would climb to a point called the thermal death of the universe, from which no organized energy could save itself. Modern observations show that the present visible universe will gradually advance beyond our horizon. The next situation or the final result is unknown. The CDM model, the most advanced Big Bang model, accepts dark energy as a cosmological constant. This model assumes that only limited gravitational systems such as galaxies can stay together, so they will not escape thermal death either. Other explanations for dark energy, called phantom energy theories, suggest that eventually galaxy clusters, stars, planets and atoms will eventually separate by eternal expansion. The findings are continued to be obtained by making experiments with particle accelerators in high energy systems in the laboratory environment.

Therefore, one can conclude that during the first period of the Big Bang, the conditions prevailing in the observable universe region were the same everywhere. On the other hand, it is seen that material elements are rapidly moving away from each other due to the expansion of the universe. The term Big Bang was proposed as a term to express the intensity of this expansion movement. The Big Bang model is essentially based on two basic ideas: 1) the universality of physical laws, 2) the cosmological principle. The cosmological principle assumes that the universe is homogeneous and isotropic at macro scales. These ideas used to be hypotheses, but today they are supported by observations. Observational developments in cosmology provide a definite support for the Big Bang. The steady-state theory, which is the basic theory against the Big Bang, is almost completely rejected today because of its observations on cosmic background radiation, its inability to explain the release of light elements

and the evolution of galaxies. The Big Bang is actually a result of general relativity, which observations still fail to make a mistake. Therefore, for some, rejecting the Big Bang means rejecting general relativity. On the other hand, it is a fact that many periods or phenomena are still not well known. Although Big Bang models, which have aspects to be developed, are still in development, it has become difficult enough to discuss the general concept of the Big Bang. The Big Bang does not have a center or a special aspect. How the universe was in the past can only be understood by observing the distant regions of the universe. The farther a region in the universe can be observed, the more distant past can be detected in the history of the universe. But what can be observed today is not directly the early Big Bang itself, but the cosmic background radiation, the luminous reflection of this warm phase in the history of the universe.

I would like to thank Berzem Selçuk ,one of my undergraduate students, who participated in this review study with her hard work.

REFERENCES:

Akçay, Gürkan. "Büyük Patlama Kuramı Nedir?" Bilimfili. https://bilimfili.com/big-bang-buyuk-patlama-teorisi-nedir. August 2015.

Atkatz, David and Pagels, Heinz. (1982). Origin of the Universe as a quantum tunneling event. P*hys. Rev. D 25*. (pg. 2065-2073). American Physical Society. doi = 10.1103/PhysRevD.25.2065.

Bakırcı, Ç. Mert. "Büyük Patlama Nedir? Büyük Patlama Sırasında Neler Yaşandı?". Evrim Ağacı. https://evrimagaci.org/buyuk-patlama-nedir-buyuk-patlama-sirasinda-neler-yasandi-7758 . June 2019.

Bowers, Richard L. and Deeming, Terry. (1984). *Astrophysics.* Provided by the SAO/NASA Astrophysics Data System. https://ui.adsabs.harvard.edu/abs/1984astr.book.....B

Delia Perlov and Alex Vilenkin: *Cosmology for the Curious.* Springer, 2017

Dicke, R.H., & Peebles, P.J.E. Israel, W. (Ed.). (1979). The big bang cosmology - enigmas and nostrums. United Kingdom: University Press.

Ercan, E. Nihal. (2019). Galaksiler, 6. Bölüm içinde, *Astrofizik* (1. Basım) (s.41-51). Nobel Akademik Yayıncılık.

Ercan, E. Nihal. (2019). Galaksilerin Oluşumu, 8. Bölüm içinde, *Astrofizik* (1. Basım) (s.59-65). Nobel Akademik Yayıncılık.

Gamow, George. (1961). *The Creation of the Universe.* (rev.ed.). Dover Publications, Minela, NY.

Gary Steigman, "Neutrinos and Big Bang Nucleosynthesis", Advances in High Energy Physics, vol. 2012, Article ID 268321, 24 pages, 2012. https://doi.org/10.1155/2012/268321

Germann, Julia. (2016). Astronomy Workshop. Ch 11-15 from Backman and Seeds. [Powerpoint slides]. https://www.lamission.edu/learningcenter/docs/ssc/ASTRO_WS_11-15-Handout.pdf

Hoyle, F., Burbidge, G. and Narlikar, J. V.. (2000). From a static universe through the big bang towards reality. *A Different Approach to Cosmology*. Cambridge : Cambridge University Press.

Hoyle, Fred. (1981). The Big Bang in Astronomy. *New Scientist.* https://ui.adsabs.harvard.edu/abs/1981NewSc..92..521H.

Lang, Kenneth R.. (2006). Space, Time, Matter and Cosmology, inside 5th part, *Astrophysical Formulae Vol2.* (3rd enlarged and revised ed.) (pg. 228-269). Springer. Massachusetts, USA.

M. Gasperini, G. Veneziano, Pre-big-bang in string cosmology, Astroparticle Physics,

National School Observatory. "Big Bang". https://www.schoolsobservatory.org/learn/astro/cosmos/bigbang

Roberto Unger and Lee Smolin: *The Singular Universe and the Reality of Time.* Cambridge University Press, 2014.

Sean Carroll: *From Eternity to Here. The Quest for the Ultimate Theory of Time.* Dutton, 2010.

Seeds, Michael A. and Backman, D. (2011). *The Solar System* (7th ed.) (pg: 180-185, 396-414). Cengage: Cengage Learning.

Seeds, Michael A. and Backman, D. (2018). *Astro: Introduction to Astronomy* (3rd ed.) (pg:322-337). Cengage: Cengage Learning.

Singh, Shiv S. (2014). Origin of Universe. IJEAR Vol. 4, IssuE 1. ISSN : 2348-0033. CMJ University Shillong, Meghalaya, India.

Spier, Fred. (1996). From the Big Bang until Today. *The Structure of Big History.* Amsterdam University Press, Amsterdam.

The Universe: What is it; Big Bang Theory; Future. (2017). In *ScienceAid*. Retrieved Jan 23, 2021, from https://scienceaid.net/physics/space/universe.html

Turner, M. (2009). Orıgın Of The Unıverse. *Scientific American, 301*(3), 36-43. Retrieved January 23, 2021, from http://www.jstor.org/stable/26001524

Volume 1, Issue 3, 1993, Pages 317-339, ISSN 0927-6505, https://doi.org/10.1016/0927-6505(93)90017-8.

Weinberg, S. (1977). The first three minutes A modern view of the origin of the universe. United Kingdom: Andre Deutsch.

Wikipedia contributors. (2021, January 10). Big Bang. In *Wikipedia, The Free Encyclopedia*. Retrieved 20:13, February 12, 2021, from https://en.wikipedia.org/w/index.php?title=Big_Bang&oldid=999546930

https://ned.ipac.caltech.edu/level5/Peebles1/frames.html

https://www.space.com/universe-standard-model-hubble-constant-new-measurements.html

References for Figures (Credicts):

[1*] Wikipedia contributors. (2021, January 10). Big Bang. In *Wikipedia, The Free Encyclopedia*. Retrieved 20:43, January 23, 2021, from https://en.wikipedia.org/w/index.php?title=Big_Bang&oldid=999546930

[2*] Emecan, Zafer. ”Büyük Patlama(Big Bang) Teorisi”. Kozmik Anafor. https://www.kozmikanafor.com/buyuk-patlama-big-bang-teorisi-1/. January 2018.

[3*]https://www.open.edu/openlearn/science-maths-technology/science/physics-and-astronomy/history-the-universe-timeline

[4*] https://www.nasa.gov/mission_pages/hubble/science/xdf.html

[5*] https://www.muhendisbeyinler.net/buyuk-patlama-teorisi-big-bang-nedir/

[6*] https://www.nasa.gov/content/discoveries-highlights-shining-a-light-on-dark-matter

[7*] http://abyss.uoregon.edu/~js/cosmo/lectures/lec15.html

[8*] https://www.sozcu.com.tr/2016/dunya/fizikcilerden-yeni-iddia-evrende-aslinda-2-defa-big-bang-oldu-1066326/

[9*] https://hubblesite.org/image/820/category/12-cosmology

Chapter 3

CHARACTERIZATION OF PROBIOTIC ABILITIES OF LACTIC ACID BACTERIA FROM TRADITIONAL PICKLE JUICE AND SHALGAM

Belgin ERDEM[1]
Esin KIRAY[2]
Ergin KARİPTAŞ[3]
Şener TULUMOĞLU[4]
Aslı AKILLI[5]

1 Prof. Dr., Kırşehir Ahi Evran University, Health Services Vocational College, Departments of Medical Services and Techniques, Kırşehir,Turkey, e-mail address: berdem@ahievran.edu.tr, ORCID IDs: 0000-0001-9108-5561
2 Assoc. Prof., Kırşehir Ahi Evran University, Health Services Vocational College, Departments of Medical Services and Techniques, Kırşehir,Turkey, ORCID IDs: 0000-0002-6908-5909
3 Prof. Dr., Samsun University, Faculty of Medicine, Department of Medical Microbiology, Samsun, Turkey, ORCID IDs: 0000-0001-6513-9589
4 Dr., Doctor Behçet Uz Hospital for Child Diseases Education and Research, Alsancak, İzmir-Turkey, ORCID IDs: 0000-0002-4831- 2623
5 Assoc.Prof.,Kırşehir Ahi Evran University, Faculty of Agriculture,Department of Agricultural Economics,ORCIDIDs:0000-0003-3879-710X

1. INTRODUCTION

Probiotics have been recognized in studies as vital microorganisms that benefit the health of the organism when used in sufficient quantities (Tavakoli, et al., 2017; Davis, 2014). Recently, probiotic fermented foods have attracted attention as a source of probiotic organisms (Shi, et al., 2016). Among the probiotic microorganisms most used are various strains of *Lactobacillus* and *Bifidobacterium,* as well as some strains of *Bacillus, Streptococcus, Pediococcus,* and *Enterococcus* (Fijan, 2014). Probiotic consumption is the result; beneficial effects such as increasing lactose tolerance, preventing digestive system infections, reducing digestion difficulties, reducing the risk of cancer, lowering cholesterol and preventing cardiovascular disease, increasing nutrition by synthesizing various vitamins (folate, vitamin B12), and strengthening the immune system (Saarela et al., 2000). Conventional probiotics; yogurt and other fermented dairy products are disadvantageous for consumption due to lactose intolerance and cholesterol content.

In recent years, consumer demand for milk-free probiotic products and the probiotics were added as tablets, capsules, and freeze-dried supplements into the food and beverage (Shah, 2001).

Some European countries with low COVID-19 mortality are those that consume almost high traditional fermented food. In an ecological study conducted in countries dieta traditional fermented foods, the risk of death for COVID-19 decreased by 35.4% with the increase in consumption of fermented vegetables (Fonseca et al., 2020).

Traditional fermented vegetable products such as pickle juice and shalgam are promising sources of natural probiotic microorganisms. Pickle juice is powerful probiotics, rich in vitamins and minerals that strengthen the immune system and destroy cancer-causing free radicals.

Pickle juice and shalgam are among the very old food preservation methods known by fermentation according to traditional methods.

In this fermentation, the sugar turns into acid by microorganisms (Nurul and Asmah 2012). Pickles contain large amounts of lactobacilli with beneficial probiotic properties and are good appetizers consumed by humans (Lal et al., 2010).

In fermented pickles, lactic acid bacteria (LAB) improve the nutritional content by providing vitamins, minerals, and carbohydrates, several taste ingredients, bacteriocins, and exopolysaccharides.These metabolic results present some special features in foods such as flavor, texture, and longer shelf life (Leroy and De Vuyst 2004). LAB in pickle juice and shalgam differs from other probiotics in that they can tolerate very high concentrations of salt and sugar.

The people of Turkey, consume traditional pickle juice and shalgam. In the literature reviews examined, studies were made with pickles, whereas studies with pickle juice were not encountered.

This study, it is to learn about the microflora of pickle juice and shalgam, which are consumed more than pickles.

The aims of the present study are to isolate, identify lactic acid bacteria in traditional pickle juice and shalgam, to determine low pH (2, 2.5, and 3), bile tolerance (0.3%, 0.5%, and 1% ox gal), and antagonistic activity.The effect is to investigate susceptibility to antibiotics, folic acid production and cholesterol assimilation.

2. MATERIAL AND METHODS

Bacterial Strains and Growth Conditions

In the study, a total of 40 samples were collected from homemade pickle juice and shalgam. 10 ml of pickle juice and shalgam samples were centrifuged at 3500 rpm for 10 minutes. The precipitate formed in the tube was planted in place of the MRS (De Man Rogosa Sharpe, Merck) solid medium for the isolation of bacteria. Biochemical fermentation kit API 50 CHL (BioMérieux La Bali Grottes, France) was used for the identification of prebiotically selected bacteria strains. For molecular identification, isolates were transferred to sterile Eppendorf containing 15% glycerol and stored at -80 ° C in a deep freezer (Liu et al., 2008).

Genotypic Characterization

Bacteria molecular identification was performed by extracting the genomic DNA of the isolates using a genomic DNA purification kit, and the 16S rDNA gene sequence of the isolates was 27F forward (5'AGA GTT TGA TCM TGG CTC AG3 ') and 1429R back (3' GGT TAC CTT GTT ACG ACT T5') using universal primers and PCR using Thermo Fisher Scientific Arktik Thermal Cycler 5020 instrument (Beasley et al., 2004). PCR conditions were 30 cycles of 2 minutes at 94 ° C, 45 seconds at 94 ° C, 1 minute at 55 ° C and finally 10 minutes at 72 ° C. The amplified fragments were displayed on 2% agarose gel electrophoresis (Vinderola et al., 2003). The identity of the isolate was analyzed by using the Blast software from the National Center for Biotechnology Information (NCBI).

Screening for Probiotic Properties

Resistance to Low pH and Bile Salts

Cultures of all strains were grown in MRS medium for 24 hours, subjected to centrifugation, washed twice with PBS buffer, and resuspended in PBS to a final concentration of 10^8-10^9 CFU / mL. Bacteria were incubated at pH 2.0 , 2.5, 3.0 and 6.2 for 3 h 37° C 5% CO_2 to investigate the effect of pH (Cukrowska et al., 2009).

100 µl of different pH adjusted media were inoculated from overnight culture of over night bacterial cultures and incubated at 37° C 5% CO_2 for 3 hours. The bacterial viability rate was determined as the log 10 value of colony forming units per mL (CFU mL^{-1}). In the laboratory bile salt tolerance test, MRS broth enriched with 0.3%, 0.5 and 1% (w / v) bile (Merck, Germany) were evaluated for all strains. Later, after 0 and 3 hours of incubation, viable colony counts were made using the pour plate method by making appropriate dilutions.

Determination of antimicrobial activity

Antimicrobial activity in probiotic specific lactic acid bacteria are make on an agar well diffusion technique defined by Reinheimer and Demkow (Reinheimer and Demkow 1990).The isolated strains were centrifuged at 37°C in activated cultures at MRS broth, and the resulting supernatant was sterilized by passing through a 0.45 µm. Separately, indicator microorganisms were activated and the bacterial suspension was inoculated to Muller Hinton agar and yeast SDA. The wells with a diameter of 8 mm were cut and100 µL of filter-sterilized supernatant was placed in each well.

Antibiotic Susceptibility

The susceptibility test of lactic acid bacteria was determined according to the agar disc diffusion method as described by Charteris et al. (Charteris et al., 2001). The results were evaluated according to the CLSI criteria (CLSI, 2010).

Cholesterol Assimilation

To determine the cholesterol assimilation capacities of strains, the serum of patients with serum cholesterol level 250-300 mg / dL at Ahi Evran University Training and Research Hospital was collected. Cholesterol (filter sterilized) was added to the MRS broth containing 0.3% (Oxgall, Sigma) bile salt to give 100 mg / mL. The cultures were allowed to incubate at 37 ° C for 24 hours and then the cells were centrifuged at 4 ° C for 10 minutes at 5,000 x g. As a control, bacterial cell uninoculated sample containing 3% bile salt and cholesterol was used. The residual cholesterol level was analyzed in the supernatant by Cobas 8000 (Roche, USA) model autoanalyzer. The amount of% cholesterol removed in the liquid medium was assessed by reversing the amount of cholesterol from the bacterial inoculated control medium (Tulumoglu, et al., 2014).

Folic acid production

To determine the ability of the strains to produce folic acid, the cultures were incubated at 37 ° C for 24 hours, and then centrifuged at 5,000 x g for 10 minutes at 4 ° C to remove supernatant into sterile ependorf tubes.

The amounts of folic acid produced in cultured supernatant fractions were measured on a Cobas e601 (Roche, USA) device.

In vitro Adhesion to Uroepithelial Cells

The adhesion of lactic acid bacteria isolates was determined by healthy female uroepithelial cells. Uroepithelial cells and cultures activated overnight were washed twice with potassium phosphate buffer (PBS) (pH 7.4). The collected cells were dilute to 5 x 10^6 cells/ml and 100 µl of bacteria isolate (10^6 CFU/ml) are mixed with 400 µl of epithelial cells and then incubated for 30 minutes in a 37°C water bath. The mixture was the centrifuge three times at 3,000 rpm and was wash twice with sterile PBS to remove bacteria from the pellet, resuspended in 100 µl PBS, stained with crystal violet and examined under a microscope. Bacterial adhesion was analyzing in 10 microscopic fields and considered positive when at least 10 bacteria adhered to each epithelial cell.The degree of adhesion of bacterial cells to epithelial cells is ranked between +1 and +4. Uroepithelial cells without bacterial culture were used as negative control (Feng et al., 2018).

Statistical Analyses

A completely randomized experimental design was used with three replications in 10 x 2 and 6 x 4 factorial arrangements. One-way analysis of variance was also used. Tukey HSD and Dunnet multiple comparison tests were used to find out which group originated the difference between the groups. The normality assumption in the analyses was examined by Kolmogorov-Smirnov and Shapiro Wilk tests. Statistical analyses were performed using SPSS (version 20.0, SPSS Inc, USA) statistical package program. In the analyses, the significance level was determined as $p < 0.05$ and $p < 0.01$.

3. RESULTS AND DISCUSSION

IdentificationUsing 16S rRNAGene Sequences.

The results of comparative 16S rRNA gene analysis showed that sixteen bacteria isolates belonged to the genus *Lactobacillus* and two isolates belong to the genus *Pediococcus* (Table 1). Five isolates isolated from the pickle were 99% similar to *L. plantarum* and the other five isolates were 98% similar to *L. brevis*. Two isolates isolated from shalgam were 99% similar to *L. plantarum*, two isolates were 98% similar to *L. brevis* and 2 isolates were 98% similar to *P. acidilactici.* The 16S rRNA gene sequences of the fourteen *Lactobacillus* strains and two *Pediococcus* strains were deposited in NCBI GenBank database under the accession numbers MF098783 to MF098798 for isolates T1, T2, T3, T4, T5, T6, T7, T8, T9, T11, Ş1, Ş2, Ş3, Ş4, Ş5 and Ş6, respectively (Figure 1).

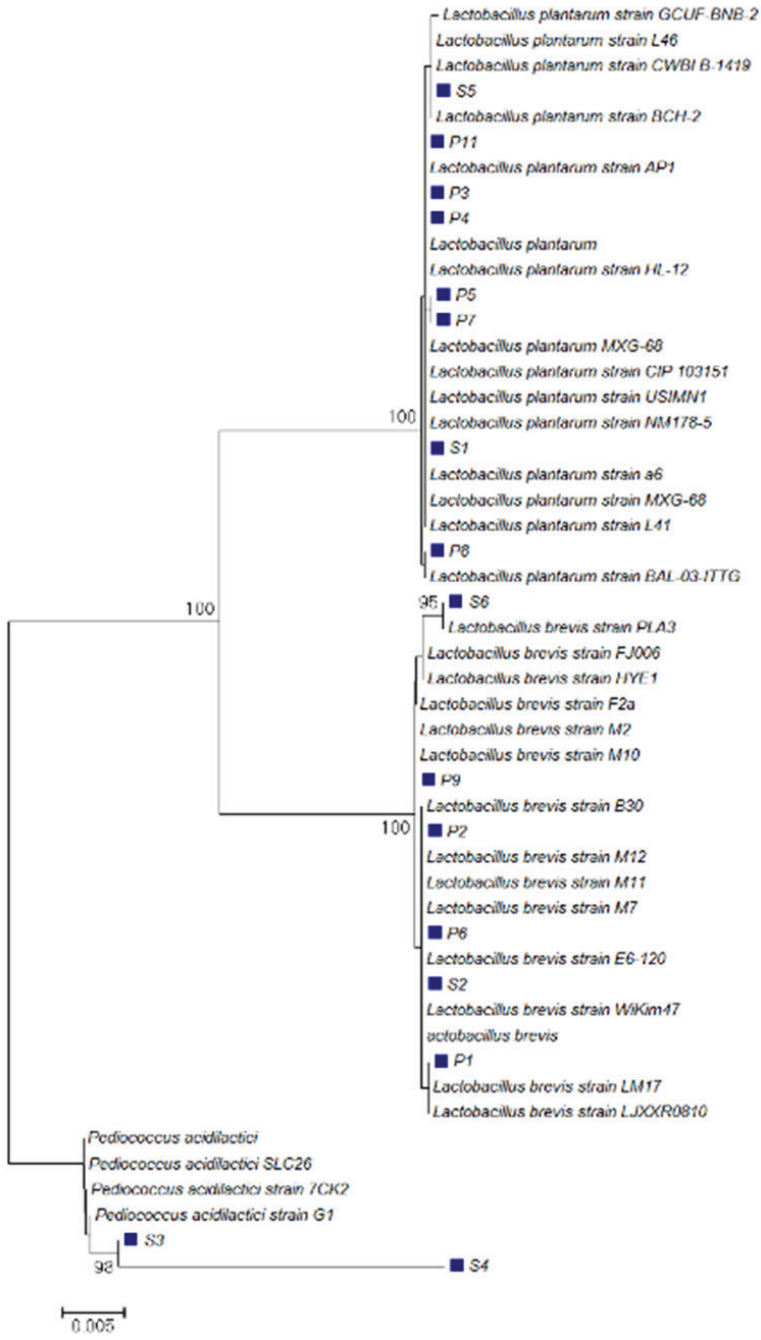

Figure 1. *Phylogenetic tree based on adjacent joining of 16S rRNA gene sequences. Dendogram was performed by neighbor-joining (NJ) method using MEGA 4.0 phylogenetic program. The numbers next to the nodes indicate the bootstrap values. The scale below Shaklin shows the similarity.*

Lactic Acid Bacterial Isolation

In the study, a total of 16 bacterial isolations were carried out, with 10 pickle and 6 shalgam. For identification of isolates, gram staining, catalase, morphological, biochemical and physiological properties were tested. In addition, API 50 CHL (BioMérieux La Bali Grottes, France) kit was used in the identification. In this study, 14 *Lactobacillus* spp. and 2 *Pediococcus* spp. the strain has been isolated. Five *Lactobacillus plantarum* and five *Lactobacillus brevis* were detected in the pickle. Shalgam was identified as 2 *Lactobacillus brevis*, 2 *Lactobacillus plantarum* and 2 *Pediococcus acidilactici.*The names and numbers of strains isolated from pickle and shalgam are given in Table 1. Scientific researches have found that *Lactobacillus* and *Pediococcus* are found at high level in microbiota of pickle samples. Tamminen et al., (2004) found that a large portion of the lactic flora in the cucumber pickle was formed by *Lactobacillus* species (*L. plantarum* and *L. pentosus*) while *Leuconostoc* species from other lactic acid bacteria were found to be in low abundance. Chiu et al., (2008) isolated *P. pentosaceus* and *L. plantarum* from cabbage and cucumber pickles. Çon and Karasu (2009) found that *L. plantarum* and *L. pentosus* strains isolated from pickled and fermented green olives produced 1.60-1.95 g / 100 mL lactic acid.

Table 1.*Tolerance of lactic acid bacteria to low pH (2.0, 2.5 and 3.0) grades (after 3 hours)*

Bacterial development (3 hours)					
pH values (cfu/ml)					
Isolates	**pH:6.2[a]**	**pH: 2.0 (%) Percent survival[b]**	**pH: 2.5 (%) Percent survival**	**pH: 3.0 (%) Percent survival**	**Total**
L. rhamnosus GG (Control)	8.86±0.01	7.42±0 (83.7)	7.82±0 (88.2)	8.27±0.01 (93.3)	8.09±0.55^{j}
L. brevis T1	8.87±0.01	0±0 0.00	5.68±0.01 (64.0)	7.63±0.01 (86.0)	5.54±3.54^{b}
L. brevis T2	8.67±0.01	0±00.00	6.27±0.01 (72.3)	7.74±0.01 (89.2)	5.67±3.53^{c}
L. plantarum T3	8.85±0.01	5.24±0.01 (59.2)	6.87±0.01 (77.6)	8.17±0.01 (92.3)	7.28±1.43^{g}
L. plantarum T4	8.98±0	4.43±0.01 (49.3)	7.88±0.01 (87.7)	8.23±0.01 (91.6)	7.38±1.82^{i}
L. plantarum T5	8.88±0.01	0±0 0.00	5.21±0.01 (58.6)	7.84±0.01 (88.2)	5.48±3.58^{a}
L. brevis T6	8.37±0.01	0±0 0.00	6.85±0.01 (81.8)	7.49±0.01 (89.4)	5.67±3.46^{cd}
L. brevis T7	8.94±0	0±0 0.00	5.45±0.01 (61.0)	8.36±0.01 (93.5)	5.68±3.69^{d}
L. platarum T8	8.92±0.01	3.27±0 (36.6)	5.56±0 (62.3)	8.26±0.01 (92.7)	6.50±2.35^{f}
L. brevis T9	8.79±0	0±0 0.00	7.17±0.01 (81.5)	7.95±0 (90.4)	5.97±3.65^{e}
*L. plantarum T*11	8.99±0	5.65±0.01 (62.8)	6.32±0 (70.3)	8.51±0.01 (94.6)	7.36±1.47^{h}
L. plantarum Ş1	8.44±0.01	3.75±0.01 (44.4)	5.87±0.01 (69. 5)	8.07±0 (95.6)	6.53±1.96^{d}
L. brevis Ş2	8.91±0.01	0±0 0.00	6.52± 0.01 (73.1)	7.59± 0.01 (85.1)	5.75±3.58^{b}
P. acidilactidi Ş3	8.71± 0.23	0±0 0.00	5.69±0 (64.2)	7.19± 0.01 (81.2)	5.39±3.44^{a}
P. acidilactidi Ş4	8.56±0	0±0 0.00	6.27±0 (73.2)	8.27± 0.01 (96.6)	5.77±3.60^{b}
L. plantarum Ş5	8.78± 0.01	6.26± 0.01 (71.2)	6.39± 0.01 (72.6)	8.34± 0.01 (94.8)	7.44±1.18^{e}
L. brevis Ş6	8.81±0	0±0 0.00	6.11± 0.01 (69.3)	8.61±0 (97.7)	5.88±3.71^{c}

[a] Control, [b] Percent survival =Final (cfu/mL)/control (cfu/mL) x 100.

The differences between the different letter averages in the same column are significant (p <0.01).

Resistance to Low pH and Bile Salts

Each microorganism has a minimum, maximum and optimum pH value that it can reproduce.Bacteria are more selective in terms of the pH of the environment in which they are growing.At the species level, *L. brevis* (T1, T2, T6, T7, T9, Ş2 ve Ş6) and *P. acidilactidi* (Ş3, Ş4) did not develop at pH 2.0 whereas *L. plantarum* (T3, T4, T5, T8, T11, Ş1, Ş5) were well developed; *L. brevis, P. acidilactidi* and *L. plantarum* strains were at pH 2.5; It was found that all strains were well developed at pH 3.0 and pH 6.2 At pH: 2, the highest level of survival of *L. plantarum* Ş5 strain (71.2%) was observed after 3 hours of incubation. Adnan and Tan (2007) reported that *L. brevis* and *L. plantarum* isolated from two traditional Malaysian products and red pepper powder developed at pH 4.5, pH 7.0 and pH 9.0 Tangüler and Erten (2012) reported that *Lactobacillus* strains isolated from shalgam showed improvement at pH 4.4, but no bacteria could develop at pH 9.6. These bacteria must have high bile salt tolerance to survive. Table 2 shows the bile salt resistance of *Lactobacillus* and *Pediococcus* strains at different bile concentrations (0.3%, 0.5% and 1.0%) after 3 hours of incubation. Bile salt tolerance in pickle samples T4, T9 and T8 strains; In shalgam samples, Ş2 and Ş6 had highest values. All of the isolates had growth capacities of 0.3 % bile salts concentration (69-95% cells) after 3 hours of incubation. A recent study reported that a total 14 strains were identified as *Lactobacillus* spp. from cucumber and cabbage pickled samples.The incubation well developed with 0.2 % bile salt solution resulted in a survival rates of 81–94 % after 24 h (Zielińska et al., 2015). Bao et al., (2010) reported that *L. fermentum* strains isolated from from traditional dairy products fermented were good tolerance to 0.3% concentration of bile salts. In another study, *L. plantarum* 100% were inhibited at the 0.3 % and 0.1% bile salts concentration (Papamanoli et al., 2003).

Table 2. *Lactic acid bacteria at different concentrations (0.3%, 0.5% and 1.0%), bile salt (oxgall) tolerance*

Bacterial development (3 hours)					
Bile salt concentration (cfu/ml)					
Isolates	**Control[a]**	**% 0.3 (%) Percent survival[b]**	**% 0.5 (%) Percent survival**	**% 1 (%) Percent survival**	**Total**
L. rhamnosus GG (Control)	8.86±0.00	8.22±0 (92.7)	6.52±0 (73.5)	6.02±0 (89.4	7.40±1.22[j]
L. brevis T1	8.87±0.01	7.46±0.00 (84.1)	0±0 (0.00)	0±0 (0.00)	4.08±4.29[b]
L. brevis T2	8.66±0.01	8.25±0.00 (95.1)	0±0 (0.00)	0±0 (0.00)	4.22±4.41[c]
L. plantarum T3	8.84±0.00	8.27±0.00 (93.4)	4.52±0.01 (51.0)	4.12± 0.00 (46.5)	6.43±2.22[h]
L. plantarum T4	8.98±0.00	7.33±0.00 (81.6)	3.68±0.01 (45.0)	0±0 (0.00)	4.99±3.61[d]
L. plantarum T5	8.88±0.01	7.42±0.00 8(83.5)	5.75±0.00 (64.7)	0±0 (0.00)	5.51±3.51[g]
L. brevis T6	8.37±0	7.4±0.01(88.4)	5.46±0.00 (65.2)	0±0 (0.00)	5.30±3.38[e]
L. brevis T7	8.94±0.01	6.42±0.00 (71.8)	6.82±0.01 (76.2)	6.08±0.00 (68.0)	7.06±1.16[i]
L. platarum T8	8.92±0.00	7.24±0.00 (81.1)	7.11±0 (79.7)	6.45±0.00 (72.3)	7.43±0.95[k]
L. brevis T9	8.79±0	8.33±0.00 (94.7)	4.39±0 (49.9)	0±0 (87.8)	5.37±3.70[f]
*L. plantarum T*11	8.81±0.17	7.63±0.59 (70.6)	4.42±2.48 (0.00)	2.26±2.88 (0.00)	5.78±3.22[a]
L. plantarum Ş1	8.44±0.00	6.33±0 (75.0)	4.66±0.00 (55.2)	4.21±0.00 (49.8)	5.67±1.73[e]
L. brevis Ş2	8.91±0.00	7.46±0 (83.7)	3.58±0.00 (40.1)	0±0 (0.00)	4.98±3.63[c]
P. acidilactidi Ş3	8.85±0	7.42±0.00 (83.8)	5.64±0.01 (63.7)	0±0 (0.00)	5.47±3.51[d]
P. acidilactidi Ş4	8.56±0.01	7.33±0.00 (85.6)	0±0 (0.00)	0±0 (0.00)	3.97±4.17[a]
L. plantarum Ş5	8.79±0.01	6.26±0.00 (69.6)	4.25±0 (48.3)	0±0 (0.00)	4.82±3.35[b]
L. brevis Ş6	8.81±0	7.29±0.00 (82.7)	6.48±0.01 (73.5)	6.21±0 (70.4)	7.19±1.05[f]

[a]Control did not receive oxgall, [b]Percent survival =Final (cfu/mL)/control (cfu/mL) x 100.

The differences between the different letter averages in the same column are significant (p <0.01)

Antibiotic Susceptibility

Lactobacillus spp. and *Pediococcus* spp. isolated from pickle and shalgam. susceptibility of strains to 10 antibiotics was evaluated according to CLSI criteria. Test results are given in Table 3. In Table 3, the difference between the group averages of the isolates obtained in all antibiotic applications was statistically significant ($p < 0.01$). Susceptibility against 10 antibiotics was tested and all *Lactobacillus* and *Pediococcus* strains were found to be resistant to vancomycin (30 µg) and teicoplanin (30 µg); T3, T4, and T6, T7 and T11 are resistant to amoxicillin-clavulanic acid (20 + 10 µg); and T7 and T8 are resistant tetracyclines (30 µg). It is desirable that the probiotics be susceptible to widely prescribed antibiotics at low concentrations. However, some antibiotic resistance of probiotic strains can be used for protective and therapeutic purposes in the control of intestinal infections (El-Naggar, 2004). In various studies, antibiotic resistance was reported previously like Ashraf et al., (2011) found that *Lactobacillus* species were resistant to tetracycline, vancomycin, and erythromycin. Lactobacillus isolated from dairy products tetracycline and erythromycin-resistant were tested for the presence of genes (Gad et al., 2014).

Table 3. *Antibiotic susceptibility results of lactic acid bacteria isolated from pickle juice and shalgam (mm)*

	Antibiotics									
Isolates	**AMC**	**RA**	**SAM**	**TE**	**C**	**VA**	**MEM**	**TE**	**E**	**P**
T1	12±1.41a	16±1b	13±1a	11±0.1ab	25±0.1e	R	20±0.1a	R	16±0.1a	13±0.1a
T2	14±1.41b	19±1c	18±1abc	12±0.1ab	21±0.1c	R	26±0.1def	R	18±0.1ab	**25±0.1c**
T3	R	15±1b	23.3±4.9de	15±1cd	18±1b	R	23±1bc	R	18±0.1ab	26±1c
T4	R	19±1c	14±1ab	18±1e	25±1e	R	28±1f	R	18±0.1ab	27±1c
T5	20±1.41bc	10±1a	18±1abc	10±1a	15±1a	R	25±1cde	R	16±1a	12±1a
T6	R	21±1c	18±1abc	13±1bc	24±1de	R	21±1ab	R	20±1b	19±1b
T7	R	15±1b	20±1cde	R	18±1b	R	20±1a	R	20±1b	20±1b
T8	15±1.41ab	20±1c	19±1bcd	R	20±1bc	R	27±1ef	R	18±1ab	25±1c
T9	24±1.41c	20±1c	19±1bcd	16±1de	21±1c	R	24±1cd	R	25±1c	19±1b
T11	R	14±1b	25±1e	17±1de	22±1cd	R	25±1cde	R	19±1b	26±1c
Ş1	18±1.41b	30±1c	12±1a	15±1a	20±1a	R	30±1d	R	20±1bc	25±1b
Ş2	23.5±0.7c	17.6±0.57a	22±1d	17.6±0.57b	21±1a	R	25±1c	R	18±1b	25±1b
Ş3	13.5±0.7ab	22±1b	15±1b	14±1a	25±1b	R	14±1a	R	20±1bc	30±1c
Ş4	11.5±0.7a	20±1ab	15±1b	15±1a	24±1b	R	12±1a	R	22±1c	30±1c
Ş5	23.5±0.7c	20±1ab	26±1e	19±1b	19±1a	R	26±1c	R	22±1c	30±1c
Ş6	15.5±2.1ab	18±1a	19±1c	17.6±0.57b	20±1a	R	21±1b	R	14.6±0.57a	15±1a

C: Chloramphenicol (30 µg), TE: Tetracyclin (30 µg), E: Eritromisin (15 µg), VA: Vancomycin (30 µg), RA: Rifampicin (5 µg), P: Penisilin (6 µg), TEC: Teicoplanin (30 µg), AMC: Amoxcillin Clavulanic Acid (20 + 10 µg), SAM: Ampicilin/ Sulbactam (10/10 µg), MEM: Meropenem (10 µg)

R = resistant

The differences between the different letter averages in the same line are significant (p <0.01).

Antagonistic Activity of Lactic Acid Bacteria

Table 4 shows the antagonistic effects of probiotics bacteria against various pathogenic bacteria. The difference between the mean values of the groups except the *C. albicans* bacterial group was found statistically significant in turnip samples ($p < 0.01$). The overall antimicrobial activity of the LAB against 11 indicator microorganisms was determined. Inhibitory zone diameters of probiotics bacteria were measured against *E. feacalis, P. aeruginosa,* 3 *S. aureus, B. subtilis, B. cereus, E. coli,* and 3 *C. albicans,* which were selected as indicator microorganisms. Antimicrobial activity was considered to be absent in samples with inhibition zones of less than 0.5 cm. *L. brevis* (T1 and T2) and *L. plantarum* (T4) were unable to show antimicrobial activity against all indicator microorganisms. The strains did not show antimicrobial activity against *P. aeruginosa* and *S. aureus*, but other microorganisms showed antimicrobial activity. It has been found that the size of the inhibition zone diameters against *L. plantarum* (T5 and Ş5), *L. brevis* (T7), and *P. acidilactidi* (Ş4) against *E. feacalis* (ATCC 9212) is greater than other bacteria (Table 4). Probiotic bacteria exhibited antibacterial activity, against *E. coli, P. aeruginosa,* and *B. cereus* (Nigam et al., 2012). .It is therefore suggested that these potent isolates could be

used as natural bio-preservatives in different food products (Bello et al., 2013).

Table 4. *Antagonistic effects of lactic acid bacteria against various pathogenic bacteria (mm)*

	Bacteria										
Isolates	A	B	C	D	E	F	G	H	I	J	K
T1	0±0a	0±0	0±0	0± 0a	0±0a	0±0	0±0	0±0	0±0a	0±0a	0±0
T2	0±0a	0±0	0±0	0± 0a	0±0a	0±0	0±0	0±0	0±0a	0±0a	0±0
T3	0±0a	0±0	0±0	13±0,5bc	11±0,5b	0±0	0±0	0±0	13±0,5b	13±0,5b	0±0
T4	0±0a	0±0	0±0	0±0a	0±0a	0±0	0±0	0±0	0±0a	0±0a	0±0
T5	15±0.5c	0±0	0±0	14±0,5c	0±0a	0±0	0±0	0±0	13±0,5b	13±0,5b	0±0
T6	14±0.5bc	0±0	0±0	11±0,5b	0±0a	0±0	0±0	0±0	13±0,5b	13±0,5b	0±0
T7	16±0,5c	0±0	0±0	14±0,5c	12±0,5b	0±0	0±0	0±0	12±0,5b	13±0,5b	0±0
T8	0±0a	0±0	0±0	12±0,5bc	12±0,5bc	0±0	0±0	0±0	0±0a	13±0,5b	0±0
T9	12±0,5b	0±0	0±0	12±0,5bc	12±0,5bc	0±0	0±0	0±0	12±0,5b	12±0,5b	0±0
T11	12±0.5b	0±0	0±0	12±0,5bc	12±0,5bc	0±0	0±0	0±0	0±0a	13±0,5b	0±0
Ş1	0±0a	0±0	0±0	0±0a	0±0a	0±0a	0±0a	0±0a	12±0,5	0±0a	0±0a
Ş2	14±0,5bc	0±0	0±0	14±0,5b	14±0,5b	0±0a	0±0a	13±0,5b	12±0,5	12±0,5b	0±0a
Ş3	12±0,5b	0±0	0±0	14±0,5b	14±0,5b	11±0,5b	0±0a	13±0,5b	13±0,5	13±0,5b	18±0,5b
Ş4	15±0,5c	0±0	0±0	14,6±0,3b	14,6±0,3b	13±0,5b	0±0a	12±0,7b	14±0,5	14±0,5b	0±0a
Ş5	16±0,5c	0±0	0±0	14±0,5b	14±0,5b	13±0,5b	12±0,5b	14±0,5bc	14±0,5	14±0,5b	0±0a
Ş6	14±0,5bc	0±0	0±0	0±0a	0±0a	12±0,5b	0±0a	16±0,5c	13±0,5	13±0,5b	0±0a

The differences between the different letter averages in the same line are significant (p <0.01).

A: E. feacalis ATCC 9212, B: P. aeruginosa ATCC 27853, C: S. aureus ATCC 29213, D: B. subtilis ATCC 6633, E: B. cereus RSKK 709, F: E .coli ATCC 25922, G: C. albicans ATCC 90028, H: C. albicans ATCC 10098,I: C. albicans Y1200, J: S. aureus ATCC 25923, K: S. aureus MRSA

Cholesterol Assimilation

Figure 2 presents numerical findings of cholesterol assimilation capacities of probiotic bacteria. There is a statistically significant difference between the groups in terms of cholesterol ratio in lactic bacteria ($p < 0.01$). High cholesterol blocks the vessels and causes heart attacks and deaths. Probiotic bacteria are known to assimilate cholesterol and lower serum cholesterol levels. In Figure 2, the cholesterol assimilation capacities of the Lactobacillus and Pediococcus in the human plasma serum are shown. Cholesterol assimilation was studied using 0.3% bile salt and cholesterol 100 mg/ml in MRS broth. In our study, it was determined that all strains had cholesterol assimilation but% cholesterol assimilation values were different

among species. *L. plantarum* T4 strain observed cholesterol assimilating of 49.6% while *L. platarum* T8 and *L. brevis* Ş6 strains were found cholesterol assimilating 42% and 36.3%, respectively (Fig. 2). In various studies, researchers have proved that some of the probiotics containing *Lactobacillus* and *Bifidobacterium* can assimilate high cholesterol (Pereira and Gibson 2002). In vitro studies have examined the ability *of L. plantarum* strains and *L. paracasei* strains showed the highest cholesterol assimilation of 19.4% and 6.8%, respectively (Belviso et al., 2009). In the recent studies, the results observed were similar Shehata et al., (2016) observed up to 43.7% of the cholesterol removal capacity of *Lactococcus lactis* subsp. *lactis.* Tokatlı et al., (2015) proved that *L. plantarum* and *L. brevis* had assimilation of cholesterol by 48.56-1.57%, 16.62% -61%, respectively.

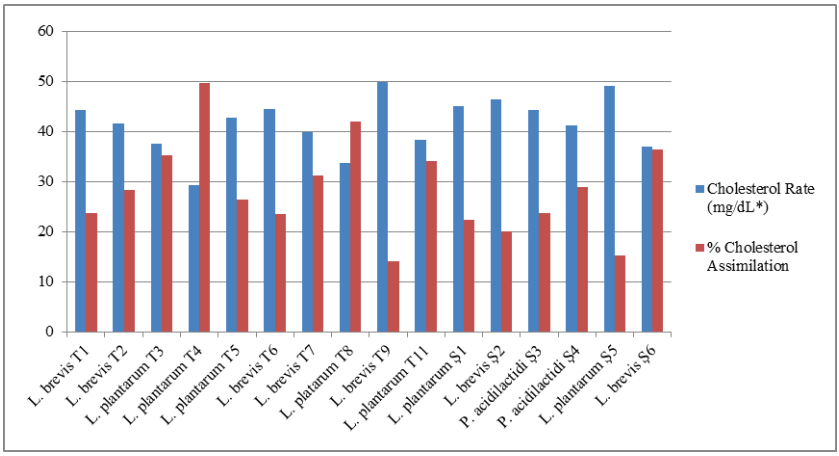

Figure 2. *Determination of cholesterol assimilation capacities of lactic acid bacteria (mg / dL)*

Folic acid production

Figure 3 shows that there is a statistically significant difference between the group averages of folic acid production rates of probiotic bacteria ($p < 0.01$). Folate is involved as a cofactor in many metabolic reactions, and it has to be an essential component in the human diet (Divya et al., 2012). In this study, out of the 16 isolates screened, 6 were found to produce folate, of which two better producers T3 and Ş6. *L. plantarum* T3 isolated from pickle produced 236±1.41 ng/ml folate and *L. brevis* Ş6 isolated from şalgam produced 317±1.41 ng/ml (Fig. 1). Among the 10 isolates from the pickle, 5 strains of *L. plantarum* (236 ng / ml) and 5 strains of L. brevis extracellularly produced high levels of folate (about 192 ng/ml). Two strains of *L. plantarum* (228 ng / ml) and two strains of *L. brevis* (about 317 ng/ml) produced extracellular folate at high levels between 4 isolates of probiotic bacteria isolated from the pickle. In addition, 2 *P. acidilactici* (about 279 ng/ml) isolated from shalgam produced folate at a high level.

Hugenschmidt et al. (2010) have reported that 96% of *L. plantarum* produced extracellular folate. In this study, *L. brevis* and *L. plantarum* isolated from the pickle were able to produce folate at different levels of 192 ng/ml and 236 ng / ml, respectively. Masuda et al., (2012) reported that high level (about 100 µg / L) folate produced *L. sake* and *L. plantarum* isolated from Japanese pickle juice.

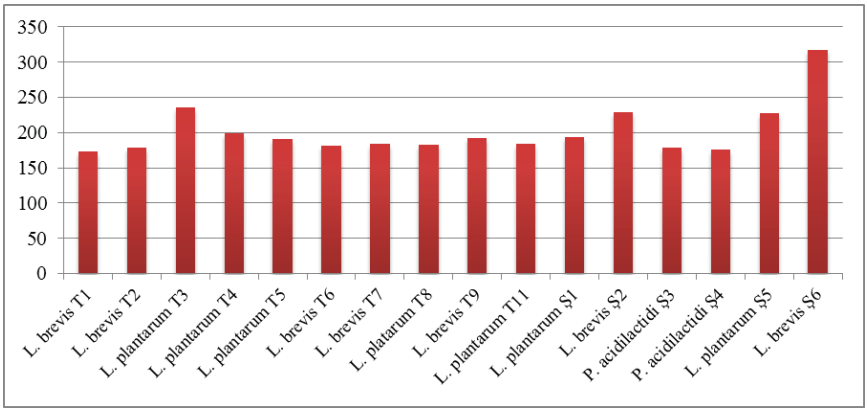

Figure 3. *Folic acid production rates of lactic acid bacteria (ng/ml)*

Adhesion to uroepithelial cells

In this study, the adhesion degree of 16 Lactic acid bacteria isolated from pickle juice and shalgam to uroepithelial cell was investigated. The highest level of adhesion to uroepithelial cells was observed for T3, T4, T5 and T8 strains were rated (+4), T1, T2, T6, T11, Ş1 and Ş5 strains were rated (+3) , T7, T9, Ş2 and Ş6 strains were rated (+2) and Ş3 and Ş4 strains were rated (+1) per microscopic field (Table 5).

Table 5. *The bacterial adhesion capacity of lactic acid bacteria to Uroepithelial cells*

Strain	**16S rRNA sequencing**	[a] **In vitro adhesion (Uroepithelial cells)**
L. rhamnosus GG (Control)	Not done	++++
T1	*L. brevis*	+++
T2	*L. brevis*	+++
T3	*L. plantarum*	++++
T4	*L. plantarum*	++++
T5	*L. plantarum*	++++
T6	*L. brevis*	+++
T7	*L. brevis*	++
T8	*L. platarum*	++++
T9	*L. brevis*	++
T11	*L. plantarum*	+++
Ş1	*L. plantarum*	+++
Ş2	*L. brevis*	++
Ş3	*P. acidilactidi*	+
Ş4	*P. acidilactidi*	+
Ş5	*L. plantarum*	+++
Ş6	*L. brevis*	++

[a] *The number of bacteria attached per uroepithelial cells. Score: +++, >100; ++, 10–100; +, 1–10; –, 0.*

A study has shown that probiotics can be useful in the treatment and prevention of urogenital infections in women (Pendharkar et al., 2015). In another study, they reported that uropathogenic bacteria have the ability to interfere with the adhesion, growth, and colonization of human bladder cells by lactobacilli (Delley et al., 2015).We performed adherence assays to the woman uroepithelial cells line to select potential Lactic acid bacteria (LAB) strains from pickle juice and shalgam. The results showed that LAB could inhibit the adherence of uroepithelial cells.

4. CONCLUSION

Probiotic bacteria enable the digestible substances to be easily digested thanks to the vitamins and minerals found in pickle juice and shalgam. In addition, the development of disease-causing microorganisms is also hampered. Probiotics should be considered to be among the cholesterol-lowering successful therapeutics by cholesterol assimilation. Probiotic bacteria are becoming more important with the production of folic acid. As a result, the lactic acid bacteria we isolated in this study can be used as probiotics. Probiotic bacteria isolated from pickle juice and shalgam show that it can be used in preventing infections.

REFERENCES

Adnan AFM, Tan IK (2007) Isolation of lactic acid bacteria from Malaysian foods and assessment of the isolates for industrial potential. Bioresource Technol 7: 1380-1385

Ashraf, R. and Shah, N.P. (2011) Antibiotic resistance of probiotic organisms and safety of probiotic dairy products. Int. Food Res. J. 18: 837-853

Bao Y, Zhang Y, Zhang Y, Liu Y, Wang S, Dong X, Zhang H (2010) Screening of potential probiotic properties of *Lactobacillus fermentum* isolated from traditional dairy products. Food Control 21: 695–701

Beasley SS, Saris PE (2004) Nisin producing strains isolated from human milk. Appl Environ Microbiol 70: 5051-3

Bello OO, Bello TK, Fashola MO (2013) Antibacterial activity of probiyotic bacteria isolated from fresh pepper and tomatoes against common food pathogens. Sci Agri 4: 42-47

Belviso S, Giordano M, Dolci P, Zeppa G (2009) In vitro cholesterol-lowering activity of *Lactobacillus plantarum* and *Lactobacillus paracasei* strains isolated from the Italian Castelmagno PDO cheese. Dairy Sci Technol 89: 169–176

Charteris WP, Kelly PM, Morelli L, Collins JK (2001) Gradient diffusion antibiotic susceptibility testing of potentially probiotic lactobacilli. J Food Protec 64: 2007–2014

Chiu HH, Tsai CC, Hsih HY, Tsen HY (2008) Screening from pickled vegetables the potential probiotic strains of lactic acid bacteria able to inhibit the Salmonella invasion in mice. J Appl Microbiol 104: 605-612

Clinical and Laboratory Standards Institute (CLSI) (2010) Performance Standards for Antimicrobial Susceptibility Testing, Twentieth Informational Supplement, M100-S20, CLSI, Wayne, PA.

Cukrowska B, Motyl I, Kozáková H, Schwarzer M, Górecki RK, Klewicka E, Slizewska K, Libudzisz Z (2009) Probiotic Lactobacillus strains: in vitro and in vivo studies. Folia Microbiol 54: 533–537

Çon AH, Karasu N (2009) Determination of Antogonostic Starter Cultures for Pickle and Olive Fermentation Processes. Czech J Food Sci 27: 185-193

Davis C (2014) Enumeration of probiotic strains: Review of culture-dependent and alternative techniques to quantify viable bacteria. J Microbiol Methods 103: 9-17

Delley M, Bruttin A, Richard M, Affolter M, Rezzonico E, Brück WM (2015) In vitro activity of commercial probiotic *Lactobacillus* strains against uropathogenic *Escherichia coli.* FEMS Microbiol Lett 362: fnv096

Divya JB, Varsha KK, Nampoothiri KM (2012) Newly isolated lactic bacteria with probiotic features for potential application in food industry. Appl Biochem Biotechnol 167: 1314-24

El-Naggar MYM (2004) Comparative study of Probiotic cultures to control the growth of *E. coli* O157:H7 and *Salmonella typhimurium*. Biotechnol 3: 173-180

Feng J, Li D, Liu L, Tang Y, Du R (2018) Characterization and comparison of the adherence and immune modulation of two gut Lactobacillus strains isolated from *Paralichthys olivaceus*. Aquaculture 499: 381–388.

Fijan S (2014) Microorganisms with claimed probiotic properties: an overview of recent literature. Int J Environ Res Public Health 11: 4745-67

Fonseca SC, Rivas I, Romaguera D, Quijal M, Czarlewski W, Vidal A,Fonseca J A,Ballester J,Anto J M, Basagana X,Cunha L M,Bousquet J (2020) Association between consumption of fermented vegetables and COVID-19 mortality at a country level in Europe. medRxiv 1-17

Gad GF, Abdel-Hamid AM, Farag ZS (2014) Antibiotic resistance in lactic acid bacteria isolated from some pharmaceutical and dairy products. Braz J Microbiol 45: 25-33

Hugenschmidt S, Schwenninger SM, Gnehm N, Lacroix C (2010) Screening of a natural biodiversity of lactic and propionic acid bacteria for folate and vitamin B12 production in supplemented whey permeate. Int Dairy J 20: 852–857

Lal G, Siddappa GS, Tandon GL (2010) Chutneys, sauces and pickles, preservation of fruits and vegetables. ICAR Publication, New Delhi, 235–269

Leroy F, de Vuyst L (2004) Lactic acid bacteria as functional starter cultures for the food fermentation industry. Trends Food Sci Technol 15:67–78

Liu GR, Lv Y, Li P, Zhou K, Zhang JL (2008) Pentocin 31-1, an anti-Listeria bacteriocin produced by *Lactobacillus pentosus* 31-1 isolated from Xuan-Wei Ham, a traditional China fermented meat product. Food Control 19: 353-359.

Masuda M, Ide M, Utsumi H, Niiro T, Shimamura Y, Murata M (2012) Production potency of folate, vitamin B_{12} and thiamine by lactic acid bacteria isolated from Japanese pickles. Biosci Biotechnol Biochem 76: 2061-7

Nigam A, Madhusudan HV, Bhola N ⁋(2012) In-vitro Screening of antibacterial activity of lactic acid bacteria against common enteric pathogens. J Biomed Sci 4: 1-6

Nurul SR, Asmah R (2012) Evaluation of antioxidant properties in fresh and pickled papaya. Int Food Res J 19:1117–1124

Papamanoli E, Tzanetakis N, Litopoulou-Tzanetaki E, Kotzekidou P (2003) Characterization of lactic acid bacteria isolated from a Greek dry-fermented sausage in respect of their technological and probiotic properties. Meat Sci 65: 859-67

Pendharkar S, Brandsborg E, Hammarström L, Marcotte H, Larsson PG (2015) Vaginal colonisation by probiotic lactobacilli and clinical outcome in women conventionally treated for bacterial vaginosis and yeast infection. BMC Infect Dis 15: 255-266

Pereira DI, Gibson GR (2002) Cholesterol assimilation by lactic acid bacteria and bifidobacteria isolated from the human gut. Appl Environ Microbiol 68: 4689-93

Reinheimer JA, Demkow MR (1990) Condioti MC Inhibition of coliform bacteria by lactic acid bacteria. Australian J Dairy Tech 45: 5-9

Saarela M, Mogensen G, Fondén R, Mättö J, Sandholm TM (2000) Probiotic bacteria: safety, functional and technological properties. J Biotechnol 84: 197–215

Shah NP (2001) Functional foods from probiotics and prebiotics. Food Technol 55: 46–53

Shehata MG, El Sohaimy SA, El-Sahn MA, Youssef MM (2016) Screening of isolated potential probiotic lactic acid bacteria for cholesterol lowering property and bile salt hydrolase activity. Ann Agri Sci 61: 65–75

Shi LH, Balakrishnan K, Thiagarajah K, Ismail NIM, Yin OS (2016) Beneficial Properties of Probiotics. Trop Life Sci Res 27: 73–90

Tamminen M, Joutsjoki T, Sjöblom M, Joutsen M, Palva A, Ryhänen EL, Joutsjoki V (2004) Screening of lactic acid bacteria from fermented vegetables by carbohydrate profiling and PCR–ELISA. Lett Appl Microbiol 39: 439-444

Tamminen M, Joutsjoki T, Sjöblom M, Joutsen M, Palva A, Ryhänen EL, Joutsjoki V (2004) Screening of lactic acid bacteria from fermented vegetables by carbohydrate profiling and PCR–ELISA. Lett Appl Microbiol 39: 439-444

Tangüler H, Erten H (2012) Chemical and Microbiological characteristics of Shalgam (Şalgam): A Traditional Turkish Lactic Acid Fermented Beverage. J Food Quality 35: 298–306

Tavakoli M, Hamidi-Esfahani Z, Hejazi M A, Azizi MH, Abbasi S (2017) Characterization of Probiotic Abilities of Lactobacilli Isolated from Iranian Koozeh Traditional Cheese. Pol J Food Nutr Sci 67: 41–48.

Tokatlı M, Gülgör G, Bağder Elmacı S, Arslankoz İşleyen N, Özçelik F (2015) *In vitro* properties of potential probiotic indigenous lactic acid bacteria originating from traditional pickles. Bio Med Res Inter 2015: 1-8

Tulumoglu Ş, Kaya Hİ, Şimşek Ö (2014) Probiotic characteristics of *Lactobacillus fermentum* strains isolated from tulum cheese. Anaerobe 30: 120-125.

Vinderola CG, Reinheimer JA (2003) Lactic acid starter and probiotic bacteria: a comparative “in vitro” study of probiotic characteristics and biological barrier resistance. Food Res Int 36: 895-904

Zielińska D, Rzepkowska A, Radawska A, Zieliński K (2015) In vitro screening of selected probiotic properties of *Lactobacillus* strains isolated from traditional fermented cabbage and cucumber. Curr Microbiol 70: 183-194

Chapter 4

GENERAL CHARACTERISTICS OF BATS

Emine Pınar PAKSUZ[1]

1 Dr. Öğr. Üyesi, Trakya University, Faculty of Education, Department of Basic Education, Edirne, Turkey. ORCID ID: 0000-0001-6304-3532

Classification of Bats

Bats (Order Chiroptera) are the most abundant, diverse and successful mammal species with a wide distribution in the entire world. The earliest confirmed records of bats come from the early Eocene in North America (approximately 55 million years ago) (Simmons and Geisler, 1998). They spread in tropical and temperate regions of the world, except in polar regions and some isolated islands. Their flying and echolocation abilities are very effective in this success of bats. In addition, it is a very different and special group in terms of their anatomy, different feeding habits, reproductive strategies, habitat preferences and roles in the ecosystem.

Until now, over 1400 species of bats have been described worldwide, making up approximately 1/4 of the known mammal species (Wilson and Mittermeier, 2019; Schipper et al., 2008; Simmons, 2005). It is also the largest group of mammals after rodents. The order of Chiroptera, spread all over the world, consists of 2 suborder Megachiroptera (Fruit bats, Flying foxes, "Megabats") and Microchiroptera (Echolocating Bats, "Microbats"). The Megachiroptera is represented by only one family, the Pteropodidae, whereas the Microchiroptera comprise all the other families (Rhinopomatidae, Craseonycteridae, Megadermatidae, Rhinonycteridae, Hipposideridae, Rhinolophidae, Emballonuridae, Myzopodidae, Nycteridae, Mystacinidae, Phyllostomidae, Furipteridae, Mormoopidae, Noctilionidae, Thyropteridae, Natalidae, Miniopteridae, Cistugidae, Vespertilionidae, Molossidae).

There are some features that distinguish these two suborders from each other. Body size in bats varies according to groups, and species in the Microchiroptera group are generally smaller than those in the Megachiroptera group. The smallest bat is in the Microchiroptera group (*Craseonycteris thonglongyai*) and its weight is only 2-3 grams. The largest bat is in the Megachiroptera group and can weigh over 1500 grams. The largest bat in the world is a megabat called the Gigantic Flying Fox (*Pteropus vampyrus*). Another difference between the two groups is their echolocation abilities. Megachiroptera members use their eyes to orient in the dark and thus have large and prominent eyes. However, the orientation of Microchiroptera members is by echolocation and usually has small eyes. Megabats have a claw on the second finger of forelimb that supports their wings, which is not found in any microbats. Most microchiropterans also have tragus, which is a projection from the lower margin of the pinna. Tragus that is functional in echolocation is not found in Megachiroptera. Some external anatomical features such as skull, teeth, nose structure, ear structure, hair, skin and wings play an important role in the diagnosis and classification of bats.

Flying Ability

Although the body structure and shape of bats are very similar to those in other mammals, the main differences are the shape of the forelimbs and the presence of the wing membrane. Morphologically, the most important feature of bats is that they have wings. The name Chiroptera derives from the Greek words chiros and pteron, meaning 'hand' and 'wing', respectively. The development of these highly specialized flight organs is undoubtedly the most important factor in the success of bats. Many changes have occurred in their bodies regarding the ability of bats to fly. These changes show a reflection of their evolutionary development. The bat wing is a modified forearm, consisting of very elongated fingers and a skin membrane supported by the arm. The radius bone in the arm is long and curved. Apart from the bones of the hand (metacarpus) and the thumb, all other fingers are thin and very long.

The development of the wing membrane called the patagium, which is unique to bats, is important. Patagium consists of different parts: chiropatagium, propatagium, plagiopatagium and uropatagium. Chiropatagium extends as a thinner membrane between the second and fifth digits of the forelimbs. Propatagium extends from the shoulder to the wrist. Plagiopatagium, which is the wing membrane will extend between the body and fifth digit. The uropatagium, which is the tail membrane, stretch between the bases of the hindlimbs and the ventral base of the tail (Figure 1A).

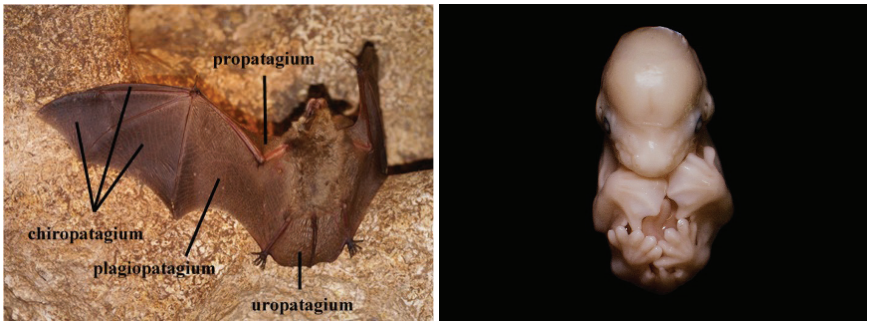

Figure 1. A: *Wing membrane of bat specimen.* **B:** *Photograph of the development of the forelimb and hindlimb of Myotis myotis in stage 18.*

Difference in the forelimb and hindlimb of bats can be seen during embryonic development. The morphogenesis of the forelimb and hindlimb is quite different in bats. All vertebrates have interdigital tissue between the fingers during embryonic development, and this tissue is lost by cell death during development in most species. (Salas-Vidal et al., 2001; Zou and Niswander, 1996). In bats, while interdigital tissue disappears in the hindlimb, this tissue does not disappear in the forelimb and forms the wing membrane called chiropatagium (Figure 1B). Interdigital tissue regresses between the 1st

and 2nd digits in the forelimbs of bats and the thumb remains free. However, the tissue between the second and fifth digits of the forelimbs remains to form the chiropatagium. In mammalian embryos, the tissue between the digits recedes by apoptosis via the expression of bone morphogenic proteins (Bmps) in the later stages of the development (Sears, 2008). Apoptosis is inhibited by the Bmp-inhibitor Gremlin and fibroblast growth factor (Fgfs, anti-apoptosis survival factors) expressed from the interdigital tissues of bats (Weatherbee et al., 2006). Another adaptation related to flight in bats is the modifications in autopodial elements. Metacarpals and the phalanges are considerably elongated and therefore the front members are longer than in other mammals (Cretekos et al., 2005).

Echolocation in Bats

Besides the ability of bats to fly, their echolocation abilities are also responsible for the success and diversity of bats in the world. More than half of all bat species use the echolocation system to navigate and catch prey at night. Echolocation is actually an adaptation that makes it possible for bats to see their surroundings with the help of sound. Echolocation is based on the propagation of sounds coming from the mouth and nose and the reflection of these sounds as an echo by hitting the surrounding objects. The echoes that occur in echolocation allow bats to evaluate the distance, shape, size, and surface structure of objects, especially in the dark (Falk et al., 2011; Simon, 2014; Moss and Surlykke, 2001). From the echoes that occur in this way, bats learn about things around them, their proximity, distance or shape.

This ability, which is present in Microchiroptera and not in Megachiroptera (except Rousettus genus), is one of the main features that distinguish two suborders. Echolocation signals and their production in bats differ according to groups. Also, frequency, call duration and call intensity of signals differ according to the bat species and bat habitat. While the majority of bats produce echolocation sounds in the larynx, a few species produce echolocation signals with the tongue clicks (Holland and Waters, 2005; Thomas et al., 2004). The majority of bats in Microchiroptera produce echolocation sounds by the larynx (Laryngeal echolocation) (Griffin, 1958). Microchiropteran bats may emit their echolocation signals through the mouth or, less commonly, through the nostrils (Griffin, 1958). The sounds are above the human hearing range and the frequencies included in the call can range from about 10 kHz to 200 kHz. A few species (*Rousettus aegyptiacus, Rousettus leschenaulti*) of Megachiroptera produce echolocation signals with the tongue clicks (Lingual echolocation). (Holland and Waters, 2005; Thomas et al., 2004). The clicks of *Rousettus aegyptiacus* are generated in pairs with a frequency range of 12–70·kHz and peak frequency at 20–40·kHz (von Herbert, 1985). In addition, some bat species have been reported to produce echolocation clicks with their wings (Gould, 1988; Fenton and Ratcliffe, 2014).

Reproductive Strategies of Bats

Order Chiroptera shows a wide variety in reproductive strategies, morphology and physiology. As seen in many other animal species, bats have energetic requirements for reproduction (Studier et al., 1972; Kurta et al., 1989), Since the energy required will be obtained from the nutrients in the environment, there is a relationship between availability of high amounts of food and breeding time (Bronson, 1985). For example, the breeding of insectivorous species in temperate regions takes place in a short period when insects are abundant (Racey, 1982). Females of such species are seasonally monoestrous, and reproductive events such as gametogenesis, gestation and lactation occur during certain months of the year when food is available (Tuttle and Stevenson, 1982). However, as nutrients are generally available all year round in tropical regions, frugivorous species living in these regions show a seasonal bimodal polyoestry (Fleming, 1971; Heithaus et al., 1975). Delayed ovulation and fertilization (Pipistrellus ceylonicus, Racey, 1979), delayed implantation (*Rhinolophus rouxi*, Rasweiler, 1993), embryonic diapause (*Artibeus jamaicensis*, Altringham, 1996) and sperm storage are reproductive strategies used by bats to cope with changing environmental conditions. Most bat species using these reproductive strategies belong to the Rhinolophidae or Vespertilionidae families (Racey, 1979). Most of these bats are found in temperate regions of the world where hibernation has an impact on the reproductive cycle.

Delayed fertilization and sperm storage occurs in Rhinolophidae and Vespertilionidae families living in temperate regions. Spermatogenesis in the testis occurs in the summer and mating takes place in the autumn (Racey, 1972). Spermatozoa are stored in the female reproductive tract during hibernation until ovulation occurs. Spermatozoa do not lose their ability to fertilize during hibernation. After arousal from hibernation ovulation occurs and the egg is fertilized by one of the spermatozoa stored in the female reproductive tract (Wimsatt, 1969). In addition, in some species, sperms are stored in the cauda epididymis in males during the winter.

Delayed implantation is seen in some bat species living in temperate and tropical regions. Spermatogenesis in the testicles occurs in the summer, and mating takes place in the autumn after the offspring are weaned. The egg formed by ovulation in autumn is immediately fertilized. The fertilized egg goes through many cell divisions to form the blastocyst. The blastocyst then stops dividing and remains in diapause throughout hibernation. Thus, implantation does not occur. After arousal from hibernation, implantation takes place and development continues.

Another of the reproductive strategies is sperm storage. Sperm storage can take place in both the male and female reproductive tract (Crichton and Krutzsch, 2000). The vast majority of sperm-storing species belong to

the Rhinolophidae and Vespertilionidae families. Most of these species are temperate zone species that spend the winter months in hibernation (Racey, 1979). In addition, it has been reported that some tropical species also store sperm. Therefore, the reproductive cycle is also affected by hibernation.

Although the gestation length in bats varies according to the species, it is between 40 and 205 days (Barclay and Harder, 2003). While the majority of bats produce one offspring, some species can produce twins. Newborn bats are completely dependent on their mothers for protection and nutrition. After the babies are born, they feed on milk by hanging on to their mothers. Because newborn bats are unable to fly when they are born, baby bats either stay in roosts while their mothers are feeding, or hanging on to their mothers during flight. Young individuals grow rapidly and gain the ability to fly within a few weeks after birth.

Feeding Habits

Bats exhibit a great variety of eating habits. The majority of bats in the Megachiroptera feed mainly on fruit (frugivorous). Some Megabats feed on nectar produced by flowering plants (nectarivorous). Old World fruit bats (family Pteropodidae) include 166 frugivorous and nectarivorous species (Koopman, 1993; Mickleburgh et al., 1992). Other food resources include leaves, shoots, buds, pollen, seed pods, sap, cones, bark, and twigs.

The species in the suborder Microchiroptera mostly feed on insects. Dietary composition is mostly Lepidoptera, Orthoptera, Coleoptera, Hemiptera, Hymenoptera, and Diptera (Kunz and Fenton, 2005; Reis et al., 2017). Insectivorous bat species can catch insects in different ways: "aerial insectivores" catch insects in flight, while "gleaning insectivores" take them from the substrate (Findley, 1993, Schnitzler and Kalko, 1998). The aerials locate their prey using the oral echolocation while the gleaners find them using the sound generated by prey (Kunz and Fenton, 2005; Santana and Cheung, 2016). In addition, some bats feed on small mammals, birds, rodents, lizards, frogs and other bats (carnivorous), or fish (piscivorous) (Tuttle and Ryan, 1981; Bonato and Facure, 2000; Delpietro and Simon, 1987; Medellín, 1989). Some Microchiropteran bats also consume fruit and nectar (Ferrarezzi and Gimenez, 1996). There are three species of vampire bats (*Desmodus rotundus*, *Diaemus youngi,* and *Diphylla ecaudata*) from the subfamily Desmodontinae (Phyllostomidae) and feed exclusively on the blood of other vertebrates (Greenhall and Schmidt, 1988). *D. rotundus* feeds on blood of mammals such as horse, pig, sheep, and cattle while *D. youngi* and *D. ecaudata* prefer to feed on bird blood. They can drink blood by cutting the skin of animals with their incisors, as the anticoagulant protein in their saliva provides the blood flow.

Different dietary patterns of bats are associated with skull, tooth, and tongue morphologies (Neuweiler, 2000; Santana et al., 2011; Tschapka et

al., 2015). For example, snout and tongue are elongated and the teeth are smaller in those who feed on nectar and pollen. Molar teeth have sharp cusps to their crowns in the insectivorous bats.

Habitat Preferences

Bats live in a variety of terrestrial habitats except polar regions. Terrestrial habitats generally comprise forests, deserts, open areas, farmland and urban areas. However, bats also use caves, mines, hollows of trees, cracks in the walls of buildings and roofs. Bats often have very specific roost preferences that differ between species.

Bats spend more than half of their life on the roost. Most bat species need daily roosts to protect themselves from the weather conditions and predators. Therefore, roost selection is very important for bats to survive (Neuweiler, 2000). Bats do not build roosts, except for a few species, and different bat species show varying levels of dependence on roosts. (Kunz, 1982; Kunz et al., 2003). Therefore, the social structure and distribution of bats is affected by the presence of roosts (Chaverri et al., 2007). In general, Megachiroptera species use trees as roosts, while Microchiroptera species use all types of roosts (Altringham, 1996). Studies have shown that the largest bat colonies were formed in caves under natural conditions (Russell et al., 2005).

When the underground and terrestrial habitats are compared, it is seen that the caves have more stable environmental conditions. Unlike terrestrial habitats, caves have an almost constant humidity and temperature throughout the year. Although microclimatic conditions generally affect the habitat quality of bats, the microclimatic requirements of bats show seasonal changes according to their annual life cycle (Baudinette et al., 2000). The preferences of roosts in bats according to different periods of the year are also variable. For example, some species may hibernate in cave during the winter, while in warmer months they may use crevices in tree cavities. Temperate zone bats use roosts to raise their young in the summer, to mate in late summer and autumn, and to hibernate in the winter.

Longevity

Bats have a surprisingly long lifespan. There is a relationship between lifespan and body size in mammals. It has been reported that smaller animals have a shorter lifespan, while larger animals have a longer lifespan. For example, lifespan is over 200 years for whales, the largest animal, and 1-2 years for shrews, which are small mammals (Finch, 1994; George et al., 1999). This relationship between longevity and body size is not in bats like that in other mammal species. Although bats are very small animals, their lifespan is quite long. The average life expectancy of bats is 30-40 years, which is considerably longer compared to other

mammals of the same body size. It has been reported that the longevity of bats is three times longer than non-flying mammals of the same size (Wilkinson and South, 2002). Longevity record has been established for some bat species such as *Myotis brandtii* (7 gr; 38 years), *Myotis lucifugus* (8 gr; 34 years), *Rhinolophus ferrumequinum* (23.5 gr; 30.5 years) and *Rosettus aegyptiacus* (146 gr; 22.9 years) and some non-flying mammals such as *Blarina brevicauda* (6 gr; 2 years), *Rattus norvegicus* (350 gr; 5 years), *Peromyscus leucopus* (25 gr; 8 years) and *Mus musculus* (30 gr; 4 years) (Wilkinson and South, 2002).

Hibernation in Bats

There are certain environmental conditions that every animal species needs in order to survive. Some physiological or morphological changes occur in response to changes in these conditions. Although the presence of food in the environment is very important for the survival of the animals, the availability of food is related to the ambient temperature. For this reason, temperature changes in the environment, which occur especially due to seasonal changes, also affect the presence of nutrients in the environment. Animals give many physiological responses to these changes related to ambient temperature and food availability in the environment in which they live. Torpor is a strategy used by many mammal species to cope with adverse environmental conditions. Torpor is characterized by a decrease in body temperature, water loss and metabolic rate (Speakman et al., 2005; Hock, 1951). The duration of the torpor can be several days in some species (daily torpor) and several months in others (hibernation).

Most of the bat species in the Microchiroptera group feed on insects. The presence of insects in the environment is closely related to the ambient temperature. There is a significant decrease in the number of insects in the environment during the cold winter months. For this reason, especially Microchiroptera species use torpor to cope with unfavorable environmental conditions caused by the decrease in the number of insects in the environment (Arlettaz et al., 2000; Willis et al., 2006; Wojciechowski et al. 2007). Many bat species hibernate to survive the harsh environmental conditions during the winter months. Hibernation, which occurs as a result of decreased nutrient availability in the environment, is a physiological and behavioral adaptation that is characterized by low body temperature, heart rate, metabolic rate, blood pressure and respiratory rate (Lyman and Chatfield, 1995). Most bats use caves for hibernation (Figure 2). The main reason for this is that caves contain roosts that have optimal microclimate for hibernating.

Figure 2. *Cave dwelling bats in hibernation.*

Roles in The Ecosystem

Bats, which are distributed almost all over the world, live in different habitats. Although bats are not well known by humans, they actually play very important roles in the ecosystem they live in. Most of the species in the Microchiroptera suborder are insectivorous, meaning they feed on insects. Therefore, insectivorous species play a very important role in controlling insect numbers. The amount of insect consumption of a bat varies significantly with the species, season, and reproductive cycle. Insectivorous bat species may consume 30%–100% of their body weight in each night (Kunz et al., 2011). For example, it has been reported that *Tadarida brasiliensis* consumes more than 70% of its body mass overnight, while *Myotis lucifugus* can consume up to 100% (Kunz et al., 1995; Kurta et al., 1989). Since most of the insects that bats consume are also agricultural pests, bats hunt these insects and benefit humans economically. It is estimated that bats are highly effective in combating agricultural pests and contribute to saving millions of dollars in the world (Boyles et al., 2011; Maine and Boyles, 2015). In addition, some bat species especially feed on mosquitoes (Rydell, 1990; Griffin et al., 1960). Therefore, they are also important in the control of many diseases transmitted by mosquitoes to humans and animals.

The different eating habits of bats are also important in terms of their role in the ecosystem. While insectivorous species are important in controlling insect numbers, frugivorous and nectarivorous species are important in the maintenance of forest ecosystems by ensuring pollination and seed dispersal in tropical and subtropical regions (Corlett, 2009). Pteropodidae and Phyllostomidae are two families that play a role in pollination and seed dispersal. Many plants that benefit from the transport of seeds and pollination by bats are also economically valuable (Kunz et al., 2011). For example, more than 100 phyllostomid species are known to be effective in dispersing and pollinating the seeds of many economically valuable plants (Dobat and Peikert-Holle, 1985).

REFERENCES

Altringham, J. D. (1999). Bats Biology and Behaviour. New York, New York: Oxford University Press.

Altringham, J. D. (1999). *Bats: biology and behavior.* Oxford Univ. Press, p. 264, Oxford.

Arlettaz, R., Ruchet, C., Aeschimann, J., Brun, E., Genoud, M., & Vogel, P. (2000). Physiological traits affecting the distribution and wintering strategy of the bat Tadarida teniotis. *Ecology*, *81*(4), 1004-1014.

Barclay, R. M. R., & Harder, L. D. (2003). Life histories of bats: life in the slow lane. InBat ecology.

Baudinette, R. V., Churchill, S. K., Christian, K. A., Nelson, J. E., & Hudson, P. J. (2000). Energy, water balance and the roost microenvironment in three Australian cave-dwelling bats (Microchiroptera). *Journal of Comparative Physiology B*, *170*(5-6), 439-446.

Bonato, V., & Facure, K. G. (2000). Bat predation by the fringe-lipped bat Trachops cirrhosus (Phyllostomidae, Chiroptera). *MAMMALIA-PARIS-*, *64*(2), 241-242.

Boyles, J. G., Cryan, P. M., McCracken, G. F., & Kunz, T. H. (2011). Economic importance of bats in agriculture. *Science*, *332*(6025), 41-42.

Bronson, F. H. (1985). Mammalian reproduction: an ecological perspective. *Biology of reproduction*, *32*(1), 1-26.

Chaverri, G., Quirós, O. E., Gamba-Rios, M., & Kunz, T. H. (2007). Ecological correlates of roost fidelity in the tent-making bat Artibeus watsoni. *Ethology*, *113*(6), 598-605.

Corlett, R. T. (2009). Seed dispersal distances and plant migration potential in tropical East Asia. *Biotropica*, *41*(5), 592-598.

Cretekos, C. J., Weatherbee, S. D., Chen, C. H., Badwaik, N. K., Niswander, L., Behringer, R. R., & Rasweiler IV, J. J. (2005). Embryonic staging system for the short-tailed fruit bat, Carollia perspicillata, a model organism for the mammalian order Chiroptera, based upon timed pregnancies in captive-bred animals. *Developmental dynamics: an official publication of the American Association of Anatomists*, *233*(3), 721-738.

Crichton, E. G., & Krutzsch, P. H. (Eds.). (2000). *Reproductive biology of bats*. Academic Press.

Delpietro, H. A., & Simon, G. (1987). Vampirfledermäuse, Desmodus rotundus rotundus (Geoffr.), als Beute des Langohr-Scheinvampirs, Chrotopterus auritus australis (Thomas). *Nyctalus*, *3*(4), 325-333.

Dobat, K., & Peikert-Holle, T. (1985). Blüten und Fledermäuse–Bestäubung durch Fledermäuse und Flughunde. *Verlag Waldemar Kramer, Frankfurt/ Main, Germany*.

Falk, B., Williams, T., Aytekin, M., & Moss, C. F. (2011). Adaptive behavior for texture discrimination by the free-flying big brown bat, Eptesicus fuscus. *Journal of Comparative Physiology A*, *197*(5), 491-503.

Fenton, M. B., & Ratcliffe, J. M. (2014). Sensory biology: echolocation from click to call, mouth to wing. *Current Biology*, *24*(24), R1160-R1162.

Ferrarezzi, H., & Gimenez, E. D. A. (1996). Systematic patterns and the evolution of feeding habits in Chiroptera (Archonta: Mammalia). *Journal of Comparative Biology*, *1*(3), 75-94.

Finch, C. E. (1994). *Longevity, senescence, and the genome*. University of Chicago Press.

Findley, J. S. (1993). *Bats: a community perspective*. CUP Archive.

Fleming, T. H. (1971). Artibeus jamaicensis: delayed embryonic development in a neotropical bat. *Science*, *171*(3969), 402-404.

George, J. C., Bada, J., Zeh, J., Scott, L., Brown, S. E., O'Hara, T., & Suydam, R. (1999). Age and growth estimates of bowhead whales (Balaena mysticetus) via aspartic acid racemization. *Canadian Journal of Zoology*, *77*(4), 571-580.

Gould, E. (1988). Wing-clapping sounds of Eonycteris spelaea (Pteropodidae) in Malaysia. *Journal of Mammalogy*, *69*(2), 378-379.

Greenhall, A. M., & Schmidt, U. (1988). Natural History of Vampire Bats. Boca Raton, FL: CRC Press.

Griffin, D. R. (1958). Listening in the Dark. Yale University Press, New Haven.

Griffin, D. R., Webster, F. A., & Michael, C. R. (1960). The echolocation of flying insects by bats. *Animal behaviour*, *8*(3-4), 141-154.

Heithaus, E. R., Fleming, T. H., & Opler, P. A. (1975). Foraging patterns and resource utilization in seven species of bats in a seasonal tropical forest. *Ecology*, *56*(4), 841-854.

Hock, R. J. (1951). The metabolic rates and body temperatures of bats. *The Biological Bulletin*, *101*(3), 289-299.

Holland, R. A., & Waters, D. A. (2005). Echolocation signals and pinnae movement in the fruitbat *Rousettus aegyptiacus*. *Acta Chiropterologica*, *7*(1), 83-90.

Koopman, K. F. (1993). Order Chiroptera. Pp.: 137–241. *Mammal Species of the World. A Taxonomic and Geographic Reference. Smithsonian Institution Press, Washington & London*.

Kunz, T. H. (1982). Roosting ecology of bats. In *Ecology of bats* (pp. 1-55). Springer, Boston, MA.

Kunz, T. H., & Fenton, M. B. (Eds.). (2005). *Bat ecology*. University of Chicago Press.

Kunz, T. H., De Torrez, E. B., Bauer, D., Lobova, T., & Fleming, T. H. (2011). Ecosystem services provided by bats. *Europe*, *31*, 32.

Kunz, T. H., Lumsden, L. F., & Fenton, M. B. (2003). Ecology of cavity and foliage roosting bats. *Bat ecology*, *1*, 3-89.

Kunz, T. H., Whitaker, J. O., & Wadanoli, M. D. (1995). Dietary energetics of the insectivorous Mexican free-tailed bat (*Tadarida brasiliensis*) during pregnancy and lactation. *Oecologia*, *101*(4), 407-415.

Kurta, A., Bell, G. P., Nagy, K. A., & Kunz, T. H. (1989). Energetics of pregnancy and lactation in freeranging little brown bats (*Myotis lucifugus*). *Physiological Zoology*, *62*(3), 804-818.

Lyman, C. P., & Chatfield, P. O. (1955). Physiology of hibernation in mammals. *Physiological reviews*, *35*(2), 403-425.

Maine, J. J., & Boyles, J. G. (2015). Bats initiate vital agroecological interactions in corn. *Proceedings of the National Academy of sciences*, *112*(40), 12438-12443.

Medellín, R. A. (1989). Chrotopterus auritus. *Mammalian species*, (343), 1-5.

Mickleburgh, S. P., Hutson, A. M., & Racey, P. A. (1992). Old World fruit bats. *An action plan for their conservation. Gland, Switzerland: IUCN*, *263*.

Moss, C. F., & Surlykke, A. (2001). Auditory scene analysis by echolocation in bats. *The Journal of the Acoustical Society of America*, *110*(4), 2207-2226.

Neuweiler, G. (2000). *The biology of bats*. Oxford University Press on Demand.

Racey, P. A. (1972). Aspects of reproduction in some heterothermic bats. *PhD diss. University of London*.

Racey, P. A. (1979). The prolonged storage and survival of spermatozoa in Chiroptera. *Reproduction*, *56*(1), 391-402.

Racey, P. A. (1982). Ecology of bat reproduction. In *Ecology of bats* (pp. 57-104). Springer, Boston, MA.

Rasweiler IV, J. J. (1993). Pregnancy in chiroptera. *Journal of Experimental Zoology*, *266*(6), 495-513.

Reis, N. R., Peracchi, A. L., Batista, C. B., de Lima, I. P., & Pereira, A. D. (Eds.). (2017). *História Natural dos Morcegos Brasileiros: chave de identificação de espécies*. Technical Books Editora.

Russell, A. L., Medellín, R. A., & McCracken, G. F. (2005). Genetic variation and migration in the Mexican free-tailed bat (Tadarida brasiliensis mexicana). *Molecular Ecology*, *14*(7), 2207-2222.

Rydell, J. (1990). The northern bat of Sweden: taking advantage of a human environment. *Bats*, *8*(2), 8-11.

Salas-Vidal, E., Valencia, C., & Covarrubias, L. (2001). Differential tissue growth and patterns of cell death in mouse limb autopod morphogenesis. *Developmental dynamics: an official publication of the American Association of Anatomists*, *220*(4), 295-306.

Santana, S. E., & Cheung, E. (2016). Go big or go fish: morphological specializations in carnivorous bats. *Proceedings of the Royal Society B: Biological Sciences*, *283*(1830), 20160615.

Santana, S. E., Strait, S., & Dumont, E. R. (2011). The better to eat you with: functional correlates of tooth structure in bats. *Functional Ecology*, *25*(4), 839-847.

Schipper, J., Chanson, J. S., Chiozza, F., Cox, N. A., Hoffmann, M., Katariya, V., ... & Young, B. E. (2008). The status of the world's land and marine mammals: diversity, threat, and knowledge. *Science*, *322*(5899), 225-230.

Schnitzler, H. U., & Kalko, E. K. V. (1998). How echolocating bats search and find food. In 'Bat Biology and Conservation'.(Eds TH Kunz and PA Racey.) pp. 183–196.

Sears, K. E. (2008). Molecular determinants of bat wing development. *Cells Tissues Organs*, *187*(1), 6-12.

Simmons, N. B. (2005). Order chiroptera. *Mammal species of the world: a taxonomic and geographic reference*, *1*, 312-529.

Simmons, N. B., & Geisler, J. H. (1998). Phylogenetic relationships of Icaronycteris, Archaeonycteris, Hassianycteris, and Palaeochiropteryx to extant bat lineages, with comments on the evolution of echolocation and foraging strategies in Microchiroptera. Bulletin of the AMNH; no. 235.

Simon, R., Knörnschild, M., Tschapka, M., Schneider, A., Passauer, N., & von Helversen, O. (2014). Biosonar resolving power: echo-acoustic perception of surface structures in the submillimeter range. *Frontiers in physiology*, *5*, 64.

Speakman, J. R., Thomas, D. W., Kunz, T. H., & Fenton, M. B. (2005). Physiological ecology and energetics of bats. *Bat ecology*, 430-478.

Studier, E.H., Lysengen, V.L. & O' Farrell, M.J. (1972). Biology of Myotis thysanodes and M. lucifugus (Chiroptera: Vespertilionidae) – II. Bioenergetics of pregnancy and lactation. Physiol. Zool. 57, 457–467.

Thomas, J. A., Moss, C. F., & Vater, M. (Eds.). (2004). *Echolocation in bats and dolphins*. University of Chicago Press.

Tschapka, M., Gonzalez-Terrazas, T. P., & Knörnschild, M. (2015). Nectar uptake in bats using a pumping-tongue mechanism. *Science advances*, *1*(8), e1500525.

Tuttle, M. D., & Ryan, M. J. (1981). Bat predation and the evolution of frog vocalizations in the Neotropics. *Science*, *214*(4521), 677-678.

Tuttle, M. D., & Stevenson, D. (1982). Growth and survival of bats. In *Ecology of bats* (pp. 105-150). Springer, Boston, MA.

Von Herbert, H. (1985). Echoortungsverhalten des flughundes Rousettus aegyptiacus (Megachiroptera). *Z Sä ugetierkunde*, *50*, 141-152.

Weatherbee, S. D., Behringer, R. R., Rasweiler, J. J., & Niswander, L. A. (2006). Interdigital webbing retention in bat wings illustrates genetic changes underlying amniote limb diversification. Proceedings of the National Academy of Sciences, 103(41), 15103-15107.

Wilkinson, G. S., & South, J. M. (2002). Life history, ecology and longevity in bats. *Aging cell*, *1*(2), 124-131.

Willis, C. K., Brigham, R. M., & Geiser, F. (2006). Deep, prolonged torpor by pregnant, free-ranging bats. *Naturwissenschaften*, *93*(2), 80-83.

Wilson DE, Mittermeier RA (2019) Handbook of the mammals of the world. Vol. 9 Bats. Lynx Ediciones, Barcelona, 1008 pp.

Wimsatt, W. A. (1969). Some interrelations of reproduction and hibernation in mammals. In *Symposium of the Society for Experimental Biology* (Vol. 23, pp. 511-549).

Wojciechowski, M. S., Jefimow, M., & Tęgowska, E. (2007). Environmental conditions, rather than season, determine torpor use and temperature selection in large mouse-eared bats (Myotis myotis). *Comparative Biochemistry and Physiology Part A: Molecular & Integrative Physiology*, *147*(4), 828-840.

Zou, H., & Niswander, L. (1996). Requirement for BMP signaling in interdigital apoptosis and scale formation. *Science*, *272*(5262), 738-741.

Chapter 5

AN INVESTIGATION ON PHYSICOCHEMICAL PARAMETERS AND POTENTIAL USE OF WASTE FRUIT PEELS AS CARBON SOURCES FOR α -AMYLASE PRODUCTION FROM *BACILLUS LICHENIFORMIS*

Abdurrahman DÜNDAR[1]

1 Mardin Artuklu University, Vocational School of Health Services, Campus, 47420, Mardin, Turkey, ORCID: 0000-0002-7930-1054, anzdundar@gmail.com

Introduction

α-amylases that break starch (EC 3.2.1.1) are widespread in nature. This enzyme randomly hydrolizes the α-1,4 glycosidic bonds and produces monosaccharides and oligosaccharides that include maltose, glucose and alpha-dextrines (Gupta et al., 2003). α-amylases are the best known significant industrial enzymes that are used in biotechnological applications and they make up 25-33 % of the enzyme market (Goyal et al., 2005; Tiwari et al., 2015; Akatı, 2019; Msarah et al., 2020). While they are widespread through nature, they can be produced by so many organisms such as microorganisms, animals, plants, etc. The main benefit of using microorganisms for producing α-amylases is the reasonable mass production capability. Additionally, they can also be oriented easily to produce enzymes that have a specific property (Shiau et al., 2003). It is well known that microorganisms including bacteria and fungi living in thermal water sources such as hot springs produce so many enzymes like α-amylases depending on the situation of their ecological niche, and habitats. At biotechnological applications microbial α-amylases are the most popular enzymes, and they are used for their potential benefits in different industries such as medicine, food, textile and detergents (Maria et al., 2019; Melnichuk et al.,, 2020; Far et al., 2020). With the advent of industrialization, new methods that can have great advantages in research applications are being developed. Production of α-amylases generally bound up with the culture systems such as liquid medium fermentation (LMF) or solid state fermentation (SSF), the bioreactor design, and the medium compounds (Sahnoun et al., 2015). SSF is the more useful, salutary and sustainable process that uses too little of water to transform plant based agricultural wastes into precious products such as biofuels, organic acids, vitamines, enzymes, and other bioactive compounds (Ozdemir et al., and Uribe, 2020). The SSF method has many properties that make it a more attractive alternative to LMF. These advantages that have been explained at scientific studies are: economical, biological, and environment friendly (López-Gómez, 2020). Choosing the substrate to be used in the SSF is a process that involves analyzing many different agricultural wastes: These substrates mostly come from wastes that are a byproduct of agricultural, forestry and food industries and include products such as fruit and vegetable peels, wood chips, and other renewable crude material. These products have a high usability rate and they are cheap namely they have a lower production cost and have lower environmental effects (since for example they are being removed) (Steudler et al., 2019). In SSF, temperature, pH, fermentation time, moisture, inoculation rate, nitrogen and carbon sources have to be optimized since they are the main factors that influence microbial reproduction and growth and hence the production of the enzymes. In this

work, the main goal is to optimize enzyme production and use alternative carbon sources such as industrial wastes for producing α-amylases from *Bacillus licheniformis,* thus reducing environmental pollution and cost of production.

Materials and methods

Microorganisms

At the study, for phylogenetic analysis (16S rRNA) the samples isolated from Belkısana hotspring (located at Düğünyurdu, Güçlükonak, Şırnak region) were send to Macrogen/South Korea. One of the sample was deposited under the accession number as KY202705.1 at National Centre for Biotechnology Information (NCBI). *Bacillus licheniformis* A12 was used as biological material. The microorganism was kept in a selective agar at 45°C to reproduce and later was transferred to a Luria-Bertani Broth liquid medium using a loop.

Substrate

In this work, melon, apple, orange and banana fruit peels were used as substrates. Before use, these plant-based wastes were ground and sieved through sieves of different diameters (500-1000-1500 and 2000 μm) and were subjected to a drying process for 3 hours at 90°C.

Solid state fermentation (SSF)

The dried plant-based wastes (at about the size of 1500 μm) with 30 %(w/v) were weighed at 3 g and were put in Erlenmeyer's of size 100 mL. 10 ML of tap water was added and they were autoclaved at 121°C for 15 minutes. The fermentation medium was inoculated with a 3 mL spore suspensionand the Erlenmeyers were left to stir for 144 hours at the rate of 150 rpm and temperature of 45°C. In order to extract the enzyme, the fermentation medium was diluted with 10 mL of tap water and was left to stir for 30 minutes. At the end of the period, the samples were filtered using sterilized gauze and were centrifuged for 8 minutes at +4°C at the rate of 7000 rpm. α-amylase activity determination was done from the supernatant.

α-amylase activity determination

In our experimental study, Bernfield (1955) method was used to determine the α-amylase activity. At this method, 200 μL of 0.5 % starch solution (0.1 M Sodium-Phosphate buffer pH:7.0) and enzyme solution (150 μL) were mixed and held on 30 minutes for catalytic activity at 37 °C. At the end of this period, 400 μL of DNS (3.5 dinitro salicilic acid) solution was added to the medium as a reaction stopper and was kept for 5 minutes in an ebullient water bath. At the end of this process,

the solution was cooled down to the room temperature after which it was diluted by adding 8 mL of pure water and the absorbance values of the samples were measured using spectrophotometric at 489 nm. All the experimental applications were over agained three times and the averages were determined with a standard deviation.

Protein amount determination

Lowry (Lowry et al., 1951) method was used for protein amount determination. For this process Bovine Serum Albumin (BSA) used as standard.

Determination of the appropriate substrate in SSF and the effect of some physical parameters on the optimal α-amylase production.

In SSFs, determining the most suitable substrate for enzyme production is an important factor. The process of finding the most optimal one for enzyme production entails investigating many agricultural wastes. In this work, while trying to find the optimal temperature and pH for *Bacillus licheniformis* α-amylase production in the fermentation media that had apple, melon, banana and orange peels as substrates, 5 °C increments were applied in the incubation in the interval of 30-70 °C for 144 hours, at intervals of 24 hours while for the pH 1 unit increments were applied in the interval of 4.0-10.0 using 0.1 N HCl and NaOH. In order to determine the optimal inoculum rate, the media were inoculated with different amounts (5, 10, 15, 20,25 30, 35, 40, 45 and %50 (w/v)) of bacteria cultures. In order to determine the effects of the Carbon and Nitrogen sources, %1 of Carbon sources such as starch, maltose, glucose, lactose, fructose galactose, xylose, and sucrose; and organic and inorganic nitrogen sources such as casein, tryptone, yeast extract, urea, Trizone, ammonium sulphate and ammonium nitrate were added to the SSF medium respectively. For determining metal ions effect at 1 mM concentrations of $CaCI_2$, $ZnCI_2$, $CdCI_2$, $HgCI_2$, $Cu(NO_3)_2$, $Co(NO_3)_2$ and $AICI_3$ were added to the fermentation medium at optimal conditions previously determined. The α-amylase activity detection was done according to the standard protocol.

Results and discussion

Parallel to the increasing population of the world, almost 35 % of all the necessary food production goes to waste or gets destroyed. With an increase in the number of fruit processing plants, the amount of fruit waste is increasing which causes new environmental waste issues. Turkey is among the top ten countries in amounts, production area and production processing plants of apples. Most of the apple production in the world is done China, USA and Turkey. Transforming solid wastes that come out of industrial fruit processing plants into valuable products is not only an

effective way to reduce environmental pollution, but is also an important way to contribute to human health and national economies (Suluk et al., 2018). To this end, apple peels, which are produced in abundance as a waste or side product in fruit juice industry, offer potential opportunities to be used for commercial use. An optimal substrate in SSFs provides all the necessary nutrients for microorganisms to grow. The carbon and nitrogen components of the substrate play an important role in a ordinary SSF application. Carbon is an important source of energy which promotes microorganism population development and can be present in basic form such as glucose as well as glucose polymers such as starch. Nitrogen is the second important element that is necessary for the microbial growth and usually it is added through an external nitrogen source to help facilitate and speed up the growth on a specific substrate (López-Gómez et al., 2020). In SSFs, the fermentation time, temperature, pH, moisture, inoculum rate, carbon and nitrogen sources need to be optimized as they are the main factors that affect microbial growth and hence enzyme production (Thippeswamy et al., 2006).

Determining the appropriate substrate and optimal incubation time in SSFs is an important factor that affects the enzyme production cost. The effect of different plant-based wastes and incubation times on the production of α-amylase was investigated. At the 48th hour if incubation, the α-amylase production reached its maximum in the fermentation that had apple peels (Figure 1). The production showed a gradual decline as incubation times got larger. A possible reason for this can be an inhibition caused by the enzyme denaturation and its coaction with other medium components as the incubation period gets extended (Abdel-Fattah et al., 2012).

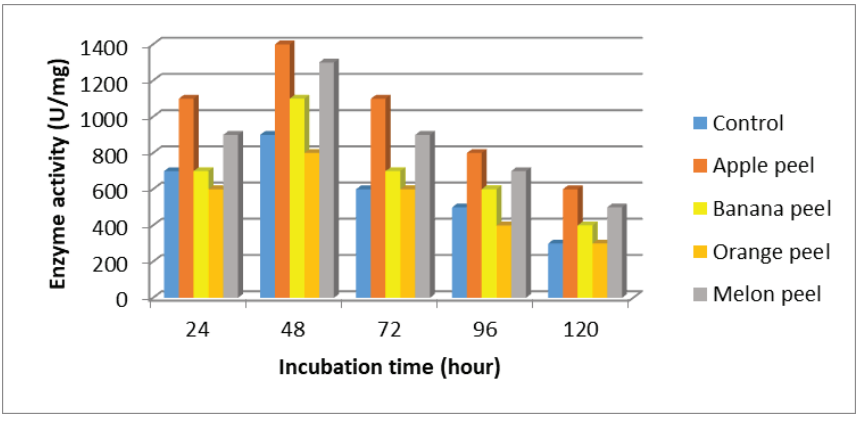

Figure 1. *Effect of different fruit peels and incubation time on α-amilaz production*

Microbial growth and thereby enzyme production affected intensely by temperature which is a vital physical factor (Abdel-Fattah et al., 2012). In order to examine the effect of temperature on the production of

α-amylase, we investigated the incubation of the organism in optimized conditions under different temperatures (30-70 °C). *Bacillus licheniformis* exhibited highest α-amylase production level at 45 °C (Figure 2). There was a decline in the enzyme production at temperatures higher than 45 °C. Most likely, the high temperature suppressed the bacterial growth and thus inhibiting the enzyme formation (Nusrat and Rahman, 2007). The optimal α-amylase production under optimized conditions was achieved at 45 °C, which is very similar to other reported results (Nwagu & Okolo, 2011; El-Shishtawy et al., 2014; Issac & Prince, 2015). The previous results report that the optimal temperature for maximum α-amylase output in the SSF medium were 30, 37, 40 and 50 °C respectively (Raul et al., 2014; Salim et al., 2019; Pranay et al., 2019).

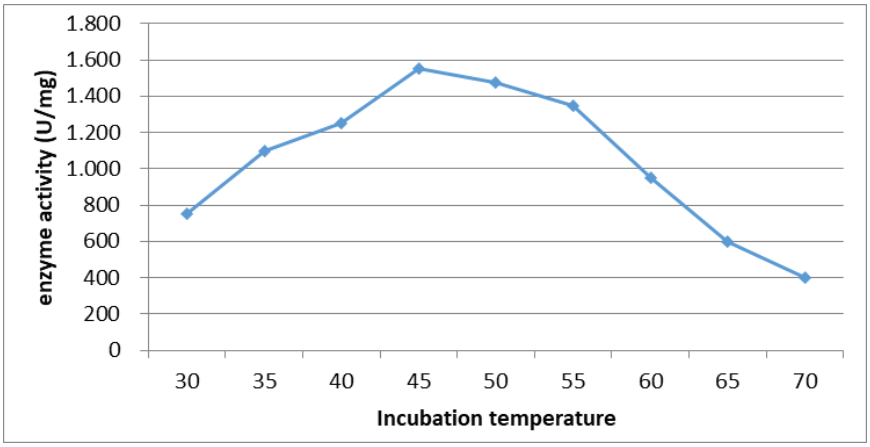

Figure 2. *Effcet of incubation temperature on α-amilaz production*

Previous studies results demonstrated that one of the most sensitive variable physicochemical parameters is pH that affects the SSF (Mitchell et al., 2006; López-Gómez et al., 2020). So that to observe the effect of the preliminary pH on the production of α-amylase, pH values between 4.0 and 10.0 were investigated. When we look at Figure 3 which shows the effect of the onset pH on the α-amylase production by the *Bacillus licheniformis,* we see that the highest enzyme production was achieved at pH 6.0. In the previous works, this has been reported at different pH values of 5.5, 6.5, 7.0, and 8.0 respectively (Balkan & Ertan et al., 2007; Saxena & Singh 2011; Issac & Prince, 2015). In general, most species of *Bacillus* produce maximal amounts of α-amylase at different pH values between 7.0 and 9.0.

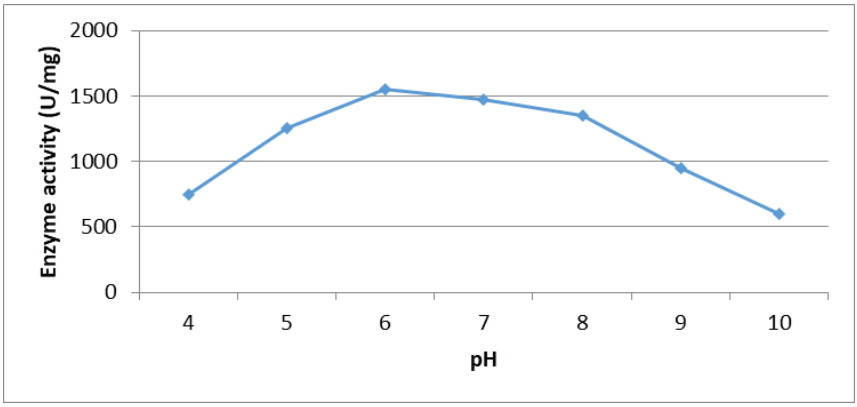

Figure 3. *Effect of medium pH value on α-amilaz production*

The inoculum rate has a significant effect on the α-amylase production in the SFF. According to our results, the maximum α-amylase production from *Bacillus licheniformis* was achieved at the fermentation medium with a 30 %(w/v) inoculum rate (Figure 4). Our results are consistent with other works on enzyme production in media with various inoculum rates (Issac and Prince, 2015; Pranay et al., 2019). The inoculum age and rate is an important parameter for the fermentation efficiency. That is why inoculum rate is an important fermentation factor that needs to be considered at all times.

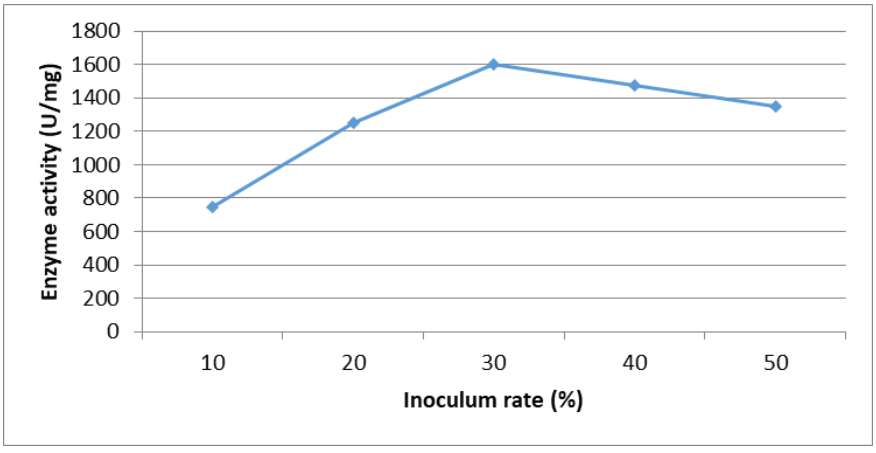

Figure 4. *Effect of inoculum ratio to fermentation medium on α-amilaz production*

When the effect of different source of carbohydrate monomers and polymers were investigated on α-amylase production from *Bacillus licheniformis*, the highest enzyme production was observed in the SFF medium that had 1%s starch (Figure 5). Starch is a widely accepted nutrient compound for the induction of amylolytic enzymes (Lonsane & Ramesh et al., 1990). This results is consistent with many works that report starch

to be a good inducer for α-amylase production (Mukherjee et al., 2009; Maity et al., 2015; Pranay et al., 2019; Almanaa et al., 2020). One possible reason for an increased output of α-amylase, an induceable enzyme, in a fermentation medium with starch can be a gradual metabolization of starch (Abdel-Fattah et al., 2012). On the other hand, a decline in the α-amylase production was observed when some other carbon sources were added to the fermentation medium. Different carbon sources have different effects on extracellular enzymes, especially different types of amylases (Rao & Satyanarayana, 2009).

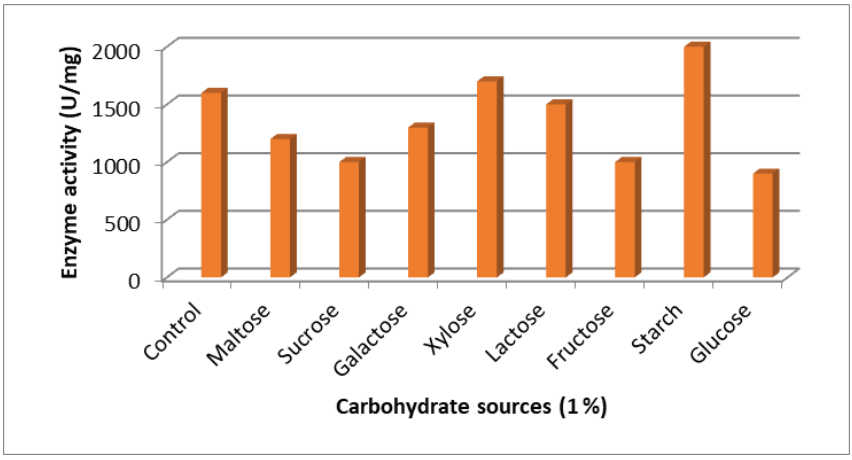

Figure 5. *Effect of different carbohydrate sources on α-amilaz production*

Growth of microorganisms highly influenced from the nitrogen ingredients of the culture media (Far et al., 2020). In this work, when the effect of various inorganic and organic nitrogen sources such as yeast extract, urea, tryptone, casein, tyrosine, ammonium sulphate and ammonium nitrate) at 1% concentration on the α-amylase production from *Bacillus licheniformis* was investigated, the best enzyme production was observed at the yeast extract medium as seen at Figure 6. This could be caused by the yeast extract's supporting effect on the bacterial growth (Dash et al., 2015). However, these necessary nitrogen types can vary from species to species. Similar results have been obtained on *Bacillus* sp. (Elmansy et al., 2018; Pranay et al., 2019); *Bacillus cereus* (Wayne et al., 1987) and *Bacillus subtilis* D19 (Almanaa et al., 2020).

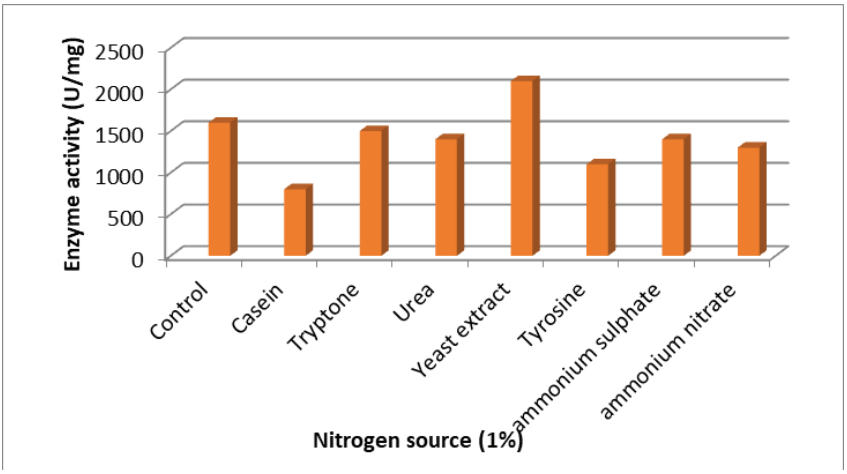

Figure 6. *Effect of different nitrogen sources on α-amilaz production*

When the effect of different metal ions on α-amylase production from *Bacillus licheniformis* was investigated, the highest enzyme production was observed in the SFF medium that had a 1mM concentration of $CaCl_2$ (Figure 7). Due to its presence in α-amylase, Ca^{2+} ions play an important role in α-amylase production and that is why Calcium Chloride ($CaCl_2$) is added to most culture media for producing α-amylase (Far et al., 2020). Similarly, some previous works have also reported that adding Ca^{2+} to the culture media increases the α-amylase production (Sun et al., 2010; Shafiei et al., 2010). The α-amylase production was mostly suppressed in the fermentation media that had $CdCl_2$ and $HgCl_2$.

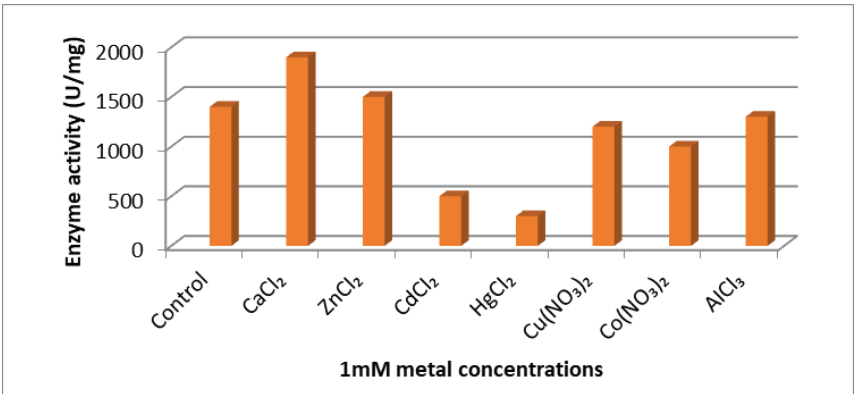

Figure 7. *Effect of metal ions on α-amilaz production*

Conclusion

In recent years, species of bacteria, especially the *Bacillus* type and the related types have gained importance at industrial levels and are seen as a potentially promising α-amylase producers. α-amylase have different

industrial applications. In this respect it is essential to reduce enzyme production costs in industrial fields that use amylases and supply the demand of consumers. It is well known that the process of α-amylase production by microorganisms is affected by several physicochemical factors; namely the combination of substrate, the inoculum rate, the incubation time, pH, temperature, nitrogen and carbon sources and mineral elements. In this study, the bacteria strain, *Bacillus licheniformis*, was inoculated in SSF on media that had apple, melon, banana and orange peels. Among the tested solid substrates, the most efficient α-amylase production was determined in the medium with apple peels. When physical factors that affect the enzyme production such as fermentation time, fermentation temperature, initial pH and inoculum rate were investigated, maximum enzyme production was observed at 45 °C, pH 6.0, 35 % inoculum rate, and at the 48th hour. An increase in α-amylase production was observed when 1% starch and yeast extract were added. The results show that the new biological transformation of apple peels that are used as substrates in SFFs for α-amylase production provides an ideal system. The biomass that remains after the fermentation can be removed or reuseable for to produce other microbial products such as bioethanol, organic acids, vitamines etc. Finally, these applications can also help prevent environmental pollution that these agricultural wastes can cause in apple producing countries including Turkey.

Acknowledgements

This study was financialy supported by Scientific Research Projects Unit of Mardin Artuklu University (Project no: MAÜ-BAP-15-SHMYO-01).

REFERENCES

Abdel-Fattah, Y. R., Soliman N. A., El-Toukhy, N. M., El-Gendi, H., & Ahmed, R. S. (2012). Production, Purification and Characterization of Termostable α-amilase Produced by *Bacillus licheniformis* Isolate AI20. *Journal Chemistry*, 2013: 1–11.

Goyal, N., Gupta, J. K., & Soni, S. K. (2005). A novel raw starch digesting thermostable α-amylase from *Bacillus* sp. I-3 and its use in the direct hydrolysis of raw potato starch. *Enzyme Microbial Technology*, 37 (2005) 723–734.

Balkan, B, & Ertan, F. (2007). Production of α-Amylase from *Penicillium chrysogenum* Under Solid State Fermentation by Using Some Agricultural By-Product. *Food Technolology and Biotechnology*, 45: 439-442.

Shiau, J. R., Hung, H. C., & Jeang, C. L. (2003). Improving the thermostability of raw starch digesting amylase from a *Cytophaga* sp. by site directed mutagenesis. *Applied Environmental Microbiology*, 69: 2383–2385.

Almanaa, T. N., Vijayaraghavan, P., Alharbi, N. S., Kadaikunnan, S., Khaled, J. M., & Alyahya, S. A. (2020). Solid State Fermentation of Amylase Production from *Bacillus subtilis* D19 using Agro-Residues. *Journal of King Saud University-Science*, 32 (2): 1555-1561.

Bernfield, P, (1955). Amylases, α and β. In, Methods in Enzymology, Vol. 1, pp. 149-158. *Academic Press*, New York, USA.

Dash, B. K., Rahman, M. M., & Sarker, P. K. (2015). Molecular İdentification of a Newly Isolated *Bacillus subtilis* BI19 and Optimization of Production Conditions for Enhanced Production of Extracellular Amylase. *BioMed Research International*, 2015 (ID: 859805): 1-9.

Elmansy, E. A., Asker, M. S., El-Kady, E. M., Hassanein, S. M., & El-Beih, F. M. (2018). Production and Optimization of α- Amylase from Thermo-Halophilic Bacteria Isolated from Different Local Marine Environments. *Bulletin of the National Research Centre*, 42 (31): 1-9.

El-Shishtawy, R. M., Mohamed, S. A., Asiri, A. M., Gomaa, A. M., Ibrahim, I. H., & Al-Talhi H. A. (2014). Solid Fermentation of Wheat Bran for Hydrolytic Enzymes Production and Saccharification Content by a Local Isolate *Bacillus megatherium*. *BMC Biotechnology*, 14 (29): 1-8.

Far, B. E., Ahmadi, Y., Khosroushahi, A. Y., & Dilmaghani, A. (2020). Microbial Alpha-Amylase Production: Progress, Challenges and Perspectives. *Advanced Pharmaceutical Bulletin*, 10 (3): 350-358.

Gupta, R., Gigras, P., Mohapatra, H., Goswami, V.K., & Chauhan, B. (2003). Microbial α-amylases: A biotechnological perspective. *Process Biochemistry*, 38: 1599–1616.

Issac, R., & Prince, R. (2015). Production of Alpha-Amylase by Solid State Fermentation using *Bacillus cereus* MTCC 7524 and *Bacillus licheniformis* MTCC 7445 from Dairy Sludge-A Comparative Study. *International Journal of Pharmtech Research*, 8: 111-117.

López-Gómez, J. P., Manan, M, A., & Webb, C. (2020). Solid-State Fermentation of Food İndustry Wastes: In Food Industry Wastes (Second Edition). Elsevier, pp, 135-161. London-United Kingdom.

Lowry, O. H., Rosebrough, N. J., Farr, A., L., & Randall, R. J. (1951). Protein Measurement with the Folin-Phenol Reagents. *Journal of Biology and Chemistry*, 48: 17-25.

Lonsane, B, K., & Ramesh M. V. (1990). Production of bacterial thermostable alphaamylase by solid-state fermentation: a potential tool for achieving economy in enzyme production and starch hydrolysis. *Advances in Applied Microbiology*, 35: 1-56.

Maity, S., Mallik, S., Basuthakur, R., & Gupta, S. (2015). Optimization of Solid State Fermentation Conditions and Characterization of Thermostable Alpha Amylase from *Bacillus subtilis* (ATCC 6633). *Journal of Bioprocessing and Biotechniques*, 5 (4): 1-7.

María, A. C., Ravanal, C., Andrews, B. A., & Asenjo, J. A. (2019). Heterologous Expression and Biochemical Characterization of a Novel Cold-Active α-Amylase from the Antarctic Bacteria *Pseudoalteromonas* sp. 2-3. *Protein Expression and Purification*, 155: 78-85.

Melnichuk, N., Braia, M. J., Anselmi, P. A., Meini, M. R., & Romanini, D. (2020). Valorization of Two Agroindustrial Wastes to Produce Alpha-Amylase Enzyme from *Aspergillus Oryzae* by Solid State Fermentation. *Waste Management*, 106: 155-161.

Mitchell, D. A., Berovic, M., & Krieger, N. (2006). Introduction to Solid-State Fermentation Bioreactors. In: Solid-State Fermentation Bioreactors: *Fundamentals of Design and Operation*, Springer-Verlag, Berlin, Heidelberg, pp 33-45.

Msarah, M. J., Ibrahim, I., Hamid, A. A., & Aqma, W. S. (2020). Optimisation and Production of Alpha Amylase from Thermophilic *Bacillus* spp. and İts Application in Food Waste Biodegradation. *Heliyon*, 6 (6): 1-9.

Mukherjee, A. K., Borah, M., & Rai, S. K. (2009). To Study The Influence of Different Components of Fermentable Substrates on Induction of Extracellular α-Amylase Synthesis by *Bacillus subtilis* DM-03 in Solid-State Fermentation and Exploration of Feasibility for Inclusion of α-Amylase in Laundry Detergent. *Biochemical Engineering Journal*, 43 (2): 149-156.

Nusrat, A., & Rahman, S. R. (2007). Comparative Studies on the Production of Extracellular α-Amylase by Three Mesophilic *Bacillus* Isolates. *Bangladesh Journal of Microbiology*, 24 (2): 129-132.

Nwagu, T. N., and Okolo, B. N. (2011). Extracellular Amylase Production of a Thermotolerant *Fusarium* sp. Isolated from Eastern Nigerian Soil. *Brazilian Archives of Biology and Technology*, 54 (4): 649-658.

Ozdemir, S., Agüloğlu, F. S., Karakaya, A., & Enez, B. (2018). A novel raw starch hydrolyzing thermostable α-amylase produced by newly isolated *Bacillus mojavensis* SO-10: purification, characterization and usage in starch industries, *Brazilian Archives of Biology and Technology*, 61, e18160399.

Pranay, K., Padmadeo, S. R., & Prasad, B. (2019). Production of Amylase from *Bacillus subtilis* sp. Strain KR1 Under Solid State Fermentation on Different Agrowastes. *Biocatalysis and Agricultural Biotechnology*, 21 (ID: 101300): 1-8.

Raul, D., Biswas, T., Mukhopadhyay, S., Das, S. K., & Gupta, S. (2014). Production and Partial Purification of Alpha Amylase from *Bacillus subtilis* (MTCC 121) Using Solid State Fermentation. *Biochemistry Research International*, (ID: 568141): 1-5.

Rao, U. M. J. L., & Satyanarayana, T. (2009). Hyperthermostable, Ca2+ Independent, and High Maltose-Forming *α*-amylase Production by an Extreme Thermophile *Geobacillus thermoleovorans*: Whole Cell Immobilization. *Applied Biochemistry and Biotechnology*, 159: 464-477.

Sahnoun, M., Kriaa, M., Elgharbi, F., Ayadi, D. Z., Bejar, S., & Kammoun, R. (2015). *Aspergillus oryzae* S2 Alpha-Amylase Production Under Solid State Fermentation: Optimization of Culture Conditions. *International Journal of Biological Macromolecules*, 75: 73-80.

Salim, A. A., Grbavcic, S., Sekuljica, N., Sekulic, M. V., Jovanovic, J., Tanaskovic, S J., Lukovic, N., & Knezevic-Jugovic, Z, 2019. Enzyme Production by Solid-State Fermentation on Soybean Meal: A Comparative Study of Conventional and Ultrasound-Assisted Extraction Methods. *Biotechnology and Applied Biochemistry*, 66 (3): 361-368.

Saxena, R., & Singh, R., (2011). Amylase Production by Solid-State Fermentation of Agro-Industrial Wastes Using *Bacillus* sp. *Brazilian Journal of Microbiology*, 42 (4): 1334-1342.

Shafiei, M., Ziaee, A. A., & Amoozegar, M. A. (2010). Purification and biochemical characterization of a novel SDS and surfactant stable, raw starch digesting, and halophilic α-amylase from a moderately halophilic bacterium, *Nesterenkonia* sp. strain. *Process Biochemistry*, 45: 694–699.

Silva, I. F., Langbehn, R. K., Silva, R. G. C., Pantoja, L. D. A. , Vanzela, A. P. F. C., & Santos, A. S. D. (2016). α-amylase Production by *Bacillus Amyloliquefaciens* Utilizing Macauba Cake (*Acrocomia aculeata*) and Peach Palm Flour (*Bactris gasipaes*-Kunth) as Substrates. *Biocatalysis and Biotransformation*, 34 (2): 76-82.

Steudler, S., Werner, A., & Walther, T. (2019). It Is the Mix that Matters: Substrate-Specific Enzyme Production from Filamentous Fungi and Bacteria Through Solid-State Fermentation. *Advances in Biochemical Engineering Biotechnology*, 169: 51-81.

Sun, H. Y., Zhao, P. J., Ge, X. Y., Xia, Y. J., Hao, Z. K., Liu, J. W., & Peng, M. (2010). Recent advances in microbial raw starch degrading enzymes. *Applied Biochemistry and Biotechnology*, 160; 988-1003.

Thippeswamy, S., Girigowda, K., & Mulimani, V. H. (2006). Isolation and identify cation of α-amylase producing Bacillus sp. from dhal industry waste. *Indian Journal of Biochemistry & Biophysics*, 43: 295-298, 2006.

Tiwari, S. P., Srivastava, R., Singh, C. S., Shukla, K., Singh, R. K., Singh, P., Singh, R., Singh, N. L, & Sharma, R. (2015). Amylases: An Overvıew with Special Reference to Alpha Amylase. *Journal of Global Biosciences*, 4 (1): 1886-1901.

Wayne, L. G., Brenner, D. J., Colwell, R. R., Grimont, P. A. D., & Kandler, O. (1987). Report of the ad hoc committee on reconciliation of approaches to bacterial systematics. *International Journal of Systematic and Evolutionary Microbiology*, 37: 463-464.

Chapter 6

SOME EXAMPLES FOR SCHIFF BASE METAL COMPLEXES TO REFLECT THEIR CATALYTIC ACTIVITIES

Barbaros AKKURT[1]
Altuğ Mert SEVİM[2]

1 Lecturer, PhD, İstanbul Technical University, Mustafa İnan Central Library, Maslak 34469, Sarıyer-İstanbul.
2 Assoc. Prof. Dr., İstanbul Technical University, Faculty of Science and Letters, Department of Chemistry, Maslak 34469, Sarıyer-İstanbul.

Schiff bases were discovered by Hugo Schiff (1834-1915) and are products of aldehydes or ketones with primary amines; the resulting condensation products are highly sought in coordination chemistry, hence the metal ions inside the coordination cavity causes a plethora of catalytic activities. Salen and salophen (see Figure 1) are among the most investigated Schiff bases since their preparation is easy and they are obtained with fair yields. Both of them have the ONNO donor set with tetradentate chemistry. In this work, we will give some examples from the literature, in the form of research articles and review articles, to show the reader their possible applications.

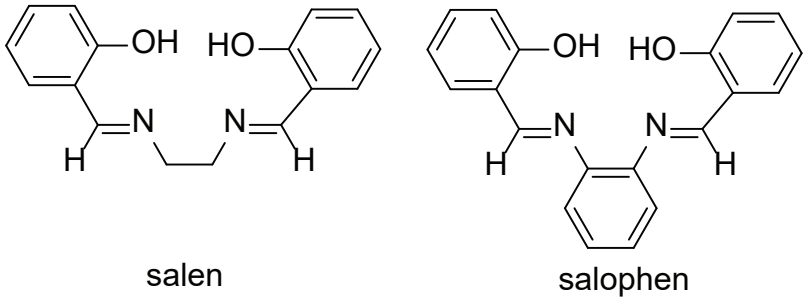

Figure 1. *The structures of salen and salophen.*

Chemical catalysis

Click reaction: Abbaspour and coworkers prepared 1,2,3-triazoles with a click reaction, in which a copper(II) salophen complex and sodium ascorbate served as catalysts and the starting compounds were based on 1,4-naphthoquinone which contains one or two prop-2-yn-1-ol moieties. The reaction times were short, reactions were conducted in room temperature, operational conditions were simple, and reaction yields are high to excellent (see Scheme 1; Abbaspour et al., 2018).

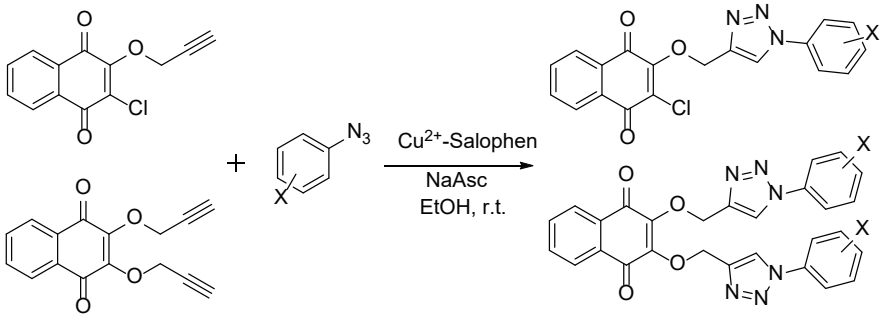

Scheme 1. *Copper(II) salophen-catalyzed click reaction.*

Conversion of carbon dioxide: Aomchad and coworkers investigated the presence of group III metals, namely scandium and yttrium complexed with salen-type Schiff bases, as catalysts of carbon dioxide reacting

with epoxides, finally forming cyclic carbonates (see Schemes 2 and 3; Aomchad et al., 2020).

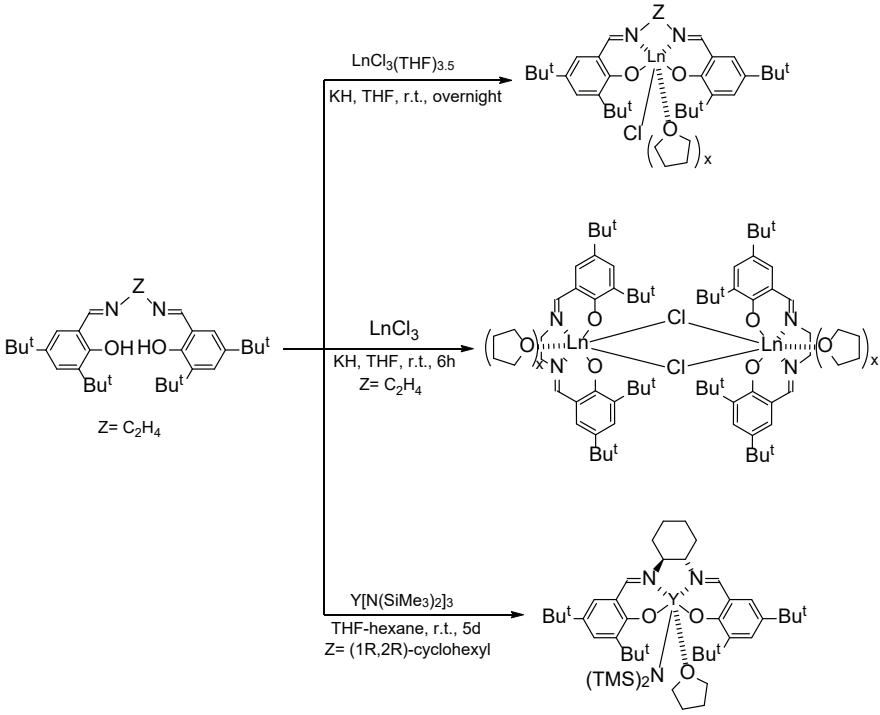

Scheme 2. *Structures of the formed complexes.*

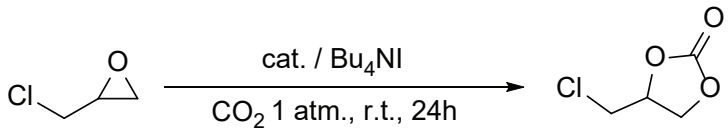

Scheme 3. *An example catalytic reaction between an epoxide and carbon dioxide.*

Copolymerization of propylene oxide (PO) and CO_2: For the copolymerization of PO/CO_2, cobalt salen complexes were used. Interestingly, the presence of oxygen gas proved a valuable co-catalyst and the reaction reached 100% of the synthesis of cyclic carbonate. Electrophility is an important parameter in letting oxygen gas a co-catalyst in the reaction. (See Figure 2; Duan et al., 2020)

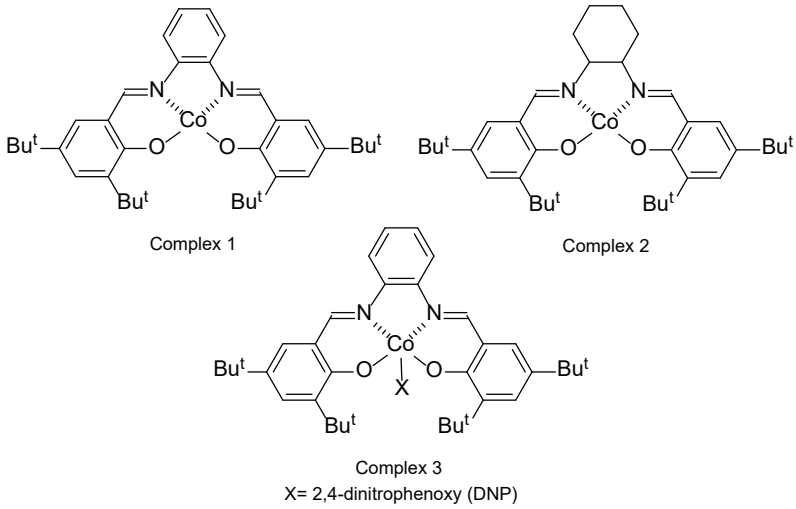

Figure 2. *The salophen and reduced salophen complexes used in the study.*

Green oxidation of sulfides: Niakan et al. have prepared an amidoamine-based dendrimeric core and synthesize a salen-derived chloroiron(III) Schiff base complex from this core. The heterogeneous catalyst was based on magnetite nanoparticles. This catalytic system was applied to the green oxidation of methylphenyl sulfide. The prepared catalyst was active even after five cycles (see Schemes 4 and 5; Niakan et al., 2020).

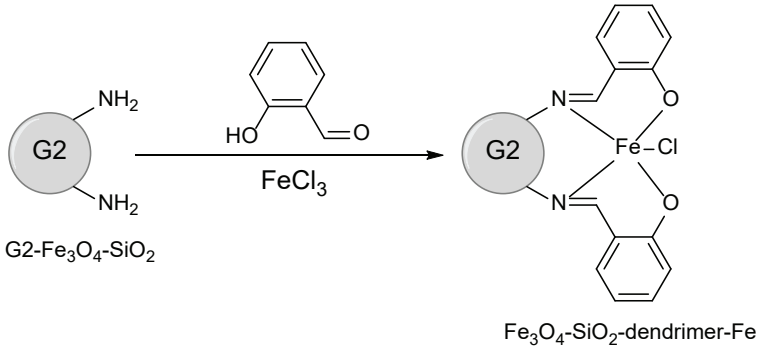

Scheme 4. *Preparation of iron-schiff base-magnetite catalytic system.*

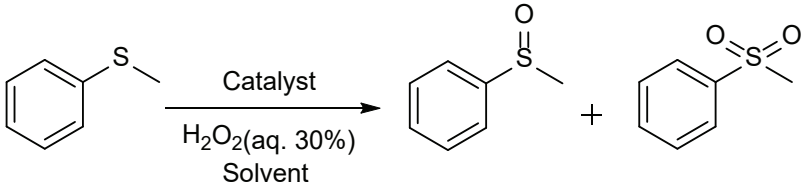

Scheme 5. *An example green oxidation of methylphenyl sulfide.*

Catalytic sulfide oxidation: Photolabile salen-chromium(III) chlorate or bromate was subjected to visible light and the result is exactly the same as the product (chromium(V)-oxo species) that was obtained with chemically oxidation by means of $PhI(OAc)_2$. In this study, chromium(III) salen complexes effectively catalyzed the oxidation of aryl sulfides to the corresponding sulfoxides with $PhI(OAc)_2$, with the presence of small amounts of water. (See Scheme 6; Klaine et al., 2020).

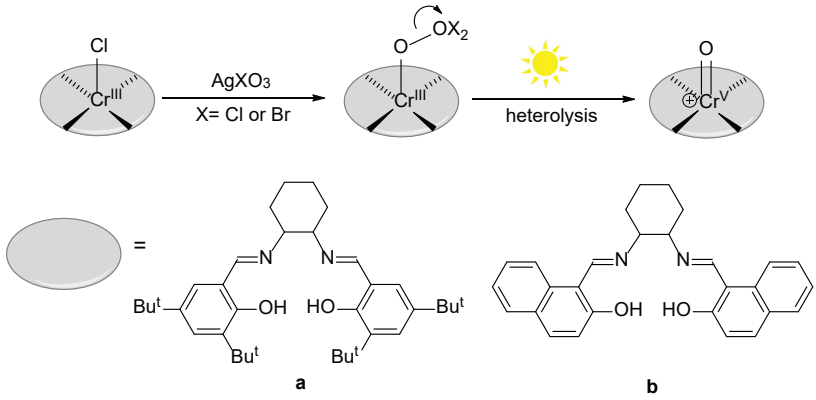

Scheme 6. *Visible light-induced oxidation of Cr(III)-reduced salophen complexes.*

Sulfoxidation of phenylmercaptoacetic acids: Kavitha and Subramaniam published two articles about sulfoxidation of phenylmercaptoacetic acids, leading to phenylsulfinylacetic acid as sole product, in which oxovanadium salen complex was the catalyst and hydrogen peroxide was the oxidant. The active oxidizing species was found to be hydroperoxovanadium(V) (See Scheme 7; Kavitha & Subramaniam, 2020a) , (Kavitha & Subramaniam, 2020b).

Heterogeneous Fenton-like catalytic activity: Keikha et al. used pyridine and thiolate anchoring groups to prepare modified γ-Fe_2O_3 nanocomposites with sizes around 20 nm. Coordinative attachment was provided with Fe(III) and Mn(III)-salophen complexes. They were exploited for the degradation of rhodamine B, methylene blue, methyl orange, and crystal violet with hydrogen peroxide as the oxidizing agent. Thiolate binding was found to provide better results than the pyridine binding (See Scheme 8 and 9; Keikha et al., 2019).

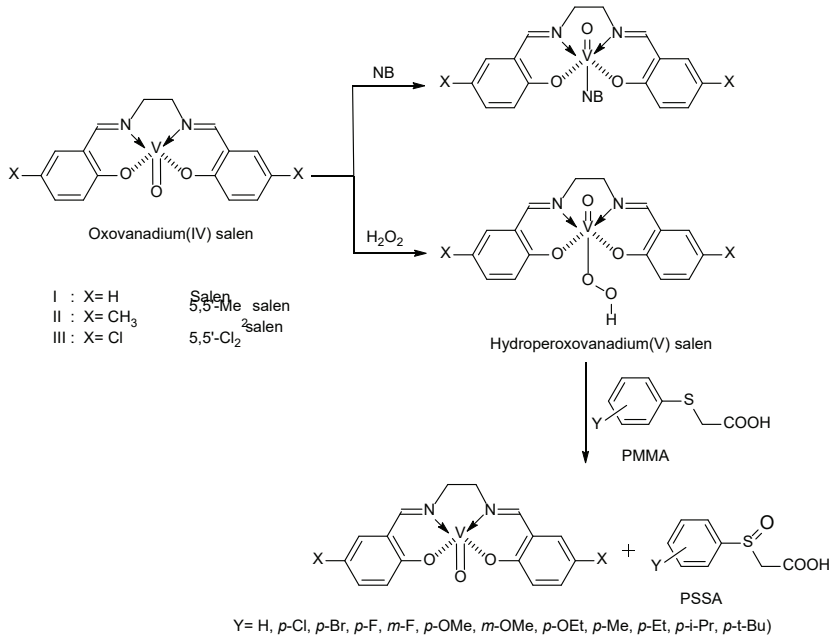

Scheme 7. *The catalytic reaction between oxovanadium salen complex and phenylmercaptoacetic acid.*

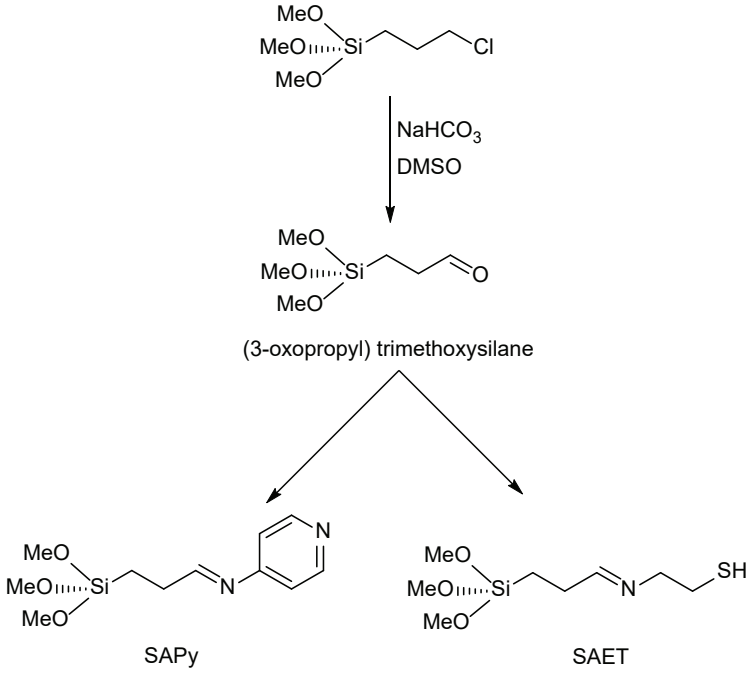

Scheme 8. *Preparation of thiolate- and pyridine-ended silane molecules.*

Heterogeneous carbon dioxide reduction: In a publication by Kong et al., molecular catalysts with a high ability to bind CO_2 coordination to the metal site to enhance their catalytic performance in the electroreduction of CO_2. Co-salophen and Co-salen were effective catalysts by coordinating CO_2, increasing its activity (See Schemes 8 and 9; Kong et al., 2020).

Cycloaddition of CO_2 to epichlorohydrin: Ullah et al. have prepared chloroaluminum ONO hydrazone complexes and they were subjected to the solvent-free chemical fixation of carbon dioxide with epoxides at ambient pressure. It was found out that the epoxide is opened by the metal center, forming an alkoxide ion, and this activates carbon dioxide at the same time (See Schemes 10 and 11; Ullah et al., 2019).

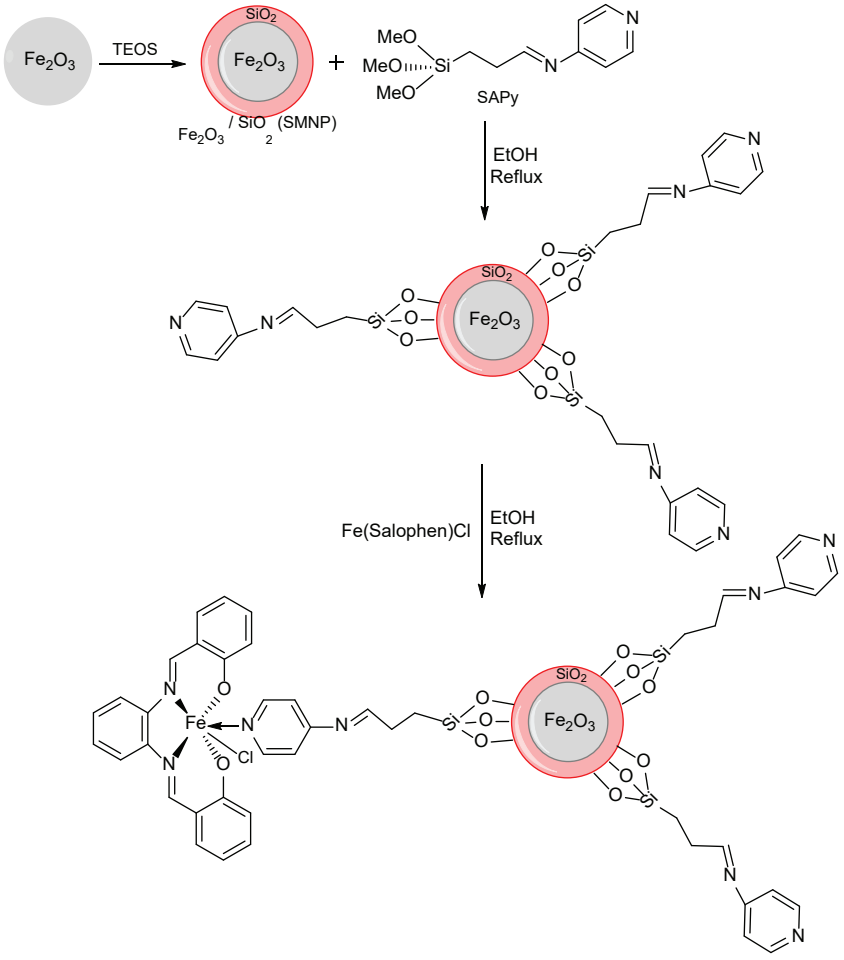

Scheme 9. *Preparation of thiolate- and pyridine-terminated nanocomposites.*

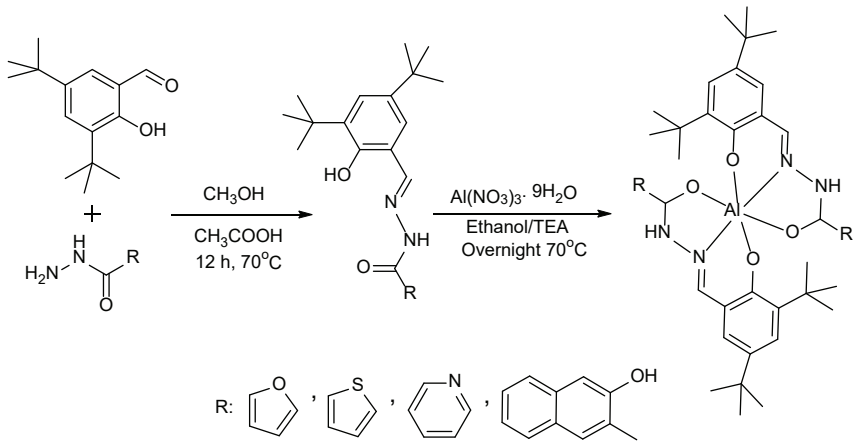

Scheme 10. *The structure of aluminum complexes.*

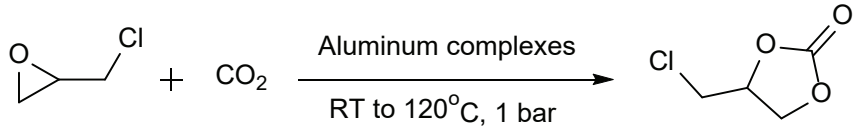

Scheme 11. *The reaction between the epoxide and carbon dioxide, yielding a cyclic carbonate.*

Phenol hydroxylation: Kumari and Ray prepared zeolite-encapsulated Ni(II) Schiff base complexes and applied them to phenol oxidation. Two different types of ligands, that is, having 1,2- and 1,3-diamino groups, were tried (See Figure 3 and Scheme 12; Kumari & Ray, 2020).

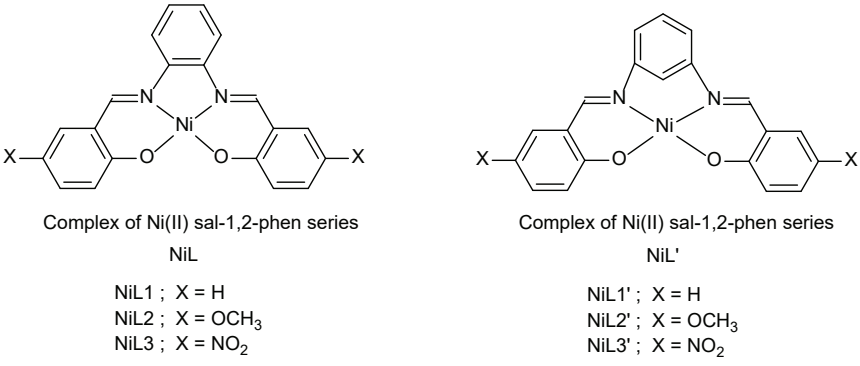

Figure 3. *The Schiff base Ni(II) complexes employed for the oxidation reaction of phenol.*

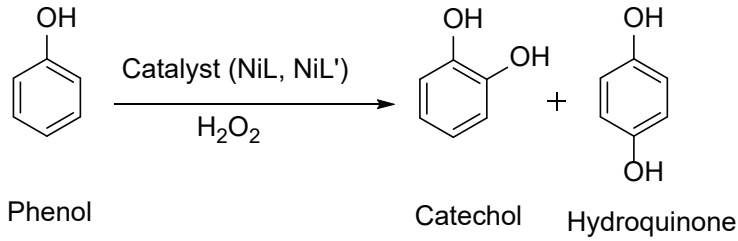

Scheme 12. *The catalytic oxidation of phenol.*

Olefin epoxidation: Pour et al. prepared a new heterogeneous Schiff base ligand having a loose OH group, synthesized the copper complex, and reacted with graphene oxide (containing COOH groups on the periphery) to obtain an ester. This covalently bound Schiff base complex and graphene oxide system was applied to the oxidation of olefins with hydrogen peroxide with sodium hydrogen carbonate and most strikingly, cyclohexene gave 100% conversion, without any by-products. Similarly, nonbornene yielded 100% conversion and 93% selectivity. The authors argue that the likely π-π interaction between graphene oxide and the Schiff base's aromatic rings is that what made the catalytic system so effective. The catalytic system was intact up to four catalytic runs (See Scheme 13; Pour et al., 2019).

Synthesis of bis(indolyl) methane derivatives: Qiao and their co-workers synthesized an air-stable μ-oxo bridged titanium(IV) salophen perfluorooctanesulfonate and applied to the synthesis of bis(indolyl) methane derivatives, which are the key components of many biological molecules. The catalytic system was intact up to five runs (See Schemes 14 and 15; Qiao et al., 2020).

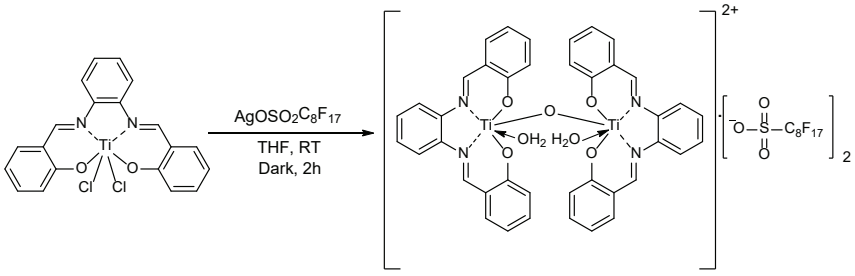

Scheme 14. *The synthetic procedure of the Schiff base titanium complex.*

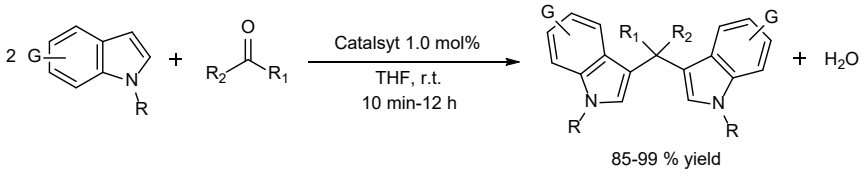

Scheme 15. *The catalytic synthesis of bis(indolyl)methanes from indoles and carbonyl compounds.*

Lactide polymerization: Rae and their co-workers prepared air-stable Aluminum salen Schiff base complexes and used them in the lactide polymerization studies. Their work about the mechanistic approach of the reaction revealed that an excess of epoxide led to classical hexacoordinated Jacobsen system whereas smaller amounts of the epoxide led to pentacoordinated species, both of which are highly active. (See Schemes 16 and 17; Rae et al., 2020).

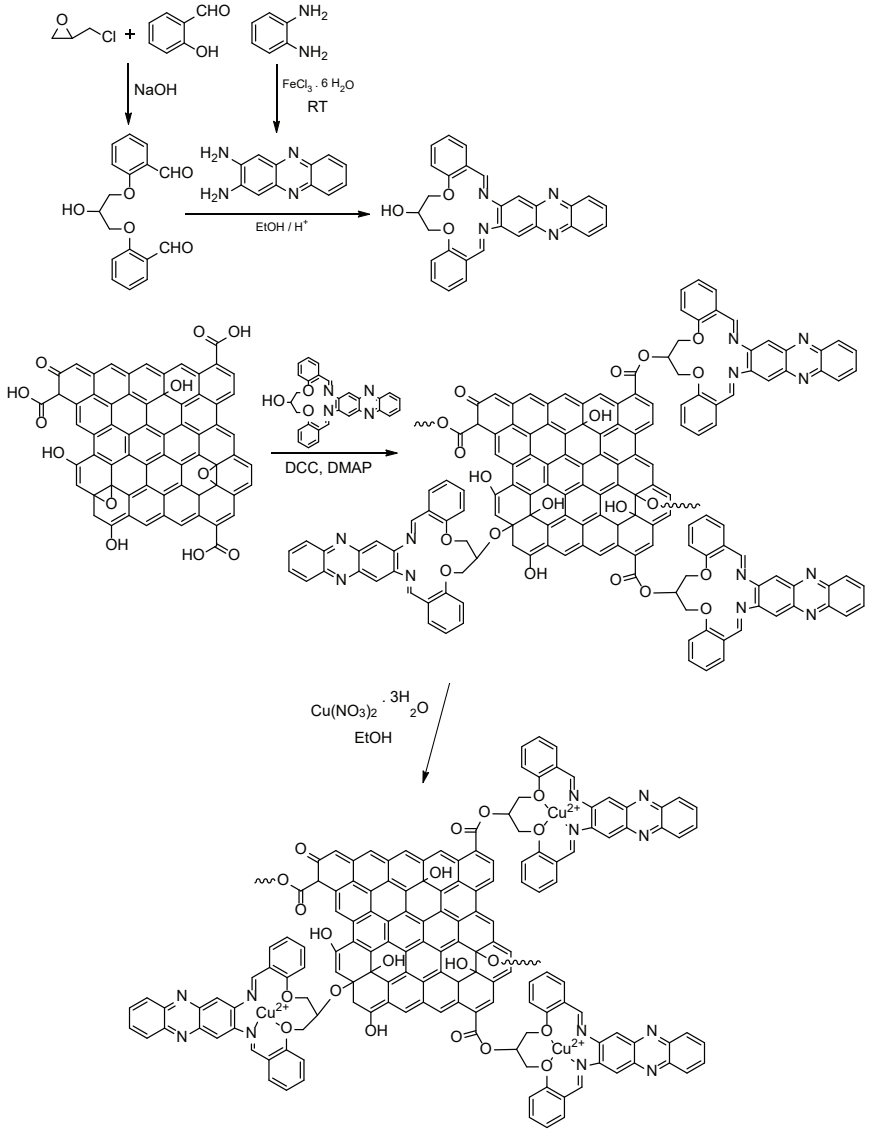

Scheme 13. *Preparation of GO-supported macrocyclic Schiff base Cu complex.*

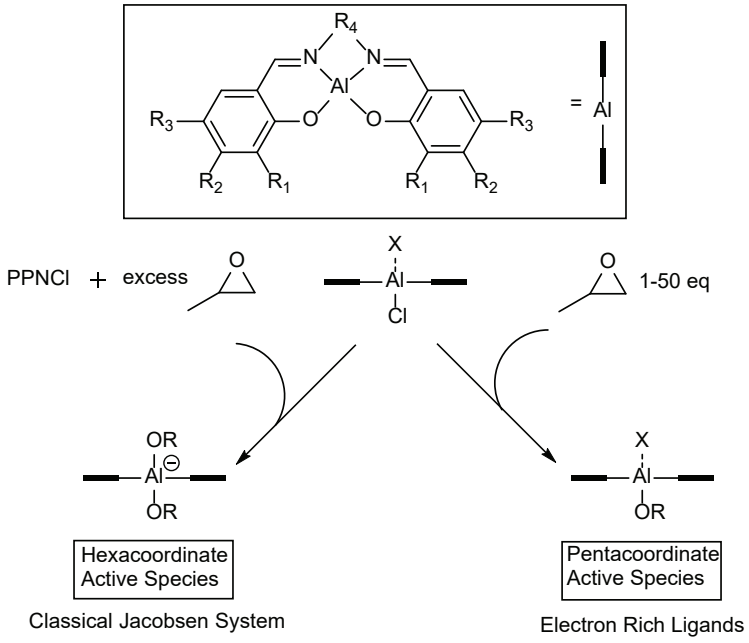

Scheme 16. *Comparison of the initiation mechanisms of polymerization, as based on the amount of epoxide.*

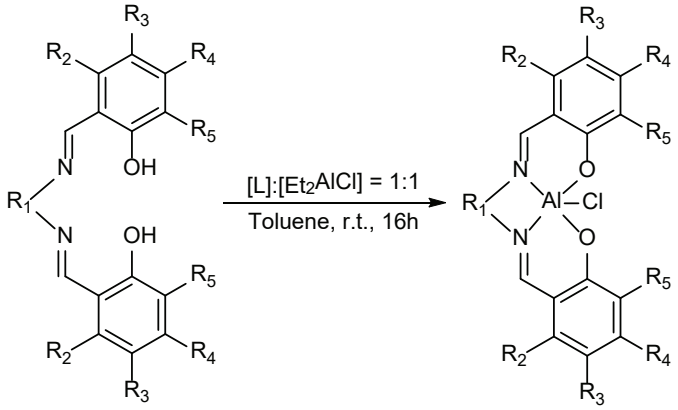

Scheme 17. *Preparation of the Al-Schiff base complex.*

Selective Aerobic Oxidative Cross-Coupling: Reiss et al. used a Co(II)salen complex for the coupling between electron-rich phenols and 2-naphthols. In the reaction, a liberated phenoxyl radical is coupled to another ligated 2-naphthoxy radical. Two Co-salen complexes were found to be scalable and sustainable, and could catalyze the reaction efficiently. Several catalysts were tried in the reaction between a phenol and a naphthol, and Co(II)salen-derived complex was very effective in yielding almost only the phenol-naphthol coupling product (See Scheme 18; Reiss et al., 2019).

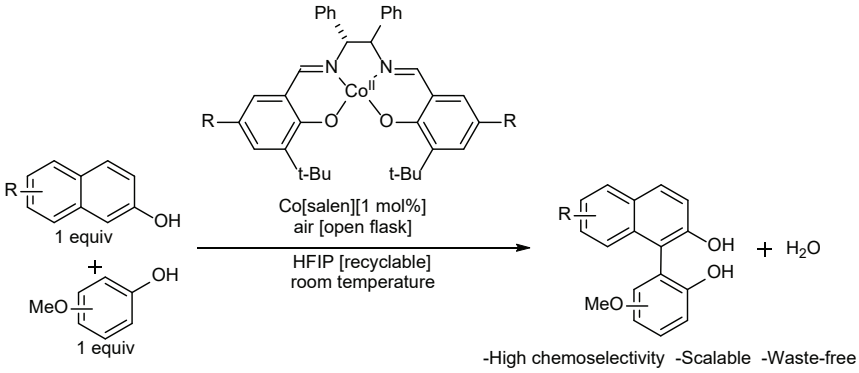

Scheme 18. *Catalytic coupling of phenols and naphthols in the presence of a Co(II)salen complex.*

Ring-opening copolymerization of epoxycyclohexane and phthalic anhydride: Epoxycyclohexane and phthalic anhydride were copolymerized in the presence of bis(triphenylphosphine)iminium chloride (PPNCl) and a non-symmetrical chlorochromium(III) salen complex as the catalytic entity. More than 90% ester linkages were found in the resulting polyester structure (See Schemes 19 and 20; Shi et al., 2020).

Electrocatalysis

Heterogeneous electrohydrocyclization: Polymer-support and zeolite-encapsulated nickel salen complexes and their homogeneous counterparts were examined in a electrohydrocyclization reaction. Heterogeneous catalysts, according to the bulk electrolytic experiments, were found to be superior than the homogeneous ones (See Scheme 21; Clendenin, 2019).

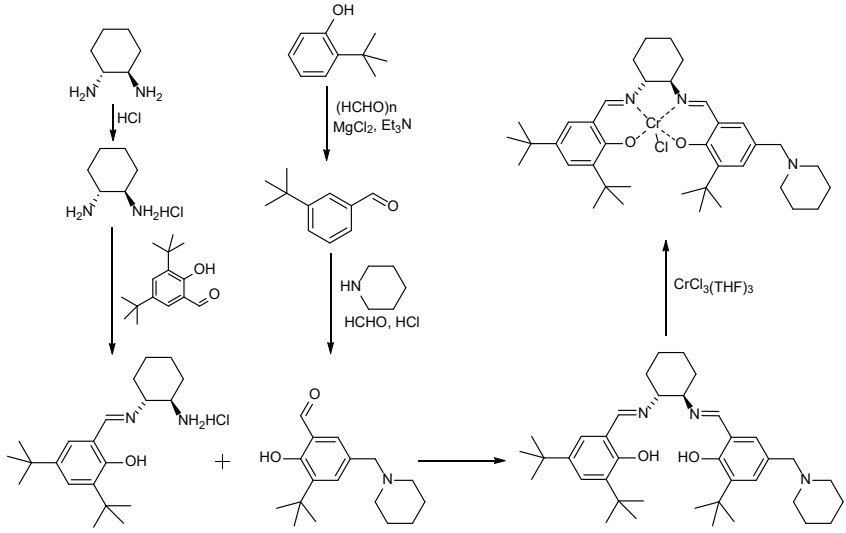

Scheme 19. *Formation of the ligands and the Cr(III) complex.*

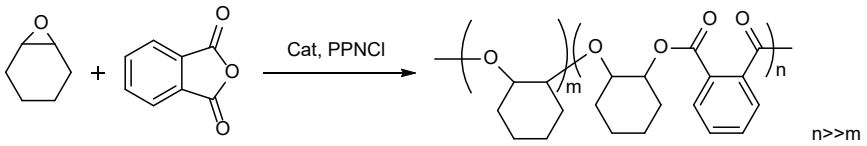

Scheme 20. *The catalytic reaction between an epoxide and phthalic anhydride.*

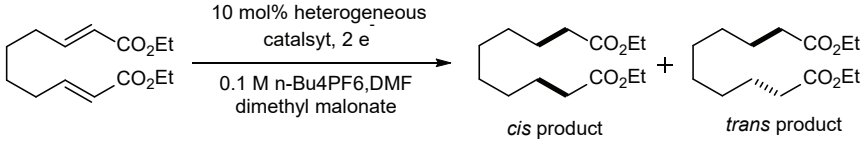

Scheme 21. *Electrohydrocyclization reaction in the presence of the prepared heterogeneous catalyst.*

Electrocatalytic water oxidation: Aligholivand et al. prepared a salophen-derived Schiff base and its Ni(II) complex to research the oxidation of water, in which the classical three electrode setup consisted of a carbon paste electrode modified by the Ni(II) salophen-type complex. Three different pH values, viz. pH = 3, 7, and 11, were studied. There were significant progress in the oxidation of water with this catalytic setup (See Figures 4-7; Aligholivand et al., 2019).

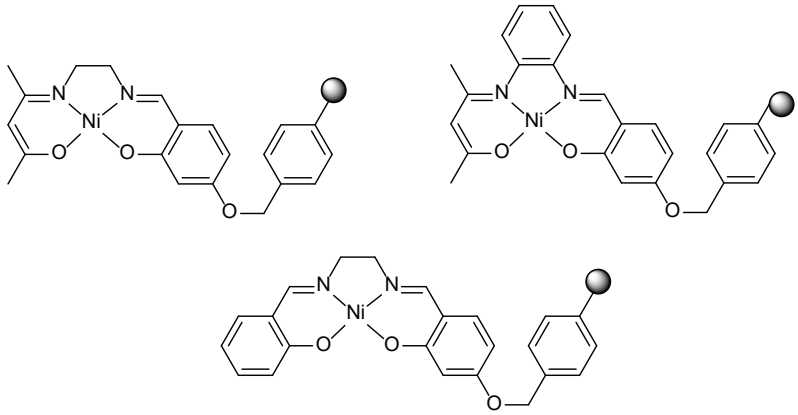

Figure 4. *Merrifield Ni-salen complexes.*

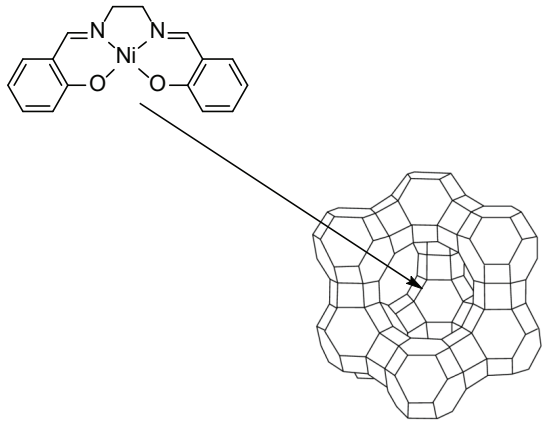

Figure 5. *The structure of Ni(salen) Zeolite Y catalyst.*

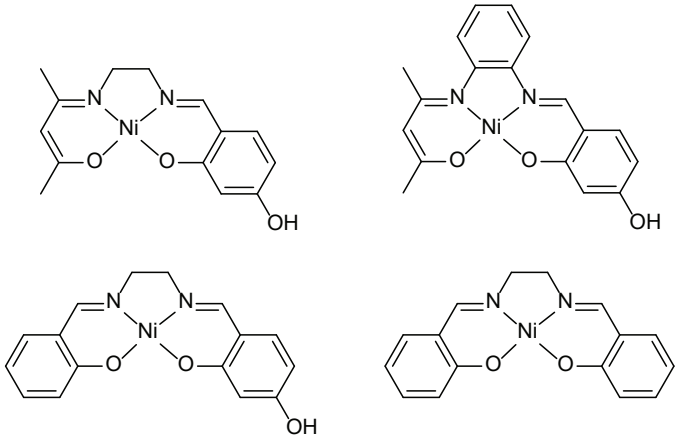

Figure 6. *Homogeneous Ni(salen) and (salophen) catalysts.*

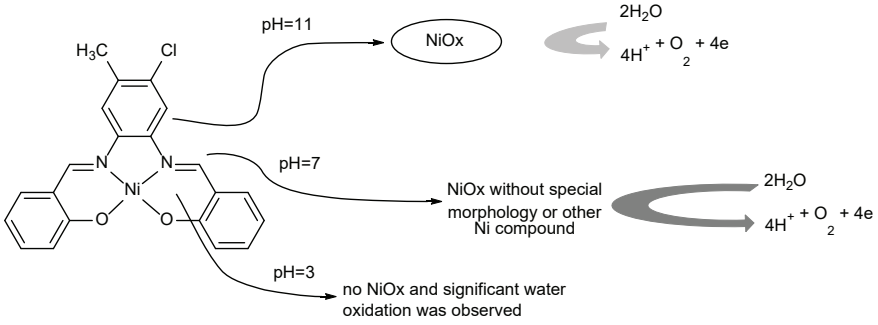

Figure 7. *Water oxidation performances of the catalytic entity at different pH values.*

Oxygen reduction reaction: Oxovanadium-4-methylsalophen complex (VOL) was employed to assess the performance of the complex in the oxygen reduction reaction (ORR), in the presence of ferrocene as a weak electron

donor. The setup is based on the interface of two immiscible solvents. The ability of reduction of oxygen by ferrocene was increased by the VOL complex. VOL complex has four positions to hold a proton and then they could be transferred to oxygen, producing water and hydrogen peroxide. Theoretical calculations showed that the oxygen in V=O moiety is the best place for the transfer of proton and electron to the molecular oxygen (See Figures 8-10; Kamyabi et al., 2021).

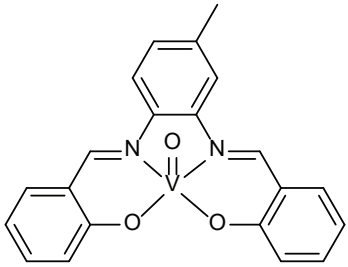

Figure 8. *The molecular structure of VOL.*

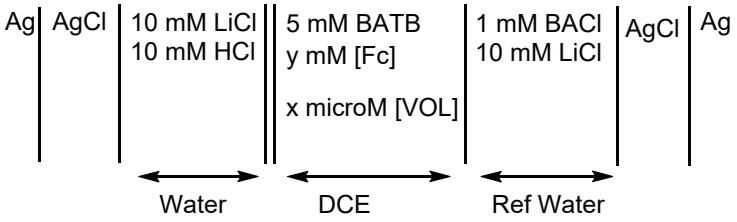

Figure 9. *The composition of the electrochemical cell.*

Catalytic hydrogen evolution in water: Khandelwal and their co-workers have found out that an inactive metal complex could be submitted for activation via using the outer sphere functionalities. They prepared cobalt(II) salen-type complexes from amino acids and amines. In Figure 12, their prepared complexes can be examined. This indeed can open new ways to prepare efficient catalysts for other small molecules' activation, involving proton transfer. The COOH groups are potential H donors towards the metallic site to produce H_2 (See Scheme 22; Khandelwal et al., 2019).

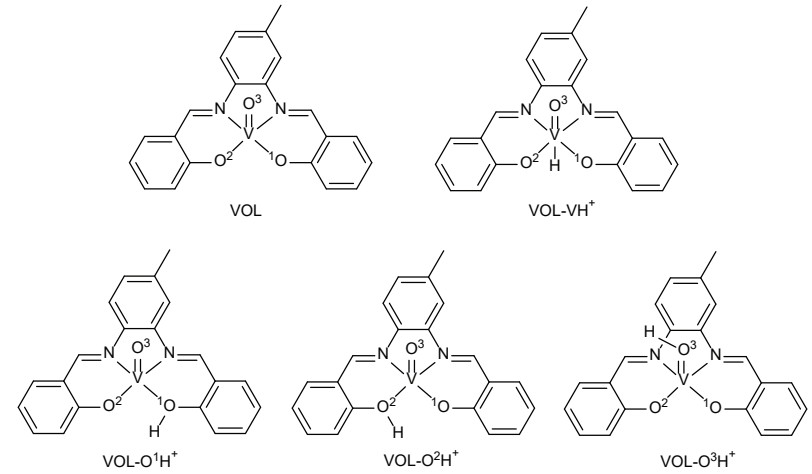

Figure 10. *Structural formulas of conjugate acids of the VOL system.*

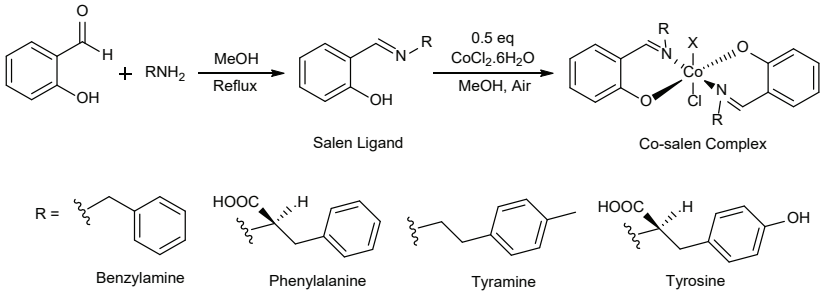

Scheme 22. *Cobalt(III)-salen complexes prepared in the study.*

Electrochemical water splitting: Some cobalt-salophen complexes were investigated in their role as water-oxidation catalysts. There was found a pattern between the stability of the complex and catalytic activity. Substituents as well presented effects on catalytic performances and stabilities. In alkaline solutions, complexes bromo- and nitro-containing Co-salen complexes proved to be efficient water-oxidation catalysts, producing oxygen (See Scheme 23; Shaghaghi et al., 2020).

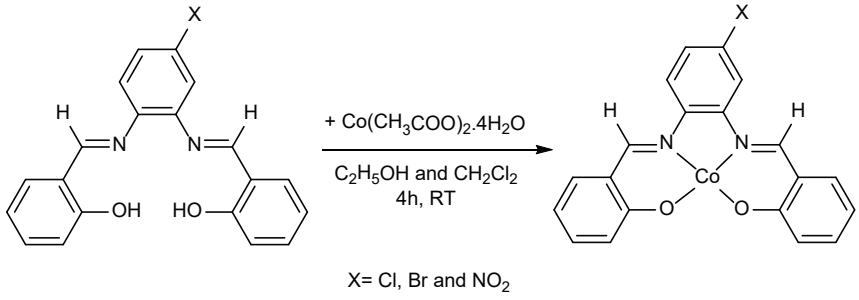

Scheme 23. *The synthesized Co complexes as water-oxidation catalysts.*

Photocatalysis

Photoredox catalysts: Luminescent properties of salen-type complexes are sought in sensing and biological applications. Al(salen)Cl is commercially available, being used as a photoredox catalyst in the synthesis of enantio-enriched α-alkylated compounds. This compound is able to replace the ruthenium complexes, and can be used as a promising photoredox catalytic reaction (See Figure11 and Scheme 24; Gualandi et al., 2020).

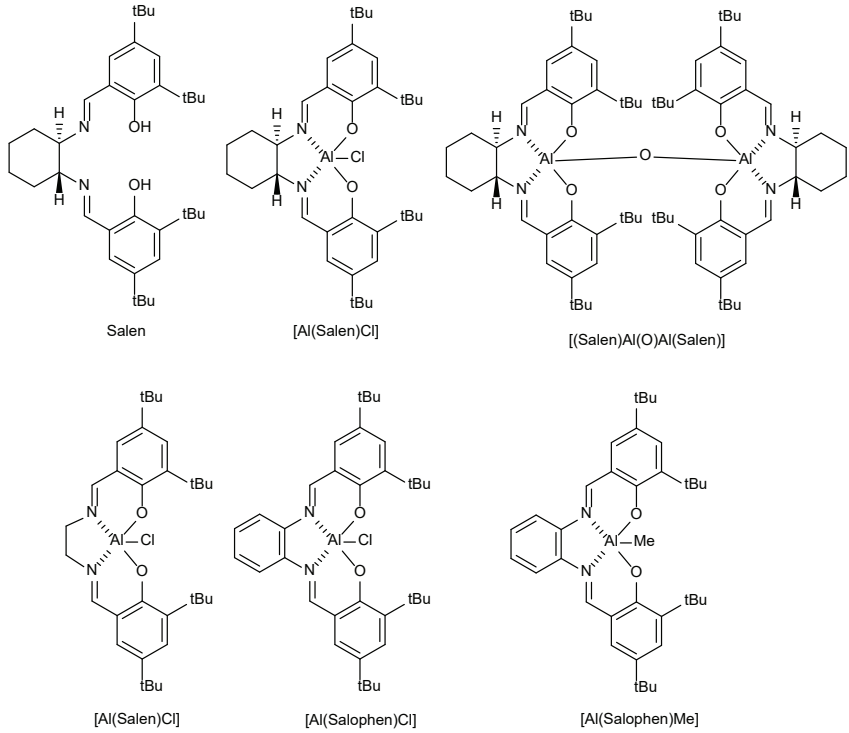

Figure 11. *The structures of salen-Al complexes used in the study.*

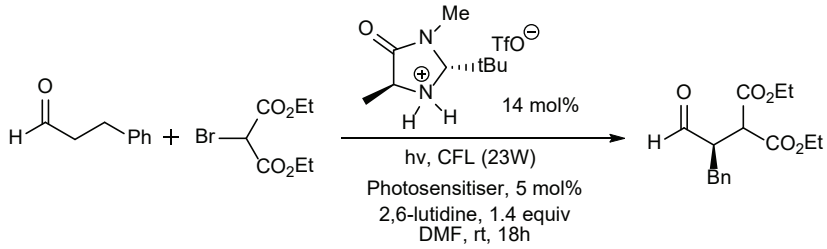

Scheme 24. *The use of aluminum complexes in a photocatalytic stereoselective alkylation of an aldehyde with a dicarboxylic acid.*

Review articles

Molecular materials and devices with tuned properties: Freire and her colleagues prepared a review article about M(salen) compounds, in which the M is V, Cr, Mn, Fe, Co, Ni, Cu, Pd, etc. The authors mentioned of immobilization onto several solid supporting materials, or supramolecular entities. Their catalytic application in the industry is covered as well. In addition, valorization of carbon dioxide in the sense of capturing it and converting into high-value products are also mentioned. These complexes are also used in the energy conversion, storage and saving, giving way to electrocatalytic entities for oxygen reducing reaction, or electrochromic materials (See Scheme 25; Freire et al., 2019).

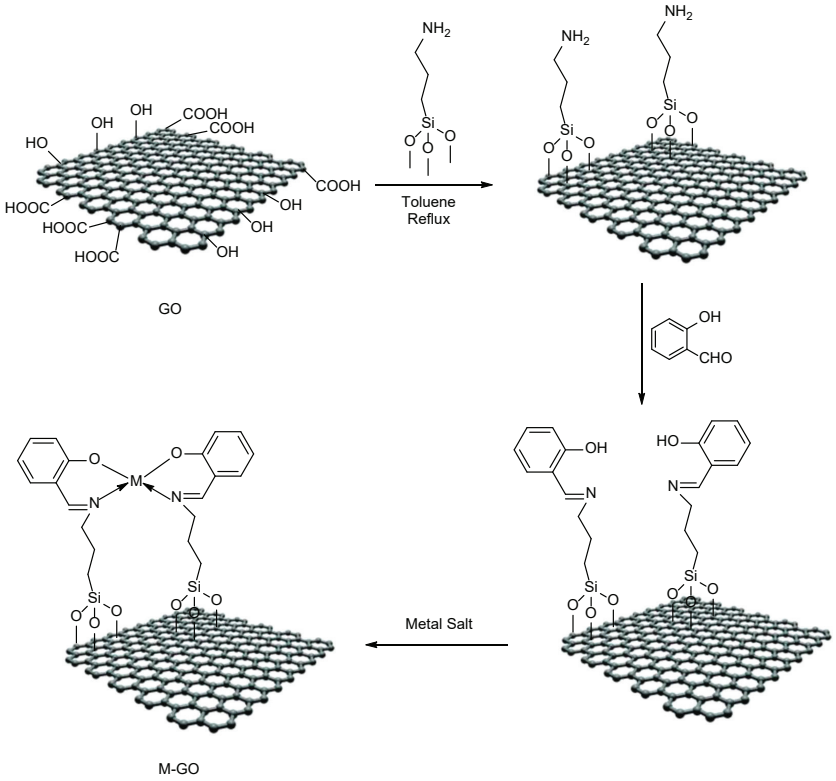

Scheme 25. *M(salen) complex covalently immobilized on functionalized graphene support.*

Synthetic radical chemistry: Kyne et al. discussed, in a review, the 5-hexenyl rearrangement of an alkylcobalt(III) complex (see Scheme 24). Also, they did mention about cobalt(II)salen precatalytic 5-exocyclization to yield sugar analogs. Epoxidation and peroxidation reactions are also mentioned. Obtaining α-amino acid precursors with nickel(II) dehydroalanine complexes was cited (See Scheme 26; Kyne et al., 2020).

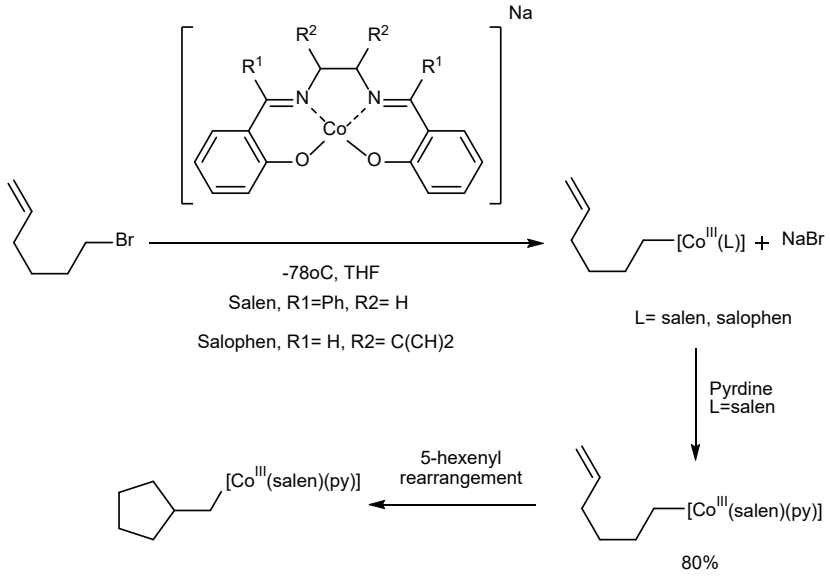

Scheme 26. *5-Hexenyl arrangement of an alkylcobalt(III) complex.*

Manganese(II,III) Schiff Base Complexes: Sarma et al. discussed the catalytic applications of manganese Schiff base complexes. To name a few, they are used in the formation of 1,2-limonene epoxide, synthesis of symmetrical disulfides, oxidation of benzyl alcohol and styrene, efficient oxidation of hydrocarbons, and decarboxylation of carboxylic acids, etc (See Schemes 27 and 28; Sarma et al., 2019).

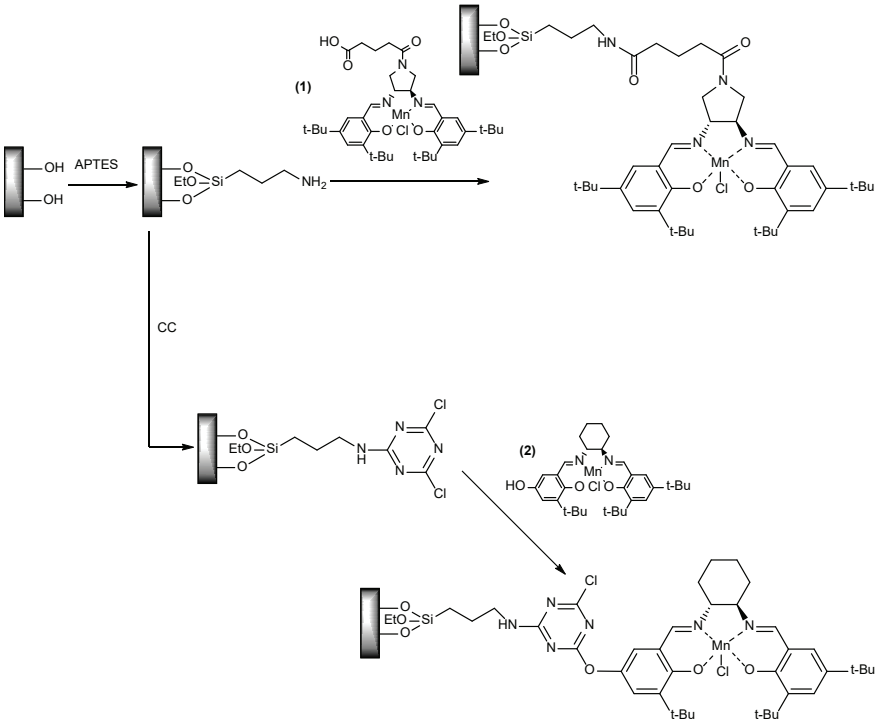

Scheme 27. *Immobilization of two Jacobsen-type complexes onto mesoporous silica.*

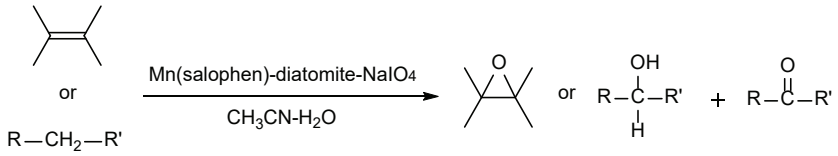

Scheme 28. *Epoxidation of an alkene or an alkane with sodium periodate and Mn complex.*

REFERENCES

Abbaspour, S., Keivanloo, A., Bakherad, M., & Sepehri, S. (2018). Salophen Copper(II) Complex-Assisted Click Reactions for Fast Synthesis of 1,2,3-Triazoles Based on Naphthalene-1,4-dione Scaffold, Antibacterial Evaluation, and Molecular Docking Studies. *Chemistry & Biodiversity*, cbdv.201800410. https://doi.org/10.1002/cbdv.201800410

Aligholivand, M., Shaghaghi, Z., Bikas, R., & Kozakiewicz, A. (2019). Electrocatalytic water oxidation by a Ni(II) salophen-type complex. *RSC Advances*, *9*(69), 40424–40436. https://doi.org/10.1039/C9RA08585H

Aomchad, V., Del Gobbo, S., Yingcharoen, P., Poater, A., & D'Elia, V. (2020). Exploring the potential of group III salen complexes for the conversion of CO2 under ambient conditions. *Catalysis Today*, S0920586120300201. https://doi.org/10.1016/j.cattod.2020.01.021

Clendenin, B. (2019). Polymer Supported Ni(salen) Catalysts and Ni(II)-salen zeolite Y as Catalysts for Heterogeneous Electrohydrocyclization Reactions. *International Journal of Electrochemical Science*, 7995–8013. https://doi.org/10.20964/2019.08.24

Duan, R.-L., Zhou, Y.-C., Sun, Z.-Q., Huang, Y.-Z., Pang, X., & Chen, X.-S. (2020). The Effect of Oxygen to Salen-Co Complexes for the Copolymerization of PO/CO2. *Chinese Journal of Polymer Science*, *38*(10), 1124–1130. https://doi.org/10.1007/s10118-020-2451-5

Freire, C., Nunes, M., Pereira, C., Fernandes, D. M., Peixoto, A. F., & Rocha, M. (2019). Metallo(salen) complexes as versatile building blocks for the fabrication of molecular materials and devices with tuned properties. *Coordination Chemistry Reviews*, *394*, 104–134. https://doi.org/10.1016/j.ccr.2019.05.014

Gualandi, A., Marchini, M., Mengozzi, L., Kidanu, H. T., Franc, A., Ceroni, P., & Cozzi, P. G. (2020). Aluminum(III) Salen Complexes as Active Photoredox Catalysts: Aluminum(III) Salen Complexes as Active Photoredox Catalysts. *European Journal of Organic Chemistry*, *2020*(10), 1486–1490. https://doi.org/10.1002/ejoc.201901086

Kamyabi, M. A., Amirkhani, F., Bikas, R., & Soleymani-Bonoti, F. (2021). Experimental and density functional theory study of oxygen reduction reaction at liquid-liquid interface by oxidovanadium(IV)-4-methyl salophen complex. *Journal of Molecular Structure*, *1228*, 129693. https://doi.org/10.1016/j.molstruc.2020.129693

Kavitha, C., & Subramaniam, P. (2020a). Alteration of electronic effect causes change in rate determining step: Oxovanadium(IV)–salen catalyzed sulfoxidation of phenylmercaptoacetic acids by hydrogen peroxide. *Polyhedron*, *175*, 114172. https://doi.org/10.1016/j.poly.2019.114172

Kavitha, C., & Subramaniam, P. (2020b). Competitive behavior of nitrogen based axial ligands in the oxovanadium(IV)-salen catalyzed sulfoxidation

of phenylmercaptoacetic acid. *Polyhedron*, *189*, 114712. https://doi.org/10.1016/j.poly.2020.114712

Keikha, N., Rezaeifard, A., & Jafarpour, M. (2019). Heterogeneous Fenton-like activity of novel metallosalophen magnetic nanocomposites: Significant anchoring group effect. *RSC Advances*, *9*(57), 32966–32976. https://doi.org/10.1039/C9RA05097C

Khandelwal, S., Zamader, A., Nagayach, V., Dolui, D., Mir, A. Q., & Dutta, A. (2019). Inclusion of Peripheral Basic Groups Activates Dormant Cobalt-Based Molecular Complexes for Catalytic H_2 Evolution in Water. *ACS Catalysis*, *9*(3), 2334–2344. https://doi.org/10.1021/acscatal.8b04640

Klaine, S., Fung Lee, N., Dames, A., & Zhang, R. (2020). Visible light generation of chromium(V)-oxo salen complexes and mechanistic insights into catalytic sulfide oxidation. *Inorganica Chimica Acta*, *509*, 119681. https://doi.org/10.1016/j.ica.2020.119681

Kong, X., Liu, Y., Li, P., Ke, J., Liu, Z., Ahmad, F., Yan, W., Li, Z., Geng, Z., & Zeng, J. (2020). Coordinate activation in heterogeneous carbon dioxide reduction on Co-based molecular catalysts. *Applied Catalysis B: Environmental*, *268*, 118452. https://doi.org/10.1016/j.apcatb.2019.118452

Kumari, S., & Ray, S. (2020). Zeolite encapsulated Ni(II) Schiff-base complexes: Improved catalysis and site isolation. *New Journal of Chemistry*, *44*(35), 14953–14963. https://doi.org/10.1039/D0NJ01590C

Kyne, S. H., Lefèvre, G., Ollivier, C., Petit, M., Ramis Cladera, V.-A., & Fensterbank, L. (2020). Iron and cobalt catalysis: New perspectives in synthetic radical chemistry. *Chemical Society Reviews*, *49*(23), 8501–8542. https://doi.org/10.1039/D0CS00969E

Niakan, M., Asadi, Z., & Masteri-Farahani, M. (2020). Fe(III)-salen complex supported on dendrimer functionalized magnetite nanoparticles as a highly active and selective catalyst for the green oxidation of sulfides. *Journal of Physics and Chemistry of Solids*, *147*, 109642. https://doi.org/10.1016/j.jpcs.2020.109642

Pour, S. R., Abdolmaleki, A., & Dinari, M. (2019). Immobilization of new macrocyclic Schiff base copper complex on graphene oxide nanosheets and its catalytic activity for olefins epoxidation. *Journal of Materials Science*, *54*(4), 2885–2896. https://doi.org/10.1007/s10853-018-3035-4

Qiao, J., Gao, S., Wang, L., Wei, J., Li, N., & Xu, X. (2020). Air-stable μ-oxo-bridged binuclear titanium(IV) salophen perfluorooctanesulfonate as a highly efficient and recyclable catalyst for the synthesis of bis(indolyl) methane derivatives. *Journal of Organometallic Chemistry*, *906*, 121039. https://doi.org/10.1016/j.jorganchem.2019.121039

Rae, A., Gaston, A. J., Greindl, Z., & Garden, J. A. (2020). Electron rich (salen) AlCl catalysts for lactide polymerisation: Investigation of the influence

of regioisomers on the rate and initiation efficiency. *European Polymer Journal*, *138*, 109917. https://doi.org/10.1016/j.eurpolymj.2020.109917

Reiss, H., Shalit, H., Vershinin, V., More, N. Y., Forckosh, H., & Pappo, D. (2019). Cobalt(II)[salen]-Catalyzed Selective Aerobic Oxidative Cross-Coupling between Electron-Rich Phenols and 2-Naphthols. *The Journal of Organic Chemistry*, *84*(12), 7950–7960. https://doi.org/10.1021/acs.joc.9b00822

Sarma, C., Chaurasia, P. K., & Bharati, S. L. (2019). Versatile Catalytic Applications of Manganese(II,III) Schiff Base Complexes (Review). *Russian Journal of General Chemistry*, *89*(3), 517–531. https://doi.org/10.1134/S1070363219030253

Shaghaghi, Z., Aligholivand, M., & Mohammad-Rezaei, R. (2020). Enhanced water splitting through different substituted cobalt-salophen electrocatalysts. *International Journal of Hydrogen Energy*, S0360319920336028. https://doi.org/10.1016/j.ijhydene.2020.09.162

Shi, D., Li, L., Wen, Y., Yang, Q., & Duan, Z. (2020). Ring-opening copolymerization of epoxycyclohexane and phthalic anhydride catalyzed by the asymmetric Salen-CrCl complex. *Polymer International*, *69*(5), 513–518. https://doi.org/10.1002/pi.5985

Ullah, H., Mousavi, B., Younus, H. A., Khattak, Z. A. K., Suleman, S., Jan, M. T., Yu, B., Chaemchuen, S., & Verpoort, F. (2019). ONO pincer type ligand complexes of Al(III) as efficient catalyst for chemical fixation of CO2 to epoxides at atmospheric pressure. *Journal of Catalysis*, *377*, 190–198. https://doi.org/10.1016/j.jcat.2019.07.033

Chapter 7

THEORETICAL INVESTIGATION OF PLATINUM ANALOGUES USED IN CHEMOTHERAPY TREATMEN

Murat AYHAN[1]

1 Dr. Murat AYHAN, Ministry of youth and sports muayhan44@gmail.com

Introduction

The basic unit of structure and behavior that contains the vital codes of a living thing and has the ability to survive under appropriate conditions is expressed as a cell. Living things can be divided into two classes according to their cell structures: unicellular and multicellular organisms. Human beings, who are among the multi-celled creatures, continue their generation thanks to cell division and also live a healthy life with the systematic work of metabolism due to regular repair activities thanks to cell division. The prerequisite for a healthy metabolism depends on the regular and balanced cell division. However, if cell divisions do not occur regularly and in a balanced way, metabolism alarms as a result of uncontrolled cell division and proliferation. Due to uncontrolled division, excessive cells that grow and multiply rapidly in the body are formed and these cells are called cancerous cells (Kantarcı, 2006). Cancer cells are a burden for metabolism. These cells act out of control and cause the body's chemistry to deteriorate as they negatively affect the functioning of normal cells. This situation prevents the metabolism from performing many vital activities. For this reason, cancerous cells in the body need to be controlled. For this purpose, chemotherapy is applied as a treatment method that kills cancer cells, prevents them from spreading and slows their growth (Sutopo, 2006). Platinum containing chemical structures are used in chemotherapy applications. Platinum element has many uses because it is resistant to high temperatures and does not undergo any change in chemical reactions. Since Platinum is not a reactive metal, it is preferred in the field of health because it does not cause any health problems (Johstone, 2016). Platinum compounds cis-platin, carbo-platin, oxaliplatin, neoplatine are preferred in cancer treatment due to their ability to penetrate the DNA structure (mckeage, 2008) In our study, we made the three-dimensional drawings of the molecular structures, which are platinum analogues and used in the chemotherapy process, using the gaussian package program based on quantum chemistry. We calculated these structures by using three basic methods, DFT (density functional theory), HF (Hatree-Fock) and semi-empirical method in the gaussian package program. We modeled and analyzed four different structures derived from the Platinum element with three different methods. We compared our results with each other. First of all, we examined the structure of cis-platin molecules, which were first used in cancer treatment. Although this structure fights and destroys cancer cells very well, it causes damage to the kidney due to the ammonia molecules it contains, and carbo-platin has been used in the following processes (Hambley, 1997). Second, we dealt with the molecular structure of Carbo-platin. Since this structure contains more carbon groups and oxygen, it has been used since it causes less damage to the kidney in its cis-

palatine structure. In the following processes, oxaliplatin and neoplatine analogues started to be preferred because they cause less damage to the body (Colley, 2008). All these pt analogs interact with guanine by affecting the DNA structure. Drawings of these four pt analog structures were created in the gaussian program to look at their interactions with guanine (Jung and Lippard, 2006). Geometric optimizations of all the structures created were made. The total energy values of the molecules formed as a result of optimization, the highest occupied molecular orbital (HOMO) and the lowest empty molecular orbital (LUMO) values were calculated. In addition, the Uv-Vis values of the molecular structures were found and their graphics were drawn. Independently of all these, the structure of guanine as a single molecule structure was also examined.

Materials and Methods

There are two main health services in studying a molecule or molecular system. One of these is the experimental method. X-ray diffraction, IR spectroscopy, NMR to examine the structure by experimental method. techniques such as are used. Besides, molecular structure is elucidated by numerical methods. In this initial three different numerical expressions, theoretical calculations were made (Bayri, 2020).

The numerical method tries to obtain the approximate mathematical solution of the Schrödinger equation for a problem. Molecular modeling has a wide range of applications in physics, chemistry, biology, pharmaceutical industry, materials science and many other places (Türkay, 2018) Molecular modeling is the elucidation of the properties of a molecule with the help of a computer, based on the laws of physics. The purpose of molecular modeling is to reveal the physical properties of the molecule. In general, molecular structures are elucidated by writing a hamiltonian that includes all interactions based on the principle of conservation of energy in the illumination of molecules (Pir and Günay, 2011). The methods to solve the problem are mostly used coded in a computer program. These programs contain all the physical properties we want to know about the molecule. These physical properties can be sizes such as structural quantities (bond length, bond angle, torsion angle), energy, dipole moment, ionization potential, electrostatic potential. The total energy of a molecule consists of approximately the kinetic energy of the electrons in the molecule, the vibration of the atoms in the molecule and the sum of the kinetic energy caused by the rotation of the molecule. In molecular modeling, the goal is mostly to reveal the electron configuration of the entire molecule. The total energy of the molecule is quantum mechanically expressed by a Schrödinger equation that takes into account the interactions between electrons and nuclei. The exact solution of this equation is impossible except in single-electron systems (Kamuran, 2018). Therefore, they usually try to obtain

numerical solutions using some approaches. Many approximate methods have been used until today. Three frequently used models, HF, DFT and Semi-empirical method, were used in our study. The HF (Hatree-Fock) method seeks the solution of the interaction of any electron in the system under the average potential energy of other electrons in the system (Tezer, 2011). Computing complex structures requires high-quality computer components. Therefore, semi-empirical methods have been developed to obtain faster and more precise calculations. In the semi-empirical method, different experimental data such as atomic spectrum and ionization energy are used to determine some parameters. DFT, Function theory deals with electrons clustered elsewhere in space. It deals with the density function of the clustered electrons (Güler, 2011). This theory is based on two foundations. The first of these; Every observable, ie energy, of a quantum mechanical system at rest can in principle be calculated precisely only from the ground state density. In other words, each observable ground state can be written as a functional of the hamiltonian. The ground state density can be calculated exactly using the variational method. With the DFT method, electronic energy is defined as follows: $E = E^T + E^V + E^J + E^{XC}$. Here, the term for the kinetic energy arising from the motion of the E^T electrons, E^V includes the columbic potential energy between the nucleus-electron, the E^J term for the electron-electron repulsion, and the other remaining electron-electron interactions in the E^{XC}. As a result, in the DFT method, the electron sees an average electron density and is included in the calculations as if interacting with a spherically symmetric potential (Uysal, 2014). These basic three theoretical methods were created by drawing platinum analogues in three dimensions with the help of the Gaussan program. The first of the platinum analogs, cis-platinum, are shown in Figure 1, the second of the platinum analogs, carbo-platinum, in figure 2, oxaliplatin in Figure 3, and finally, the plot of the neoplatine analogue in the gaussian program is shown in Figure 4.

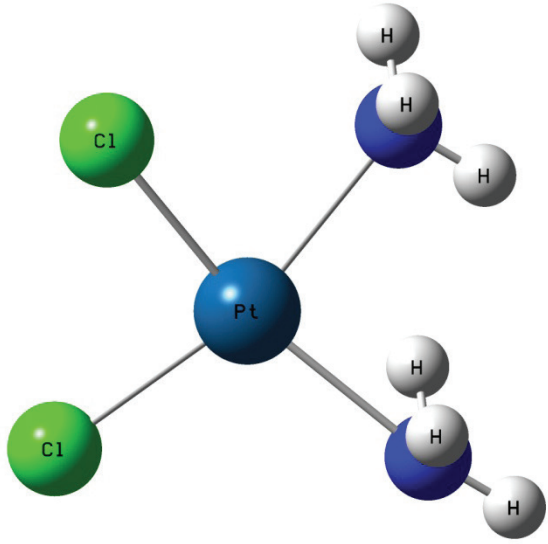

Figure 1 There dimensional drawing in Cis-Platin gaussian program

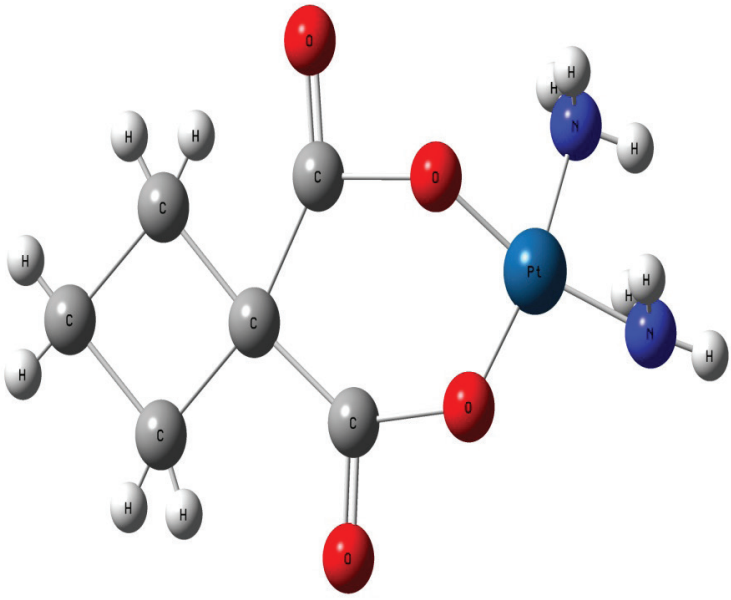

Figure 2 There dimensional drawing in Carbo-Platin gaussian program

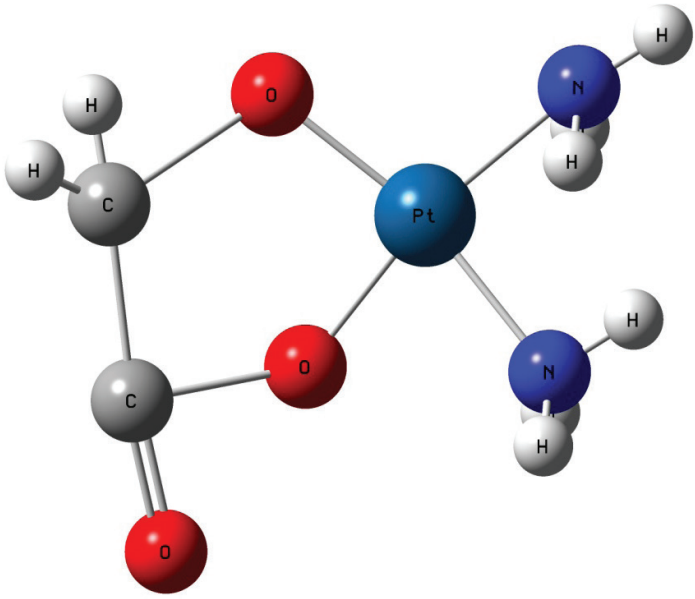

Figure 3 There dimensional drawing in Neoplatinum gaussian program

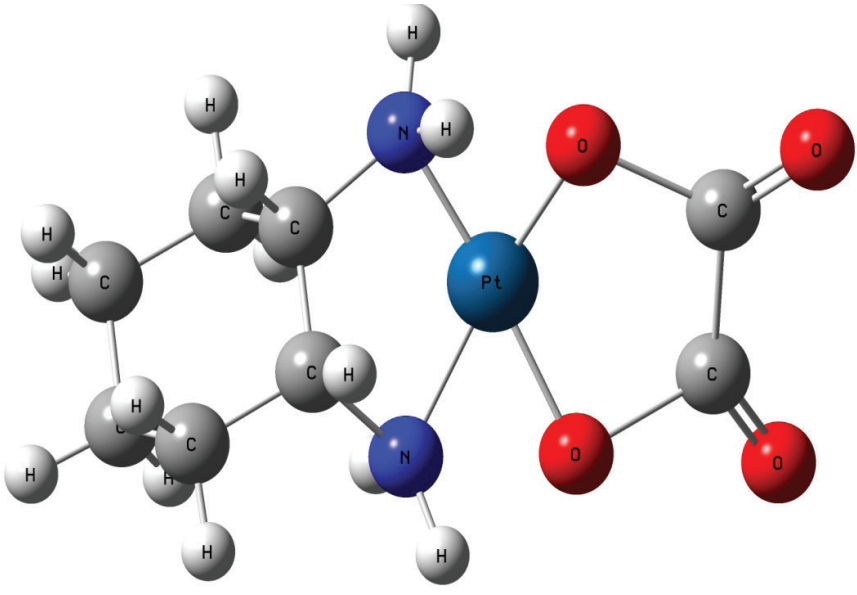

Figure 4 There dimensional drawing in Oxalioplatin gaussian program

Gaussian is a very grift program used in molecule modeling. It contains all the calculation methods mentioned above. The program, which focuses on quantum chemistry, calculates the energies of molecular structures, dipole momentums, vibration frequency values. It reveals the most ideal

form of the structure by calculating the geometric optimization of the molecular structure using the iteration cycle. With this program, it can be determined whether the molecular wave function is stable or not. Using the potential energy values of the surfaces, the program can predict the possible transition states and the paths of reactions that may occur. In addition, by presenting the HOMO (highest occupied molecular orbital energy value) and LUMO (the lowest unoccupied energy value) information, which belong to the molecular structure, the molecules are about the structure by informing us about the ionization potential, electron affinity and the structural hardness and softness that the structure will have. All these properties can be found in gas phase, solution or crystal phase. The ground state or excited state of the atom or molecule can be used in calculations

GaussView is an interface program developed for the Guassian program we used to edit the input file and visualize the output files. This interface unit provides the interaction between the user and the program. It helps us to visualize molecular structures, to rotate the structures in the directions and angles we want, to displace the structures as we want, to add or remove any atom or solvent to the molecular structure, to delete part or all of the structure, and so on. In addition, it allows us to create input files for complex calculations. In addition, it provides us with a detailed examination by graphically presenting the results we have obtained through Gaussian. The results obtained can be highly physical quantities such as optimized complex structures, orbitals of molecules, charges belonging to atoms, Infrared spectroscopy, nuclear magnetic resonance spectroscopy, polarized states and vibration frequencies

While the calculations of the platinum analogs drawn in GaussView were made using the Ground State / Lan2Dz base set for HF and DFT method, the ground state / MP6 method was used in the semi-experimental method. Calculations of four different Platinum analogs were made for these base sets. Detailed information about the buildings was obtained by interpreting the obtained results. The difference between the HOMO - LUMO values of the structures (Energy gap) Since the Eg value gives information about the chemical stability of the structures, the energy gaping values of four different platinum analogs were calculated. In addition, UV-Vis values of platinum analogs and UV graphics of the structures were also obtained as a result of these values.

Results and Discussion

The electron configuration of the molecules allows us to obtain information about the structure under study. Geometric optimization of the structure should be made to ensure that the electron configuration is clearly inviting. İn figure 1- figure 4 four different platinum molecule structures

with geometric optimization is the Eg values. Eg value is found from the energy difference between HOMO and LUMO. We can reach these values about the structure under study. Many physical and chemical quantities such as electron affinity, ionization potential, electronegativity, chemical hardness and chemical softness can be calculated using HOMO and LUMO energies (Wolf, 2004) The HOMO and LUMO energy orbitals of these four different platinum molecular structures are as follows. HOMO-LUMO electron charge distributions and Eg values obtained from three different methods of cis-platinum analog in figure 5, carbo-platinum analog in figure 6, oxaliplatin analog in figure 7 and finally neoplatin analog in figure 8.

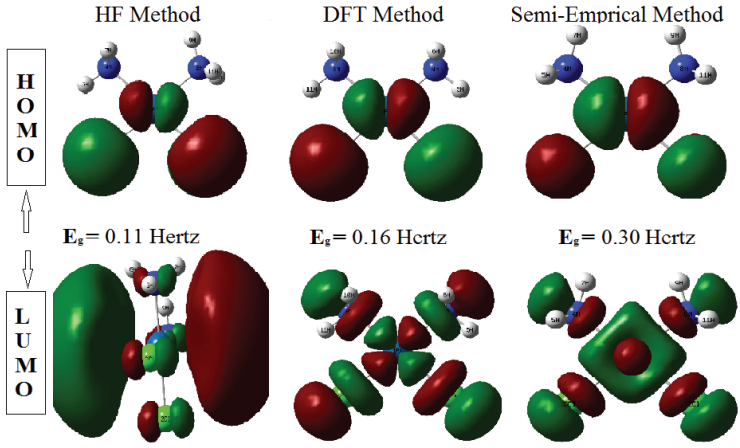

Figure 5 Cisplatin HOMO-LUMO orbital and E_g values

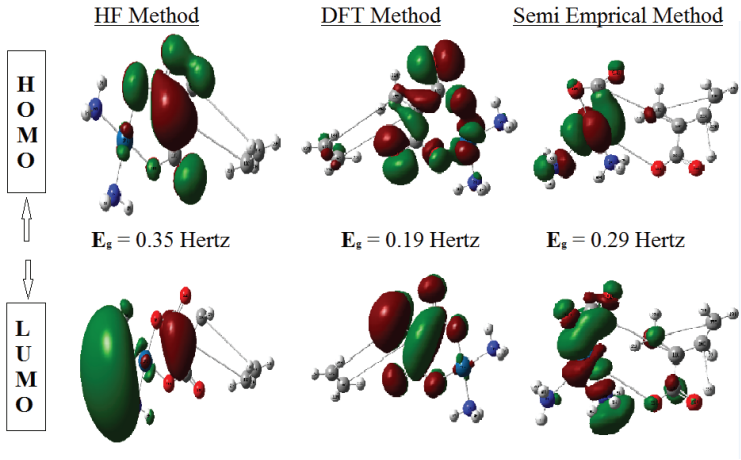

Figure 6 Carbo - platin HOMO-LUMO orbital and E_g values

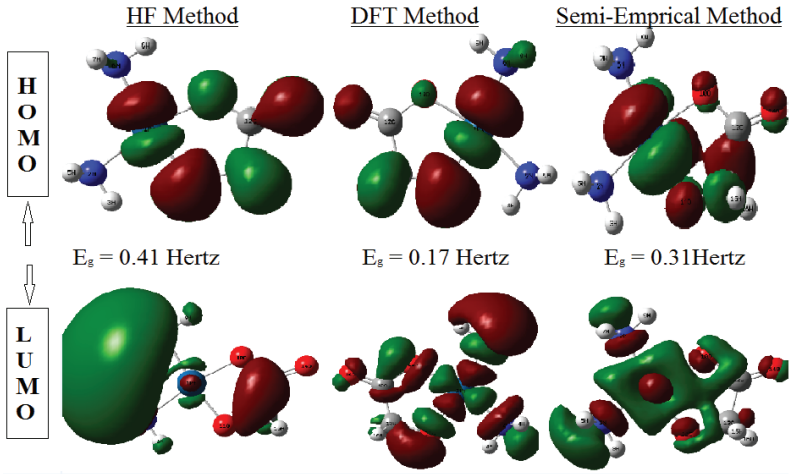

Figure 7 Oxaliplatin HOMO-LUMO orbital and E_g values

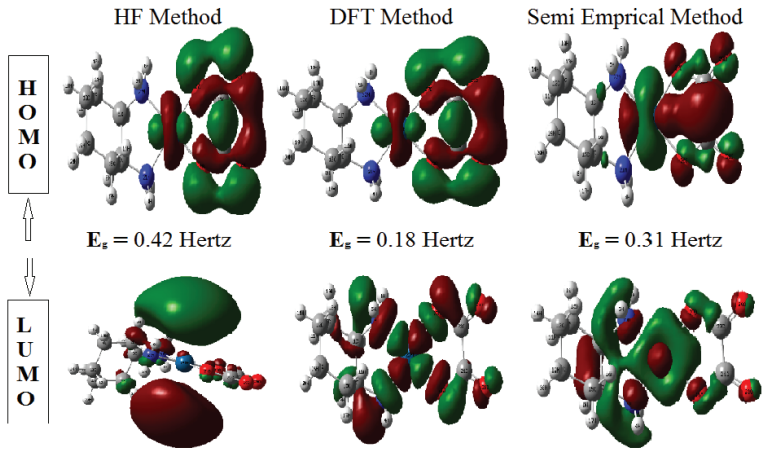

Figure 8 Neoplatine HOMO-LUMO orbital and E_g values

Energy gaping (Eg) values calculated using three different methods of cis-platinum analog are given in Figure 5. Since the value obtained from the HF method is the smallest, we know that the most stable structure in the cis-platinum analog was found by the HF method. Since the HF method is based on the effect of each electron on an independent average potential, it is thought that this method will be more effective in cis-platinum analogue studies. In Figure 6, Energy gaping (Eg) values calculated using three different methods of carbo-platinum analog are given. In the carbo-platinum analogue, the calculation made by the DFT method has the smallest value, and the most stable structure for carbo-platinum was obtained using the DFT method. Since the DFT method is based on electrons concentrated in a region of space, it can be thought that this analogue can be used in the

treatment of cancer cells that have the highest density or cancerous cells that are highly concentrated in a certain part of the body. Similarly, when Figure 7 and Figure 8 are examined, the energy value obtained by the DFT method is the smallest for neoplatin and oxaliplatin analogues. Therefore, if we make the same interpretation for these analogues, we can say that these analogues will be used in the treatment of certain parts of the body. In addition, the HF method can be used when a general treatment is aimed in the body.

Independent of all these, the molecules were studied in guanine as a structure. Because pt analogues given to the body during chemotherapy enter with guanine found in the DNA chain, making it ineffective. Therefore, the calculations of this structure were made by drawing in GaussView in the guanine structure. In Figure 9, the three-dimensional drawing of the guanine molecule structure in GaussViev, and in Figure 10 and Figure 11, the three-dimensional drawings of the interactions of the guanine molecules structure with the platinum analogues cis-platinum and carbo-platinum in gaussView are made. Thus, the data of the guanine structure before interacting with the platinum analogs can be compared with the data after interacting with the platinum analogs. In addition, three-dimensional drawings of the interactions of guanin with pt analogs were made in GaussView and the UV-Vis values of these structures were examined. Because platinum is very small with the interaction in the magnetic field and takes a value between 0 - 300A. This value indicates that the platinum element is almost not affected. Therefore, platinum is one of the indispensable elements of the healthcare industry. We have reached some data and made some predictions about platinum analogues that interfere with guanine. We aimed to control the UV changes before and after the reaction and to evaluate the result.

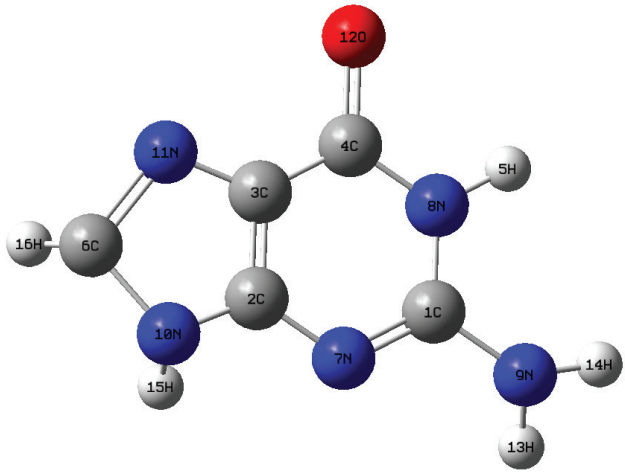

Figure 9. GaussView Three dimensional drawing of the guanine molecule

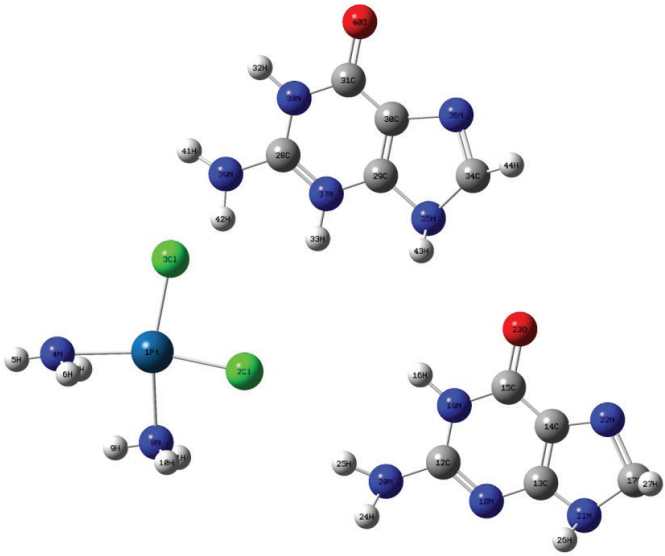

Figure 10. GaussView Three dimensional drawing of the guanine and cisplatin molecule

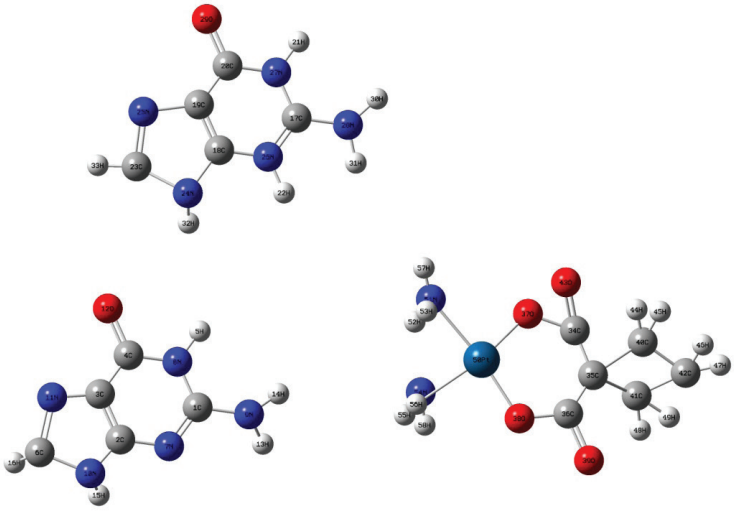

Figure 11 GaussView Three dimensional drawing of the guanine and carboplatin molecule

Conclusion

Conclusion Cis-platinum, which has the smallest Eg value among platinum analogues, has a more stable structure. Because Eg is an indicator of the chemical stability of a structure. The decrease in the Eg value makes the structure more stable and the reactions within the structure take place more easily. Despite having the steadiest structure of the four analogues,

cis-platinum is the most damaging analogue to the body. As we mentioned earlier, while cis-platinum may be successful in fighting cancerous cells throughout the body, other analogues may be more successful in fighting cancer cells collected in certain parts of the body. In addition, since the platinum element is only slightly affected by the magnetic field, this situation has been observed in the structure of platinum analogues. The uV-Vis plots of the guanine structure interacting with guanine and cis-latin are shown in figure 12. The guanine structure was found to have a UV-Vis peak of around 322 nm and a wavelength of 0.08. However, the cis-platinum Uv-Vis spectrum interacting with guanine has a value of 740, 76 nm and is almost 0.000002 of the wavelength and gives an exponential appearance to the right and left of the zero value. While it is almost a linear line to the left of the zero value, the UV-Vis peak rises rapidly when it approaches zero, and when it reaches the zero value, the peak changes direction again and the peak tends to decrease rapidly on the right side of the zero value. This shows us that there is an interaction between cis-platinum and guanine, where a reversible process is at work. We can express that, with a demolition, a repair work takes place. This is also seen in all other pt analogs that interact with guanine. But the most prominent appearance is seen in cis-platinum. Based on this, we can say that Cis-platinum is more effective and effective despite other analogues, and the damage it gives to the body is more. Therefore, it can be preferred in the first stage of cancer treatment, but it will be healthier to prefer analogs instead in the future. Even if we interpret the values obtained from the Gaussian program when all the analogs are reviewed, we can reach the following conclusion. Carbo-platinum, oxaliplatin and neoplatin analogues, which are richer in oxygen in their molecular structure, cause less damage to the body. As a result, we can say the following. If we can create a pt analog that has less ammonia content and contains more oxygen, our fight against cancer will be easier.

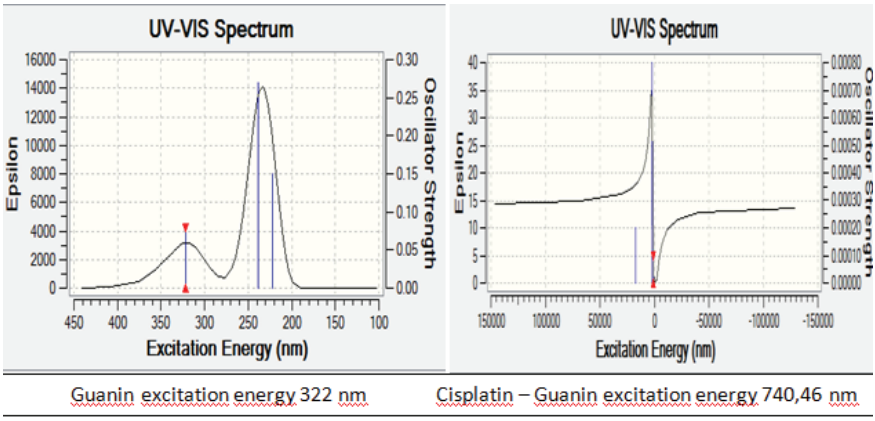

Figure 12.UV-Vis spectra of molecules structures.

REFERENCES

[1] Kantarcı G. ,Özgüney I. ,Sozer S.,Karasulu H.Y, Güneri T., Ertan G., Transdermal Delivery of Diclofenac Sodium Through Rat Skin From Various Formulations, April 10, 2006; 7 (4) Article 88

[2]Sutopo H., Reactions of Cisplatin Hydrolytes with Thiols. 3: Reactions of cis-[Pt(15NH3)2(H2O)2]2+ with Glutathione, MAKARA of Science Series, April 2006, 10 (1)

[3] McKeage M J, Pawel J Von, Reck M, Jameson M B, Rosenthal M A, Sullivan R, Gibbs D, Mainwaring P N, Serke M, Lafitte J-J, Chouaid C, Freitag L & Quoix E, Randomised phase II study of ASA404 combined with carboplatin and paclitaxel in previously untreated advanced non-small cell lung cancer, pages2006–2012 (2008),British Journal of Cancer volume 99

[4] Hambley T.W. , The influence of structure on the activity and toxicity of Pt anti-cancer drugs Author links open overlay panel, Volume 166, November 1997, Pages 181-223

[5] Colley J., Azzopardi D., Dallosso A.R., Eliason K., Hendrickson B.C., Jones N., Rawstorne E., Moskvina V., Frye C., Sampson J.R., Wenstrup R., Scholl T. and Cheadle J.P., Multiple Rare Nonsynonymous Variants in the Adenomatous Polyposis Coli Gene Predispose to Colorectal Adenomas,

[6] Lippard S.J. , Jung Y. ,RNA polymerase II blockage by cisplatin-damaged DNA. Stability and polyubiquitylation of stalled polymerase, February 2006 ,Journal of Biological Chemistry 281(3):1361-70

[7] Bayri A., Altın S., Demirel S., Oz E., Altın E., Hetherington C. and Avcı S., Synthesis of $Na_2Ti_3O_7$ nanorods by a V-assisted route and investigation of their battery performance**,** 10.1039/C9CE01955C (Paper) CrystEngComm, 2020, 22, 2483-2490

[8] Türkay R., Bakır B., Tuğcu V., Binbay M., Özden E., Erbin A., Özgör F., Prostat Kanserinde Multiparametrik Manyetik Rezonans Görüntüleme Ve Hedefe Yönelik Biyopsi Kılavuzu, 2018

[9] Pir H.Gümüş, Atalay Y., Günay N., Avcı D., Başoğlu A.,A Theoretıcal Study On 5 Chloro 8 Hydroxyquınolınıum Nıtrate, Balkan Physıcs Letters, cilt.19, ss.350-361, 2011

[10] Tezer A., Kefeli A., Yeniova A. Ö., Nazlıgül Y. , Küçükazman M., Saçıkara M., Asiltürk Z.,Şimşek G., Importance of ulcer size and localization observed at endoscopy in differential diagnosis of gastric ulcers, 2011; 2 (3): 273-276

[11] Güler G., Sarı E., Hayran M., Güllü I., Altundağ K., Özışık Y., Comparative study of the immunohistochemical detection of hormone receptor status and HER-2 expression in primary and paired recurrent/metastatic lesions of patients with breast cancer, Medical Oncology volume 28, pages57–63 (2011)

[12] Uysal A.,Oktem G., Sercan O., Güven U.,Uslu R. , Göksel G.,Ayla S.,Bilir A., Cancer stem cell differentiation: TGFβ1 and versican may trigger molecules for the organization of tumor spheroids, June 12, 2014, Pages: 641-649